Structural Effects in Network Dynamical Systems: From Reconstruction to Pattern Formation in Hypergraphs

by

Moise R. Mouyebe

A dissertation submitted in partial fulfillment
of the requirements for the degree of
Doctor of Philosophy
(Applied and Interdisciplinary Mathematics)
in the University of Michigan
2026

Doctoral Committee:

Professor Anthony M. Bloch, Co-Chair
Professor Indika Rajapakse, Co-Chair
Professor Victoria Booth
Professor Ilya Kolmanovsky

Moise R. Mouyebe

mmouyebe@umich.edu

ORCID iD 0000-0002-1030-7677

© 2026 Moise R. Mouyebe. All rights reserved.

IN GOD WE TRUST

To my father Elissa Mouyebe. and my mother Marie-Claire Balogog.,

whose love and sacrifices have made this journey possible.

You are the light that guides my path.

Acknowledgments

I would like to express my heartfelt gratitude to my advisor, Professor Anthony M. Bloch, for his guidance, insight, and constant support throughout this journey. I feel truly fortunate to have had an advisor who understood and encouraged me throughout my graduate studies. Professor Bloch has given me the opportunity to explore my own research directions, while offering deep and thoughtful guidance whenever I needed it. His mentorship has had a profound impact on both this dissertation and my growth as a researcher. Even during times when progress was slow, his patience and steady encouragement helped me persevere and complete this work. I am especially thankful for the trust he placed in my ideas and for always listening attentively, not only to my research, but also to the many practical matters surrounding it.

I am also grateful to my co-advisor, Professor Indika Rajapakse, for his valuable feedback and for the good discussions during the early stages of this work. In particular, I am grateful for his introduction to hypergraphs and their data-driven aspects , which played an important role in shaping the initial direction of this research.

I would like to thank the members of my dissertation committee, Professor Victoria Booth and Professor Ilya Kolmanovsky, for their time, and for agreeing to serve on my committee.

I am grateful to the faculty and staff of the Mathematics Department here at the University of Michigan for their support, and for fostering an environment dedicated to learning and intellectual growth.

I offer a special and heartfelt acknowledgment to my daughter Kenza Claire Mouyebe. Her patience, love, and quiet strength have been a constant source of inspiration. Through her, I have come to realize that my capacity for resilience runs deeper than I ever imagined.

I am deeply thankful to my family members, especially my sister Jemima Abiba Mouyebe and my nephew Andrew K. C. Bogmis , whose support has been a steady and reliable source of strength throughout this journey.

Finally, I acknowledge my ancestors, especially Mohis Toakole, Rachel Gafoube, Pierre Balogog, Seraphine Ngo Kam, Mali Maa Toakole and Mali Maa Gafoube whose legacy, sacrifices, and support have made this work possible in ways both seen and unseen.

Contents

Dedication ii

Acknowledgments iii

List of Figures x

List of Tables xii

List of Appendices xiv

Abstract xv

1 Introduction 1

1.1 Motivation 1

1.2 Structural Effects and Observability 2

1.3 Overview of the Approach 2

1.4 Contributions 3

1.5 Organization of the Dissertation 4

2 Hypergraph Reconstruction and the Limits of Pairwise Data 5

2.1 Motivation 5

2.2 Hypergraphs and Incidence Structure 6

2.3 Clique Expansion as a Forward Map 8

2.4 The Hypergraph Reconstruction Problem 10
2.5 Ill-Posedness of the Reconstruction Problem 11
2.5.1 Regularization by Sparsity 13
2.5.2 Clique-Contraction as a Constructive Heuristic 14
2.6 Consistency of Clique Contraction 15
2.7 Deterministic and Probabilistic Selection 17
2.7.1 Deterministic Selection 17
2.7.2 Probabilistic Selection 17
2.7.3 Clique Score and Selection Rule 18
2.7.4 Regularization and Trade-Off 19
2.7.5 Interpretation 20
2.8 Empirical Illustrations 20
2.8.1 Email networks 21
2.8.2 Drug-class Networks 23
2.8.3 Contact Networks 24
2.9 Implications for Structural Inference 26
2.10 Transition to Network Dynamics 27

3 Network Stability and Structural Effects in Graph Dynamical Systems 28

3.1 From Reconstruction to Dynamics 28
3.1.1 Coupling and Stability in Network Dynamical Systems 29
3.2 Network Dynamical Systems on Graphs 30
3.3 Homogeneous Equilibrium and Linearization 32
3.3.1 Equilibria of the Dynamics 32
3.3.2 Linearization and Variational Equation 33
3.4 Spectral Decomposition of the Network Jacobian 35
3.5 Stability Conditions 36
3.5.1 Coupling-Induced Destabilization 38

3.5.2 Coupling-Induced Stabilization 39
3.6 Obstructions to Stabilization 41
3.6.1 Functional Obstruction: Diffusive Coupling 41
3.6.2 Structural Obstruction: Bipartiteness 42
3.6.3 Examples 43
3.7 Summary of Static Stability Mechanisms 43
3.8 Switching Network Dynamical Systems 44
3.8.1 Formulation and Equilibrium structure. 44
3.8.2 Challenges of switching dynamics. 45
3.8.3 Stability objective. 45
3.9 Common Lyapunov Functions and Stability under Switching 46
3.9.1 Separable Lyapunov Structure 47
3.9.2 Existence of a Common Quadratic Lyapunov Function 47
3.10 A Network-Only Stability Condition for Switching 48
3.10.1 Quadratic-Type Lyapunov Functions 48
3.10.2 Degree-Based Switching Stability Condition 49
3.10.3 Interpretation and Structural Implications 50
3.11 Spectral and Lyapunov Structural Perspectives on Network Dynamical Systems 51
3.12 Numerical Simulation 52
3.13 Chapter Summary 60

4 Pattern Formation in Hypergraphs: Linear and Nonlinear Structural Effects 62

4.1 From Reconstruction to Pattern Formation 62
4.2 Introduction 63
4.3 Hypergraph Background and Directionality 66
4.3.1 Hypergraphs 67
4.3.2 Directed hypergraphs and B-hypergraphs 67

4.3.3 Order decomposition and uniform B-components 68
4.3.4 Adjacency tensors for uniform B-hypergraphs 68
4.3.5 Degrees for directed B-hypergraphs 69
4.3.6 Directification 70
4.3.7 Symmetric B-hypergraphs 72
4.4 A Unifying Framework for Dynamical Systems on Directed Hypergraphs . . 73
4.4.1 Dynamical systems on hypergraphs 73
4.5 Aggregator-Mixer coupling structure 75
4.5.1 Relation to existing models and unifying perspective 76
4.6 Reaction-Diffusion on B-hypergraphs and Laplacian dynamics 77
4.6.1 Diffusive coupling 78
4.6.2 Laplacian tensor formulation 78
4.7 Model specification 79
4.8 Linear Dynamics and Pattern Onset 81
4.8.1 Structural visibility hierarchy 82
4.8.2 Linearization about a reference trajectory 84
4.9 Working assumptions 86
4.9.1 Linearization theorem 87
4.9.2 Directed dispersion relation 88
4.9.3 Linear indistinguishability 89
4.9.4 Interpretation 90
4.10 Nonlinear Analysis and Pattern Saturation 90
4.10.1 Spectral setup 91
4.10.2 Weakly nonlinear reduction 93
4.10.3 Linear growth rate coefficient 93
4.10.4 Nonlinear saturation coefficients 95
4.10.5 Normal form regimes 102

4.10.6 Nonlinear distinguishability and structural effects 106
4.11 Interpretation 111
4.12 Numerical Validation 112
4.12.1 Overview 112
4.12.2 Numerical setup 112
4.12.3 Nonlinear Distinguishability under Exposure-Equivalence 114
4.12.4 Dynamical Graph Surrogacy 115
4.12.5 Reduced Dynamics versus the Full System 117

5 Conclusion and Outlook **118**
5.1 Summary of Results 118
5.1.1 Reconstruction from Data 119
5.1.2 Stability of Network Dynamical Systems 119
5.1.3 Nonlinear Reduction on Directed Hypergraphs 120
5.2 A Unified Perspective on Structural Effects 120
5.3 Implications 121
5.3.1 Limits of Structural Inference 122
5.3.2 Role of Higher-Order Interactions 122
5.3.3 Modeling Considerations 122
5.4 Future Directions 122
5.4.1 Beyond Weakly Nonlinear Regimes 123
5.4.2 Inference of Dynamically Relevant Higher-Order Structure 124
5.4.3 Control of Higher-Order Dynamical Systems 124

Appendices **126**
A Aggregator-Mixer Coupling Examples 126
A.1 Multilinear Coupling 126
A.2 Polynomial Coupling 127

A.3 Homogeneous Polynomial Coupling 127
A.4 Trigonometric Coupling 128
B Additional Derivations 130
B.1 Proof of Lemma 4.20 130
B.2 Proof of Proposition 4.22 130
B.3 Proof of Proposition 4.29 131
C Numerical Validation 133
C.1 Hypergraph Benchmark Sets 133
C.2 Reduced Dynamics Versus Full System 134

List of Figures

2.1 A 3-uniform hypergraph consisting of a single hyperedge. 12

2.2 A graph on three vertices with all three pairwise edges present. 12

2.3 Enron-email hypergraph structure and recovery results 21

2.4 Enron-email hypergraph recovery comparison 22

2.5 Email-EU hypergraph statistics and recovery results 22

2.6 Email-EU hypergraph recovery comparison 23

2.7 NDC-classes hypergraph statistics and recovery results 23

2.8 NDC-classes hypergraph recovery comparison 24

2.9 Contact-High-School hypergraph statistics and recovery results 24

2.10 Contact-High-School hypergraph recovery comparison 25

2.11 Contact-Primary-School hypergraph statistics and recovery results 25

2.12 Contact-Primary-School hypergraph recovery comparison 26

3.1 Spectral shift and stability under network coupling 36

3.2 Stable diffusively coupled Sprott systems on a 4-node network 53

3.3 Unstable diffusively coupled Sprott systems above critical coupling 54

3.4 Stabilization of signless-diffusive Sprott network dynamics 55

3.5 Instability and toroidal-like dynamics in signless Sprott network 56

3.6 Stable switched signless-diffusive network dynamics 57

3.7 Bidirectional graph on a set of four nodes. 57

3.8 Non-positive divergence graphs 58
3.9 Instability of switched diffusively coupled network system 59

4.1 A 3-uniform undirected hypergraph on four nodes 71
4.2 The B-arc set $B_{\text{arc}}(e_1)$ associated with the hyperedge $e_1 = \{2, 3, 4\}$ 71
4.3 Visibility hierarchy 84
4.4 Nonlinear distinguishability for Pair in Table C.1 115
4.5 Dynamical graph surrogacy test 117

C.1 Reduction validation across regimes 134

List of Tables

4.1 Coefficient comparison for the pair of hypergraphs in Table C.1. 114

4.2 Summary of the graph-surrogacy experiments. 116

A.1 Example of multi-index exponents for homogeneous polynomial coupling. . . 128

C.1 Pair of directed weighted hypergraphs $\mathcal{H}_A$ and $\mathcal{H}_B$ used in Figure 4.4 133

C.2 Directed weighted hypergraph $\mathcal{H}$. 133

List of Appendices

Appendix A: Aggregator-Mixer Coupling Examples 126

Appendix B: Additional Derivations 130

Appendix C: Numerical Validation 133

Abstract

This dissertation studies how interaction structure influences the behavior of network dynamical systems, and more fundamentally which aspects of that structure are dynamically observable. While complex systems are often modeled through underlying interaction networks or hypergraphs, the relationship between structure and dynamics is not direct in the sense that different analytical frameworks reveal different structural projections.

First, we study the inverse problem of reconstructing higher-order interaction structure from pairwise observations. We show that such reconstruction is fundamentally non-unique, establishing intrinsic limitations on structural inference from graph data. Next, we analyze network dynamical systems on graphs and show that, in the linear regime, structural effects are mediated through coupling operators and their associated spectral and degree-based representations. We further identify intrinsic obstructions to coupling-induced stabilization. Finally, extending these ideas to reaction-diffusion systems on directed hypergraphs, we develop a weakly nonlinear reduction framework for pattern formation near bifurcation. We show that the resulting nonlinear dynamics depend not on the full higher-order interaction structure, but on specific projected quantities, termed *packing effects*, which govern pattern selection and saturation. This leads to a characterization of the notion of *dynamical graph surrogacy*, under which higher-order interactions become dynamically indistinguishable from pairwise ones.

Chapter 1

Introduction

1.1 Motivation

Networked dynamical systems are often understood through the structure of interactions between their components. In this view, the underlying network or hypergraph is assumed to encode the essential information governing system behavior. However, this perspective raises a fundamental question:

To what extent is interaction structure actually visible through dynamics?

This dissertation shows that the relationship between structure and dynamics is not direct. Rather than being fully observable, interaction structure is revealed only through specific projections determined by the analytical framework used to study the system. Different analytical methods expose different representations of structure, and certain higher-order effects may remain dynamically invisible under particular regimes or approximations.

These questions are especially relevant because many modern systems are only partially observable, and they involve interactions that are fundamentally higher-order. Examples include biological regulation, ecological communities, social contagion, power grids, and distributed multi-agent systems. In such settings, interaction structure is often inferred indi-

rectly through data, stability properties, synchronization behavior, or emergent patterns. Understanding which aspects of structure are dynamically visible is therefore essential for inference, modeling, and control in complex interacting systems.

1.2 Structural Effects and Observability

In this dissertation, *structural effects* refer to the influence of interaction structure on system dynamics, as mediated by the analytical framework used to study the system.

Depending on the setting, structure becomes visible through different mathematical objects:

- In (static graph) network dynamical systems, structure may appear through spectral properties of coupling operators.
- In switching systems over network, it may appear through Lyapunov-compatible degree conditions.
- In nonlinear reaction-diffusion systems on directed hypergraphs, it appears through the reduced dynamics coefficients governing pattern formation near bifurcation.

A central theme of this dissertation is therefore that structure does not possess a single universal dynamical representation. Rather, the observable components of structure depend on the analytical lens used to probe the system.

1.3 Overview of the Approach

The dissertation develops this perspective across three interconnected directions.

1. **Static data and reconstruction.** We examine whether higher-order interaction structure can be recovered from pairwise observations, and study the limitations and non-uniqueness inherent in this reconstruction problem.

2. **Network dynamical systems.** We analyze how pairwise interaction structure influences stability in coupled network systems, both for static and switching topologies.

3. **Hypergraph dynamical systems and nonlinear reduction.** We study how higher-order structure influences nonlinear behavior near bifurcation in reaction-diffusion systems on directed hypergraphs.

1.4 Contributions

The main contributions of this dissertation are as follows.

Hypergraph reconstruction via optimization and clique-contraction

We formulate the hypergraph reconstruction problem from pairwise data as a regularized optimization problem, and we introduce deterministic and probabilistic clique-contraction frameworks for computing sparse hypergraph representations consistent with observed graph data. These methods provide constructive procedures for identifying candidate higher-order interaction structures from pairwise observations. At the same time, we show that hypergraph reconstruction is in generals non-unique. More specifically, multiple distinct hypergraphs may induce the same pairwise structure. This establishes a fundamental limitation of static reconstruction, and it highlights the role of modeling assumptions in selecting among admissible higher-order representations.

Operator-level characterization of structural effects in network dynamics

For network dynamical systems on graphs, we show that structural effects are mediated through coupling operators, including spectral and degree-based representations. We analyze both coupling-induced stabilization and destabilization, and we identify intrinsic structural and functional obstructions to stabilization.

Nonlinear reduction framework for hypergraph dynamical systems

We develop a systematic framework for analyzing reaction-diffusion systems on directed hypergraphs via weakly nonlinear reduction near bifurcation. This framework extends classical pattern formation theory to higher-order interaction structures.

Packing effects and nonlinear structural observability

We identify packing effects as dynamically relevant projections of higher-order structure governing nonlinear behavior near bifurcation. We show that systems with identical linear structure may nevertheless exhibit different nonlinear dynamics, therefore establishing a form of structural nonlinear distinguishability.

Dynamic graph surrogacy and reduction of higher-order interactions

We introduce and characterize the notion of dynamical graph surrogacy as the condition under which a hypergraph-coupled system is dynamically equivalent to a graph up to a given order of approximation. This provides a precise criterion for when higher-order interactions can be reduced to pairwise ones.

1.5 Organization of the Dissertation

Chapter 2 studies hypergraph reconstruction from pairwise observations. Chapter 3 develops a stability theory for network dynamical systems on graphs, including static and switching interaction structures. Chapter 4 develops a nonlinear reduction framework for pattern formation in reaction-diffusion systems on directed hypergraphs. Finally, Chapter 5 concludes with a synthesis of the results and directions for future work.

Chapter 2

Hypergraph Reconstruction and the Limits of Pairwise Data

2.1 Motivation

Many complex systems are observed through pairwise relationships even when their underlying interactions are not fundamentally pairwise [5, 7, 68]. In social systems, an observed edge may indicate that two individuals participated in the same group event [5]. In biological systems, pairwise associations may arise from a shared biochemical complex or pathway [31]. In communication systems, pairwise links may reflect participation in a larger broadcast or group exchange. Thus, a graph may represent only a projection of a richer higher-order interaction structure [11].

Hypergraphs provide a natural language for representing such multiway interactions [8, 11]. In a hypergraph, an edge may connect more than two nodes, thus encoding a group interaction directly rather than decomposing it into pairwise relations. However, in many applications the available data are already graph-valued. This raises a basic inverse problem:

Given a graph $\mathcal{G}$, can one reconstruct the latent hypergraph $\mathcal{H}$ whose projection is $\mathcal{G}$?

This chapter examines that question. The main point is not that hypergraph reconstruc-

tion is impossible, but that it is fundamentally non-unique without additional assumptions. Multiple distinct hypergraphs may induce the same graph under standard projection procedures such as clique expansion [74, 2]. Consequently, pairwise data alone do not uniquely determine higher-order structure.

This observation plays an important role in the dissertation. It motivates the later shift from static reconstruction to dynamical analysis. If higher-order structure cannot be uniquely recovered from pairwise observations, then a natural next question is whether dynamics can reveal additional structural information. Chapters 3 and Chapter 4 pursue this question from two different directions; first through stability analysis of pairwise network systems, and then through nonlinear reduction for dynamical systems on directed hypergraph.

2.2 Hypergraphs and Incidence Structure

Hypergraphs. Let V be a finite set. A *hypergraph* $\mathcal{H}$ is a pair (V, E), where $E \subseteq \mathcal{P}(V) \setminus \{\emptyset\}$, with $\mathcal{P}(V)$ denoting the power set of V. The elements of V are called *vertices*, and the elements of E are called *hyperedges*. Each hyperedge is thus a subset of vertices allowing interactions among more than two nodes. We assume throughout that hyperedges do not contain repeated vertices (i.e., hyperloops are not allowed).

Weighted hypergraphs. A *weighted hypergraph* is a hypergraph equipped with a weight function

$$w : E \to (0, \infty) \tag{2.1}$$

which assigns a positive weight $w(e)$ to each hyperedge $e \in E$.

Degrees. The *degree* of a vertex $v \in V$ is defined as

$$d(v) = \sum_{\substack{e \in E \\ v \in e}} w(e) \tag{2.2}$$

It captures the total weight of hyperedges incident to v. The *degree* of a hyperedge $e \in E$ is defined as its cardinality:

$$d(e) = |e| \tag{2.3}$$

A hypergraph is said to be *k-uniform* if all hyperedges have the same cardinality k, i.e., $d(e) = k$ for all $e \in E$.

Incidence structure. The vertex–hyperedge incidence matrix $H \in \mathbb{R}^{|V| \times |E|}$ is defined by

$$H(v, e) = \begin{cases} 1, & \text{if } v \in e, \\ 0, & \text{otherwise.} \end{cases} \tag{2.4}$$

Using this notation, the vertex and hyperedge degrees can be written compactly as

$$d(v) = \sum_{e \in E} w(e)\, H(v, e), \qquad \text{and} \qquad d(e) = \sum_{v \in V} H(v, e). \tag{2.5}$$

Degree and weight matrices. We define the following diagonal matrices:

- $D_v \in \mathbb{R}^{|V| \times |V|}$: vertex degree matrix, with diagonal entries $d(v)$,
- $D_e \in \mathbb{R}^{|E| \times |E|}$: hyperedge degree matrix, with diagonal entries $d(e)$,
- $W \in \mathbb{R}^{|E| \times |E|}$: weight matrix, with diagonal entries $w(e)$.

Equivalently, if $\mathbf{1}$ denotes the vector of all ones of appropriate dimension, then the vertex degree vector can be written as

$$d = HW\mathbf{1} \tag{2.6}$$

and the corresponding diagonal degree matrix is

$$D_v = \mathrm{diag}(HW\mathbf{1}) \tag{2.7}$$

This incidence-based representation is useful because it allows one to express certain graph projections of the hypergraph in matrix form. In particular, the matrix $HWH^\top$ encodes weighted co-membership of vertices in hyperedges. Its off-diagonal entry (i, j) records the total weight of hyperedges containing both i and j, while the diagonal entries recover the vertex degrees. It follows that the matrix $HWH^\top - D_v$ has zero diagonal entries and off-diagonal entries corresponding to pairwise co-membership weights. This matrix is the algebraic object underlying the standard clique expansion of a hypergraph.

2.3 Clique Expansion as a Forward Map

The most common way to convert a hypergraph into a graph is via *clique expansion*. Given a hypergraph $\mathcal{H} = (V, E)$, the standard clique expansion constructs a graph $\mathcal{H}^{\mathrm{cs}} = (V, E^{\mathrm{cs}} \subset V)$ by replacing each hyperedge with a clique on the same set of vertices. More specifically, for a hyperedge $e = \{i_1, \ldots, i_k\}$, edges are introduced between all pairs of vertices in e

$$E^{\mathrm{cs}} = \{(u, v) : u, v \in e,\ e \in E\} \tag{2.8}$$

Thus, the vertices of each hyperedge form a complete subgraph in the expanded graph. Throughout this work, the term *clique expansion* refers to this standard weighted construction.

When the hypergraph is weighted, the weight of an edge (i, j) in the clique expansion is defined as the total weight of all hyperedges containing both i and j. This corresponds to

the *standard clique expansion*, for which

$$w^{\text{cs}}(u, v) = \sum_{e \in E} h(u, e)\, h(v, e)\, w(e) \tag{2.9}$$

The corresponding vertex degree is

$$d^{\text{cs}}(u) = \sum_{e \in E} h(u, e)\, (d(e) - 1)\, w(e) \tag{2.10}$$

In matrix form, the weighted clique expansion has adjacency matrix

$$A^{\text{cs}} = HWH^{\top} - \text{diag}(HW\mathbf{1}) \tag{2.11}$$

and associated normalized Laplacian

$$L^{\text{cs}} = I - (D_v^c)^{-1/2} A^{\text{cs}} (D_v^c)^{-1/2} \tag{2.12}$$

This construction defines a forward map

$$(H, W) \;\mapsto\; A^{\text{cs}} \tag{2.13}$$

which is straightforward to compute but *not injective*. Distinct hypergraphs may yield the same clique expansion. For example, a triangle in a graph may arise either from a single three-node hyperedge as in Figure 2.1, or from three pairwise edges as in Figure 2.2. Both constructions produce the same graph but correspond to different underlying interaction mechanisms.

This many-to-one character of clique expansion underlies the reconstruction problem. While the forward map from hypergraphs to graphs is well-defined, the inverse problem of recovering a hypergraph from its clique expansion is in general ill-posed.

2.4 The Hypergraph Reconstruction Problem

Suppose we are given observed pairwise data encoded by a graph $\mathcal{G} = (V, E_G)$ with adjacency matrix A, and further assume that the observed data is only the *projection* of an intrinsic latent multiway data structure encoded by an unknown hypergraph $\mathcal{H} = (H, W)$. The hypergraph reconstruction problem consists in recovering the weighted hypergraph $\mathcal{H}$, equivalently specified by its incidence matrix H and weight matrix W, such that its clique expansion is consistent with the observed graph $\mathcal{G}$.

We define the natural condition of exact reconstruction as follows

$$HWH^\top - D_v = A, \tag{2.14}$$

where D_v is given in (2.7). We address this problem by formulating it into the following mixed-integer nonlinear-program

$$\min_{H,W} \|HWH^\top - D_v - A\|, \tag{2.15}$$

subject to

$$H_{ij} \in \{0, 1\}, \qquad W \text{ is a diagonal matrix with } W_{ii} > 0. \tag{2.16}$$

To ensure structural compatibility between the reconstructed hypergraph and the observed graph, we impose the support constraint

$$\mathcal{B}(HWH^\top - D_v) = \mathcal{B}(A) \tag{2.17}$$

where $\mathcal{B}$ denotes the binarization operator defined by

$$\mathcal{B}(M)_{ij} = \begin{cases} 1, & M_{ij} \neq 0, \\ 0, & \text{otherwise} \end{cases} \tag{2.18}$$

This condition requires that the reconstructed hypergraph induce precisely the same pairwise connectivity pattern as the observed graph.

Definition 2.1. *A hypergraph $\mathcal{H} = (H, W)$ is said to be a (structural)* recovery *of the graph $\mathcal{G}$ if*

$$\mathcal{B}(HWH^\top - D_v) = \mathcal{B}(A). \tag{2.19}$$

Definition 2.2. *A recovery $\mathcal{H} = (H, W)$ is said to be* nontrivial *if it contains at least one hyperedge of size greater than or equal to three.*

Definition 2.3. *A recovery $\mathcal{H} = (H, W)$ is said to be* exact *if it further satisfies*

$$\|HWH^\top - D_v - A\| = 0. \tag{2.20}$$

The hypergraph reconstruction problem is therefore inherently non-unique. Distinct hypergraphs may yield the same clique expansion. The central questions are whether a nontrivial recovery exists, whether it is unique, and how to select among multiple admissible reconstructions.

2.5 Ill-Posedness of the Reconstruction Problem

The hypergraph reconstruction problem is inherently ill-posed, as the observed graph does not uniquely determine the underlying hypergraph. In particular, distinct hypergraph structures may yield identical clique expansions.

A simple illustration is given by a triangle graph on three nodes. This observed graph admits multiple hypergraph realizations. One possibility is that it arises from three pairwise hyperedges as in Figure 2.2,

$$\{1, 2\}, \quad \{1, 3\}, \quad \{2, 3\}. \tag{2.21}$$

Alternatively, it may arise from a single higher-order hyperedge as in Figure 2.1,

$$\{1, 2, 3\}. \tag{2.22}$$

Both constructions produce the same clique expansion, and therefore the observed graph alone does not reveal whether the interaction is genuinely higher-order or merely a collection of pairwise interactions.

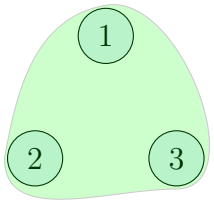

Figure 2.1: A 3-uniform hypergraph consisting of a single hyperedge on vertices 1, 2, and 3.

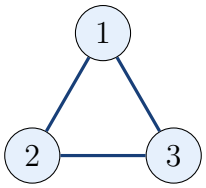

Figure 2.2: A graph on three vertices with all three pairwise edges present forming a triangle.

This ambiguity becomes more pronounced in larger graphs. Any clique of size greater than or equal to three may be interpreted as a higher-order interaction, yet cliques can overlap, carry different weights, and admit multiple decompositions into hyperedges. Consequently, the reconstruction problem is not only computationally challenging, but also *structurally underdetermined*.

It is important to distinguish these two aspects. Computational complexity concerns the difficulty of finding a solution, whereas ill-posedness concerns the lack of uniqueness of the solution itself. Hypergraph reconstruction from *static graph data* exhibits both features: clique-based methods are combinatorially expensive, and the inverse problem admits multiple feasible reconstructions. This dual difficulty is a central theme in the study of hypergraph reconstruction.

2.5.1 Regularization by Sparsity

Because the inverse problem is non-unique, we must impose additional selection criteria in order to identify a preferred solution. In this work, we adopt a sparsity-based regularization strategy, which favors hypergraph reconstructions with fewer hyperedges, and in particular discourages the introduction of higher-order interactions unless supported by the data.

This leads to our formulation of the following regularized optimization problem:

$$\min_{H,W,m} \ \|HWH^\top - D_v - A\| + \lambda m, \tag{2.23}$$

subject to

$$m \in \mathbb{N}^*, \quad H_{ij} \in \{0,1\}, \quad W \text{ diagonal matrix with } W_{ii} > 0, \tag{2.24}$$

and

$$\mathcal{B}(HWH^\top - D_v) = \mathcal{B}(A). \tag{2.25}$$

Here, m denotes the number of hyperedges and $\lambda > 0$ is a *regularization parameter controlling the trade-off between fidelity to the observed graph and model complexity.* Larger values of λ promote sparser reconstructions.

This formulation provides a principled mechanism to select among multiple admissible hypergraph representations. It is important to stress that sparsity does not resolve the intrinsic ambiguity of the inverse problem. Rather, it introduces an explicit modeling assumption that biases the solution toward simpler structures. In this sense, the reconstruction problem is naturally reformulated as a model selection problem.

This perspective is central to the present work, namely the reconstructed higher-order structure is determined not only by the observed pairwise data, but also by the regularization principles used to resolve non-uniqueness.

2.5.2 Clique-Contraction as a Constructive Heuristic

Given the ill-posedness of the hypergraph reconstruction problem, it is natural to seek constructive procedures that produce admissible solutions consistent with the observed graph. In this work, we introduce a method called *clique-contraction*, which provides an explicit mechanism for constructing such solutions.

The central idea is to iteratively identify higher-order structures in the form of cliques and reinterpret them as hyperedges. At each step, a maximal clique is selected, assigned a weight, and its contribution is removed from the graph. This process is repeated until no clique of size greater than or equal to three remains, after which the residual edges are interpreted as pairwise interactions. A schematic version of the procedure is given in Algorithm 1.

Algorithm 1: Clique–Contraction (Skeleton)

Input: Adjacency matrix A of a simple and undirected graph $\mathcal{G}$
Output: Hypergraph $\mathcal{H} = (H, W)$

```
while clique number of G is at least 3 do
    Selection step
    Filtering step
end
Collection step
```

In this work, we develop both a deterministic version of this procedure and a probabilistic variant (see section 2.7) in which the clique selection step is guided by a score combining clique strength and centrality. These variants provide a means of exploring different admissible reconstructions.

It is important to note that, the role of clique-contraction is not to resolve the non-uniqueness of the inverse problem, but to construct a hypergraph whose clique expansion is consistent with the observed graph. In particular, the procedure yields an exact recovery in the sense of Definition 2.3, as the resulting hypergraph satisfies (2.20).

Meanwhile, different choices in the clique selection step may lead to distinct hypergraphs with identical clique expansions. Thus, clique-contraction provides a constructive mecha-

nism for generating feasible solutions, while making explicit the multiplicity of admissible reconstructions inherent to the problem.

2.6 Consistency of Clique Contraction

The clique-contraction algorithm (Deterministic and Probabilistic) has a useful consistency property, namely the hypergraph it constructs reproduces the off-diagonal entries of the observed adjacency matrix. More specifically we have the following proposition.

Proposition 2.4. *Let $\mathcal{G}$ be a graph with clique number at least three, and whose adjacency matrix is non-negative valued, then there exists a non-trivial exact recovery of $\mathcal{G}$.*

The proof of Proposition 2.4 is a direct corollary of the following lemma.

Lemma 2.5. *Let H, W be the output of the* Clique-Contraction *algorithm operating on an adjacency matrix A, then the matrices HWH^T and A coincide on the off-diagonal.*

Proof. We assume that the clique number $\omega(A)$ of the graph induced by A is at least 2, since the case $\omega(A) = 1$ is vacuous hence not interesting.

The proof proceeds by induction on the number n of higher-order maximal cliques to delete from A until the resulting subgraph has clique number at most 2. Note that this is precisely the number of iterations until the algorithm terminates.

– Order $n = 0 : H$ is nothing but the incidence matrix of A, and W is the corresponding weight matrix on the edges of A.

for $i \neq j$ we have

$$\begin{aligned}(HWH^T)_{ij} &= \sum_{l=1}^{m} H_{ie_l} H_{e_l j} W_{e_l e_l} \qquad \text{where m = number of edges in A.} \\ &= W_{e_l e_l} \mathbb{1}_{\{A_{ij} \neq 0\}} \\ &= A_{ij}\end{aligned} \tag{2.26}$$

– Order $n = 1$: There is exactly one higher-order hyperedge in the graph induced by A.

for $i \neq j$ we have the following, where E_0 is the unique hyperedge in H

$$\begin{aligned}(HWH^T)_{ij} &= H_{iE_0}H_{jE_0}W_{E_0E_0} + \sum_{l=1}^{m} H_{ie_l}H_{e_lj}W_{e_le_l} \\ &= W_{E_0E_0}\mathbb{1}_{\{(i,j)\in E_0\}} + (A_{ij} - W_{E_0E_0})\mathbb{1}_{\{(i,j)\in\bigcup_{l=1}^{m} e_l\}} \\ &= A_{ij}\end{aligned} \tag{2.27}$$

Induction Hypothesis (IH): assume the result is true at order $n = k > 1$. That is if we delete k higher-order maximal cliques from an integer adjacency matrix $\tilde{A}$ before the resulting subgraph has clique number at most 2, then the matrices $\tilde{H}\tilde{W}\tilde{H}^T$ and $\tilde{A}$ coincide on the off-diagonal.

– Order $n = k + 1$: Let $\tilde{H}$ be the matrix obtained from H by dropping the first column corresponding to the E_{k+1}-st hyperedge. $\tilde{W}$ the submatrix obtained from W by dropping the $(1, 1)$ row-column pair, and finally let $\tilde{A}$ be the matrix obtained from A by decreasing by $W_{E_{k+1}E_{k+1}}$ only the (i, j) entries for which $(i, j) \in E_{k+1}$. The matrix $\tilde{A}$ satisfies the premises of (IH), hence we have:

for $i \neq j$

$$\begin{aligned}(HWH^T)_{ij} &= H_{iE_{k+1}}H_{jE_{k+1}}W_{E_{k+1}E_{k+1}} + (\tilde{H}\tilde{W}\tilde{H}^T)_{ij} \\ &= W_{E_{k+1}E_{k+1}}\mathbb{1}_{\{(i,j)\in E_{k+1}\}} + \tilde{A}_{ij} \\ &= A_{ij}\end{aligned} \tag{2.28}$$

By the principle of mathematical induction, we conclude that regardless of the number of iterations it takes before the algorithm terminates, the resulting output matrices H and W have the property that the matrices HWH^T and A coincide on the off-diagonal. ■

2.7 Deterministic and Probabilistic Selection

A central source of ambiguity in the clique-contraction procedure lies in the clique selection step. When multiple candidate cliques are available, different choices may lead to distinct hypergraph reconstructions. Thus, the reconstruction process requires a principled rule for selecting among admissible cliques.

2.7.1 Deterministic Selection

A natural deterministic strategy is to select a maximum clique at each iteration. This approach prioritizes large higher-order interactions and typically yields sparse reconstructions. However, it is inherently greedy and may be sensitive to local choices, as early selections can significantly influence subsequent steps of the algorithm. This leads to the *deterministic* Clique-Contraction described in Algorithm 2 below.

Algorithm 2: Clique-Contraction (Deterministic)

Input: Adjacency matrix A of a simple and undirected graph $\mathcal{G}$
Output: Hypergraph $\mathcal{H} = (H, W)$

while *clique number of* $\mathcal{G}$ *is at least* 3 **do**
  choose a maximum clique M
  $w \leftarrow \min\{A_{ij} \mid (i,j) \in M\}$
  for $(i,j) \in M$ **do**
    $A_{ij} \leftarrow A_{ij} - w$
  end
end
$H \leftarrow \{\text{all the remaining edges of } \mathcal{G}\} \cup \{\text{all hyperedges from step 2}\}$
$W \leftarrow diag(\{\text{weights of all the remaining edges of } \mathcal{G}\} \cup \{\text{all w's from step 3}\})$

2.7.2 Probabilistic Selection

To mitigate the sensitivity of deterministic selection, we introduce a probabilistic variant of the clique contraction procedure. Instead of selecting a clique deterministically, this approach samples from a probability distribution defined over candidate cliques at each iteration.

This modification is motivated by the combinatorial complexity of the reconstruction problem. If the algorithm requires N iterations and there are n_k candidate cliques at step k, then the total number of possible reconstructions scales as $\prod_{k=1}^{N} n_k$, rendering exhaustive search computationally infeasible. The probabilistic approach provides a tractable alternative by exploring the space of admissible reconstructions in a structured manner.This leads to the probabilistic Clique-Contraction described in Algorithm 3 below.

Algorithm 3: Clique-Contraction (Probabilistic)

Input: Adjacency matrix A of a simple and undirected graph $\mathcal{G}$
Sparsity level λ
Output: Hypergraph $\mathcal{H} = (H, W)$

while *clique number of* $\mathcal{G}$ *is at least* 3 **do**
  enumerate the maximum cliques $\mathcal{M}_k := \{M_{i_1}, ..., M_{i_k}\}$
  for $M_{i_j} \in \mathcal{M}_k$ **do**
    $\sigma(M_{i_j}) \leftarrow \frac{1}{\lambda} S_{i_j} + (1 - \frac{1}{\lambda}) \frac{1}{1+C_{i_j}^2}$
  end
  normalize σ to define the probability distribution $\mathbb{P}_k$ over $\mathcal{M}_k$
  sample a maximum clique $M \sim \mathbb{P}_k$
  $w \leftarrow \min\{A_{ij} \mid (i,j) \in M\}$
  for $(i,j) \in M$ **do**
    $A_{ij} \leftarrow A_{ij} - w$
  end
end
$H \leftarrow$ {all the remaining edges of $\mathcal{G}$} $\cup$ {all hyperedges from step 7}
$W \leftarrow diag($ {weights of all the remaining edges of $\mathcal{G}$} $\cup$ {all w's from step 8}$)$

2.7.3 Clique Score and Selection Rule

At each iteration k, let $\mathcal{M}_k$ denote the set of candidate cliques. To guide the selection process, we assign to each clique $M \in \mathcal{M}_k$ a score of the form

$$\sigma(M) = \alpha S(M) + (1 - \alpha) \frac{1}{1 + C(M)^2}, \qquad \alpha \in [0, 1], \tag{2.29}$$

where $S(M)$ denotes a measure of clique strength and $C(M)$ denotes a measure of clique centrality.

The clique strength $S(M)$ captures the internal cohesion of the clique, for example through aggregate edge weights or similarity-based measures such as Jaccard or Adamic–Adar indices. Empirical studies (e.g., [7, 6]) suggest that stronger ties correlate with the presence of higher-order interactions, motivating the inclusion of this term.

The centrality term $C(M)$ is computed in the clique graph, whose vertices correspond to cliques and where edges connect cliques sharing at least one edge. High-centrality cliques play a structural role in maintaining connectivity. Removing them may fragment the graph and lead to denser reconstructions. The inverse dependence in (2.29) therefore penalizes such selections.

The resulting score induces a probability distribution $\mathbb{P}_k$ over $\mathcal{M}_k$, obtained by normalization. The selection step then consists of sampling a clique according to $\mathbb{P}_k$. Alternatively, one could also consider some measure of hypergraph structural similarity [67] to inform the selection step.

2.7.4 Regularization and Trade-Off

The parameter α governs the trade-off between strength-driven and centrality-driven selection. In the context of the sparsity-regularized formulation, we set

$$\alpha = \frac{1}{\lambda}, \tag{2.30}$$

where λ is the regularization parameter introduced previously.

For large values of λ, the selection process emphasizes centrality, favoring cliques whose removal preserves global structure and leads to sparser reconstructions. Conversely, for λ close to one, the algorithm prioritizes clique strength, selecting cliques that are more likely to correspond to genuine higher-order interactions, potentially at the cost of increased model complexity.

2.7.5 Interpretation

This framework highlights an intrinsic trade-off between reconstruction accuracy and sparsity. Strong cliques provide evidence for higher-order interactions, while central cliques influence the global structure of the reconstruction. The necessity of such a selection rule further reinforces the underdetermined nature of the inverse problem. That is different choices lead to different, yet equally admissible hypergraph representations.

2.8 Empirical Illustrations

We have evaluated the reconstruction framework described above on several real-world datasets from the repository [7], including email networks, drug-class networks, and contact networks. These systems provide natural examples of higher-order interactions. Emails may involve multiple recipients, drugs may belong to multiple functional classes, and contact events may occur among groups of individuals.

In these studies, hypergraph structures were reconstructed from clique-expanded graph representations, and the recovered hypergraphs were compared to the original data. The analysis included comparisons of hyperedge-size distributions, adjacency matrices, and incidence structures, as well as statistics quantifying the agreement between original and reconstructed hyperedges.

These empirical results illustrate that pairwise projections can retain partial signatures of higher-order structure. However, the reconstruction remains inherently imperfect and non-unique. In particular, different hypergraphs may reproduce the same pairwise adjacency while differing significantly in hyperedge composition and size distribution. This behavior is consistent with the theoretical ambiguity established earlier.

2.8.1 Email networks

Email networks (email-Enron[32] and email-Eu[56]): Nodes are email addresses and a hyperedge consisting of all recipient addresses on an email along with the sender's address. email-Enron spans most of the duration of a company's lifetime, and email-Eu spans over 2 years of communication.

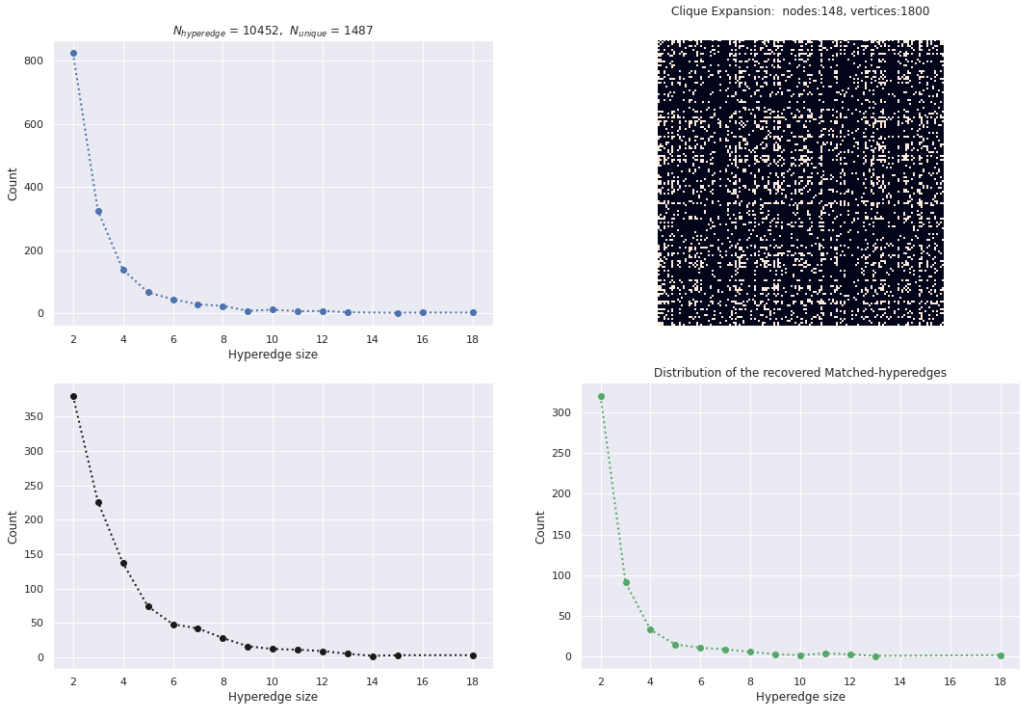

Figure 2.3: Enron-email: (Top left) distribution of hyperedge sizes in the initial hypergraph. (Top right) adjacency matrix of the standard clique expansion of the initial hypergraph. (Bottom left) distribution of the hyperedge sizes in the recovered hypergraph. (Bottom right) distribution of matched hyperedges. These are the hyperedges in the recovery that are effectively present in the initial hypergraph.

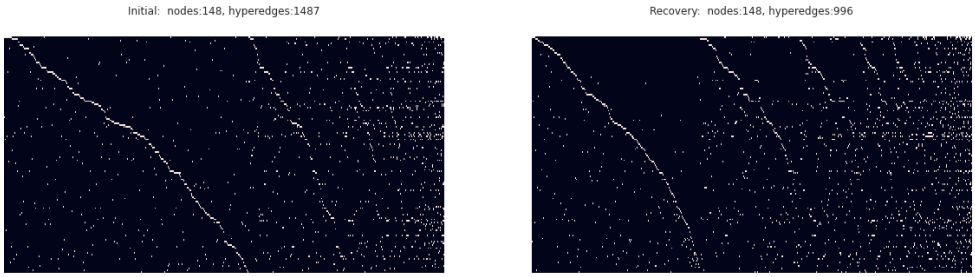

Figure 2.4: Enron-email recovery: (Left) incidence matrix of the initial hypergraph. (Right) incidence matrix of the recovered hypergraph.

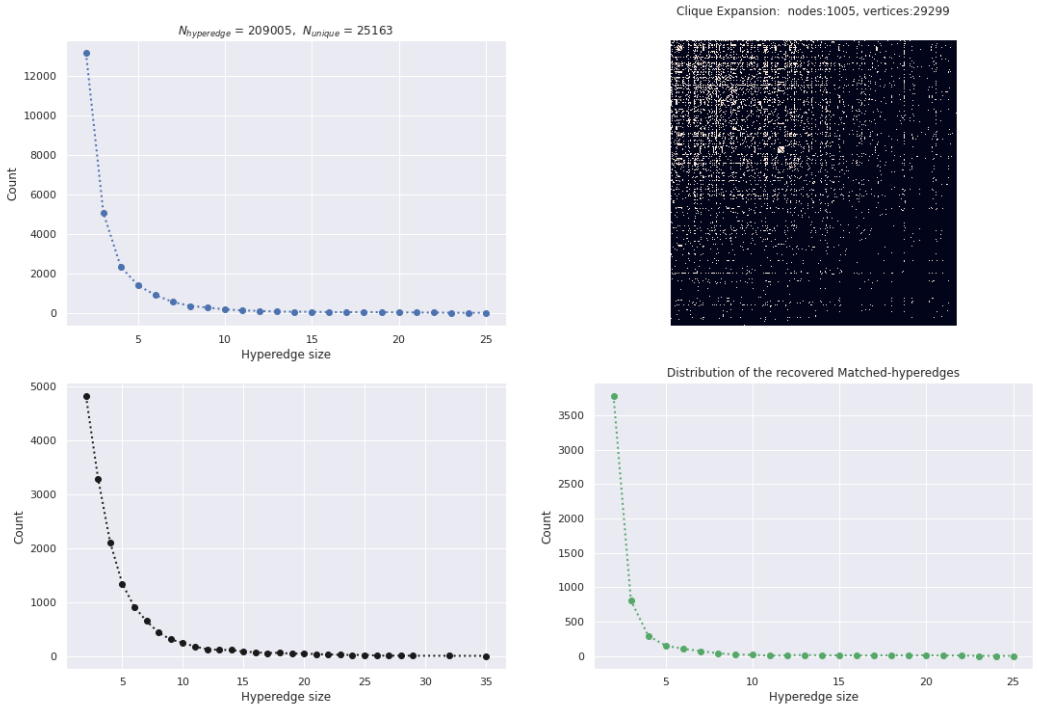

Figure 2.5: Email-EU: (Top left) distribution of hyperedge sizes in the initial hypergraph. (Top right) adjacency matrix of the standard clique expansion of the initial hypergraph. (Bottom left) distribution of hyperedge sizes in the recovered hypergraph. (Bottom right) distribution of matched hyperedges. These are hyperedges in the recovery that are effectively present in the initial hypergraph.

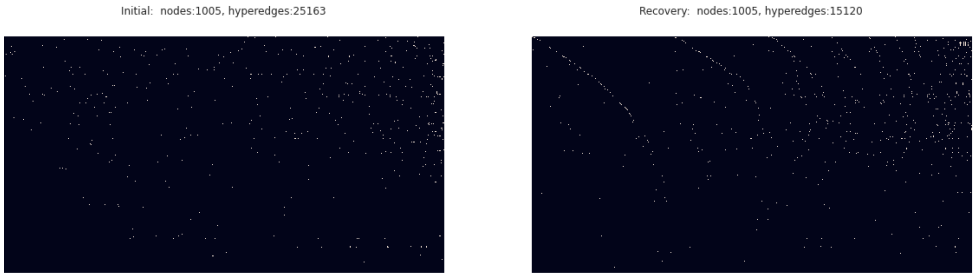

Figure 2.6: email-EU recovery: (Left) incidence matrix of the initial hypergraph. (Right) incidence matrix of the recovered hypergraph.

2.8.2 Drug-class Networks

Drug networks from the National Drug Code Directory (NDCclasses) Nodes are class labels (e.g. serotonin reuptake inhibitor) and a hyperedge is the set of class labels applied to a drug (all applied at once).

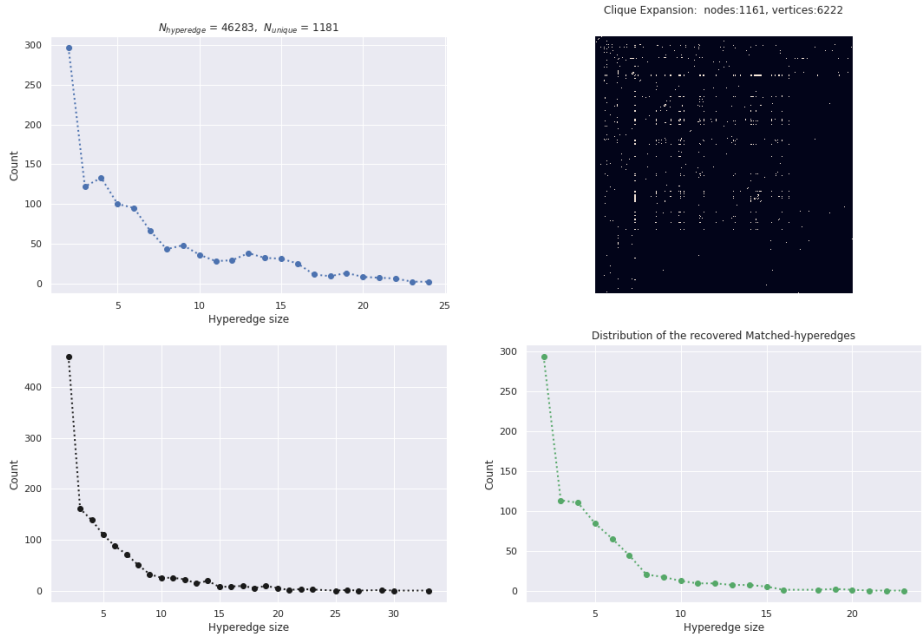

Figure 2.7: NDC-classes: (Top left) distribution of hyperedge sizes in the initial hypergraph. (Top right) adjacency matrix of the standard clique expansion of the initial hypergraph. (Bottom left) distribution of hyperedge sizes in the recovered hypergraph. (Bottom right) distribution of matched hyperedges. These are hyperedges in the recovery that are effectively present in the initial hypergraph.

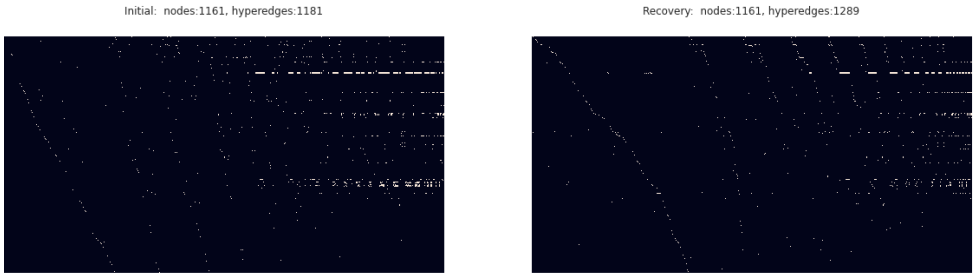

Figure 2.8: NDC-classes recovery: (Left) incidence matrix of the initial hypergraph. (Right) incidence matrix of the recovered hypergraph.

2.8.3 Contact Networks

Contact networks (contact-high-school[42] and contact-primaryschool[65]) Nodes are persons and a hyperedge is a set of persons in close proximity to each other.

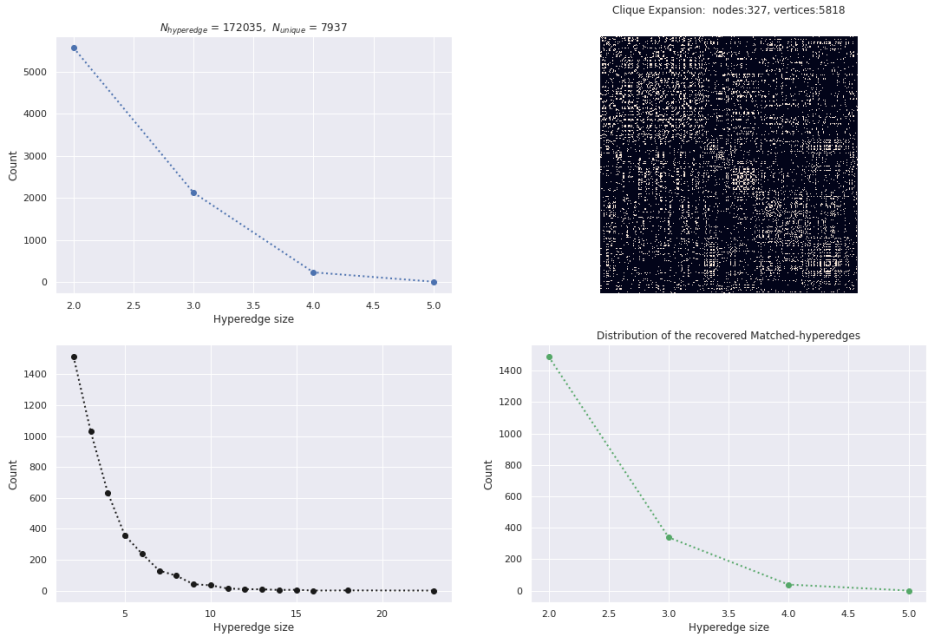

Figure 2.9: Contact-High-School: (Top left) distribution of hyperedge sizes in the initial hypergraph. (Top right) adjacency matrix of the standard clique expansion of the initial hypergraph. (Bottom left) distribution of hyperedge sizes in the recovered hypergraph. (Bottom right) distribution of matched hyperedges. These are hyperedges in the recovery that are effectively present in the initial hypergraph.

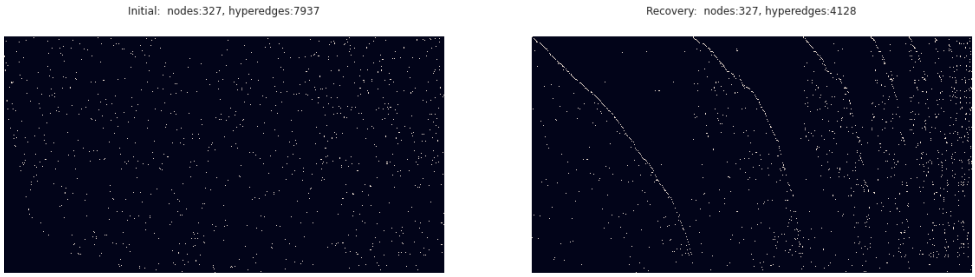

Figure 2.10: Contact-High-School recovery: (Left) incidence matrix of the initial hypergraph. (Right) incidence matrix of the recovered hypergraph.

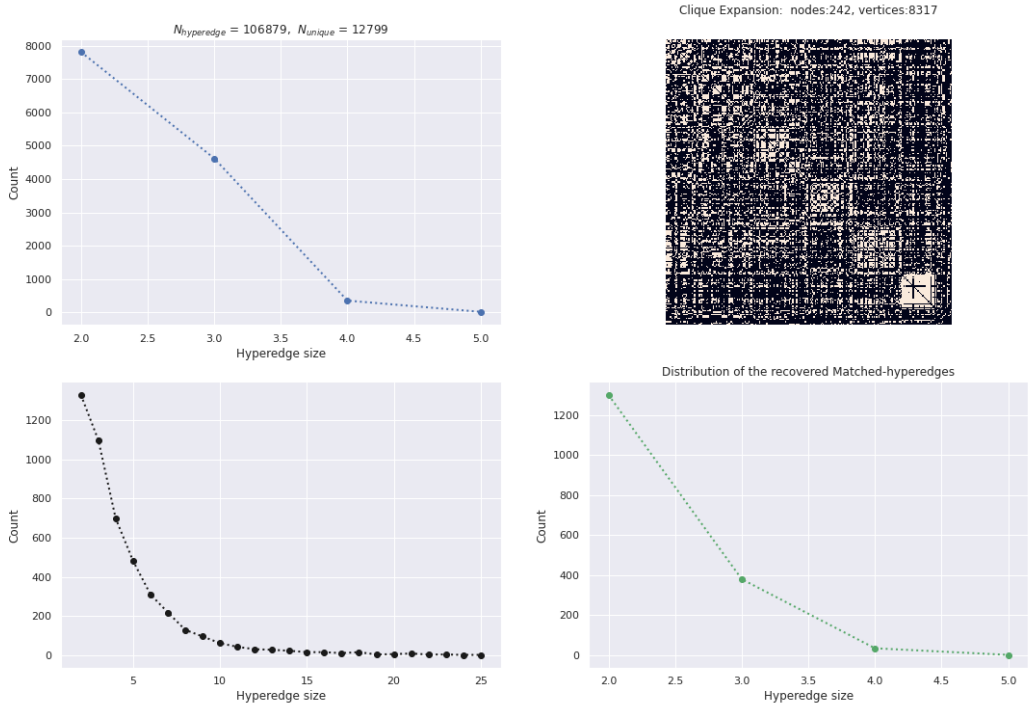

Figure 2.11: Contact-Primary-School: (Top left) distribution of hyperedge sizes in the initial hypergraph. (Top right) adjacentcy matrix of the standard clique expansion of the initial hypergraph. (Bottom left) distribution of the hyperedge sizes in the recovered hypergraph. (Bottom right) distribution of matched hyperedges. These are the hyperedges in the recovery that are effectively present in the initial hypergraph.

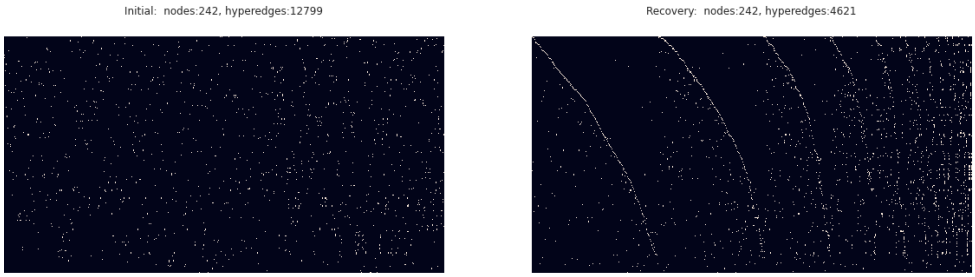

Figure 2.12: Contact-Primary-School recovery: (Left) incidence matrix of the initial hypergraph. (Right) incidence matrix of the recovered hypergraph.

2.9 Implications for Structural Inference

The analysis of the hypergraph reconstruction problem yields several key insights that inform the remainder of this dissertation.

First, pairwise observations are insufficient to uniquely determine higher-order interaction structure. A given graph may be consistent with multiple distinct hypergraphs, reflecting an intrinsic loss of information in pairwise projections.

Second, reconstruction necessarily depends on additional modeling assumptions. In this work, we develop and adopt several such approaches, including sparsity-based regularization, probabilistic priors, and clique-selection strategies as mechanisms for selecting among admissible reconstructions. However, these choices are not determined by the observed pairwise data alone, and instead they reflect external assumptions imposed on the problem.

Third, agreement at the pairwise level does not imply structural correctness. A reconstructed hypergraph may reproduce the same clique expansion as the true system and therefore match all pairwise observations, while differing significantly in its underlying higher-order interactions.

These observations establish that hypergraph reconstruction, which is understood as the recovery of the full interaction structure from pairwise data is in general an ill-posed problem. These limitations motivate a shift in perspective. Rather than attempting to uniquely recover the full hypergraph from static observations, we instead consider the following question:

Which aspects of interaction structure are observable through the dynamics?

This reframing moves the focus from *exact structural recovery* to the identification of *dynamically relevant structure*. In many applications, the primary goal is not to recover the complete interaction structure, but to identify those structural features that determine system behavior.

2.10 Transition to Network Dynamics

The limitations of hypergraph reconstruction motivate a shift from static structural recovery to a dynamical framework. In the next chapter, we examine how graph structure influences the behavior of network dynamical systems. In this setting, the relevant structural object is not a reconstructed hypergraph, but rather a coupling operator derived from the graph. Spectral analysis is used to characterize how this operator modifies the stability properties of the underlying node dynamics, while Lyapunov-based methods provide structural conditions for stability under time-varying interactions including switching.

This shift reframes the central question of the analysis. Instead of asking

Can the full underlying interaction structure be reconstructed?

we instead consider the question

How does interaction structure influence system dynamics?

This transition lays the foundation for the subsequent development. In Chapter 4, we return to higher-order interaction models and show that, within a weakly nonlinear regime, the dynamics depend not on the full hypergraph structure, but only on specific projected quantities. This perspective provides a principled link between structural inference and dynamical behavior.

Chapter 3

Network Stability and Structural Effects in Graph Dynamical Systems

3.1 From Reconstruction to Dynamics

Chapter 2 established that higher-order interaction structure cannot in general be uniquely reconstructed from pairwise observations. A given graph may arise as the clique expansion of multiple distinct hypergraphs, thus implying that static pairwise data alone are insufficient to uniquely determine the underlying interaction structure.

This limitation motivates a shift in perspective. Rather than attempting to reconstruct the full structure directly, we instead examine how interaction structure manifests itself through system dynamics. In network (graph) dynamical systems, the graph is not merely a static object. It enters the equations of motion through coupling operators which can stabilize, destabilize, or otherwise reshape the qualitative behavior of the system.

This chapter develops the pairwise setting as a foundational case. We study diffusively and signless-diffusively coupled network systems and analyze how graph structure influences stability through two complementary analytical frameworks. For static networks, the key object is the coupling Laplacian, whose spectrum governs shifts in the stability of the node

dynamics. For time-varying (switching) networks, spectral methods become less effective, and Lyapunov-based techniques instead yield structural conditions for stability under arbitrary switching.

This analysis establishes the first dynamical layer of the dissertation central theme, namely interaction structure influences system behavior through coupling operators, and different analytical approaches reveal distinct structural features of these operators. This perspective will be extended in Chapter 4 to higher-order interaction models, where nonlinear analysis reveals which components of structure are dynamically observable.

3.1.1 Coupling and Stability in Network Dynamical Systems

Network dynamical systems (NDS) provide a fundamental framework for modeling interacting dynamical units across a wide range of applications, including communication networks [4], biological systems [62], and power grids [22]. In these systems, the evolution of each node depends on both its intrinsic dynamics and its interactions with neighboring nodes.

A central challenge in NDS is the analysis and design of coupling mechanisms that ensure stability. Due to nonlinear and complex interactions between nodes, stability is not guaranteed, and instabilities such as oscillations or chaotic behavior may arise. Coupling strategies have therefore emerged as a key tool for influencing system behavior [60, 40]. Appropriately designed coupling can promote synchronization and collective behavior [19, 53], thereby stabilizing the network even when individual node dynamics are unstable. Conversely, poorly designed coupling may destabilize otherwise stable systems, highlighting the delicate interplay between local dynamics and network structure. This phenomenon is reminiscent of the destabilizing effects of dissipation in symmetric Hamiltonian systems [10].

The study of stability in interconnected systems builds on classical Lyapunov theory, as well as extensions such as input-to-state stability [63], which characterize the effect of interconnections and external inputs. Stabilization in NDS requires understanding both the local dynamics of individual nodes and their coupling structure, with careful design of

interconnections playing a critical role [57, 29]. In particular, coupling-induced stabilization occurs when interactions between nodes drive the system toward a stable equilibrium, as observed in consensus dynamics and coupled oscillator models [54, 58].

Coupling mechanisms may be local, involving interactions between neighboring nodes, or global, affecting the network as a whole. In both cases, the stability of the system depends strongly on the structural properties of the network and the strength of the coupling. Identifying coupling structures that promote stability remains a significant challenge, with recent work exploring distributed and optimization-based approaches [38]. These ideas are particularly relevant in engineering applications such as power grids, where coupling strategies are used to synchronize generator units and ensure reliable operation [19].

In many real-world systems, network structure is time-varying, leading to switching dynamical systems. Changes in connectivity due to communication constraints or operational requirements can introduce additional instability mechanisms, particularly when switching is abrupt or unpredictable [72, 44]. Ensuring stability under such conditions requires theoretical tools that account for both the dynamics of individual subsystems and the evolution of the network topology.

In this chapter, we build on these ideas to analyze how coupling structure influences stability in diffusively coupled systems, with a particular focus on identifying structural mechanisms that promote or obstruct stabilization.

3.2 Network Dynamical Systems on Graphs

Let $\mathcal{G} = (V, E)$ be a directed graph on N nodes, with adjacency matrix $A \in \mathbb{R}^{N\times N}$. We refer to A as the *network topology* or *wiring* of the system.

Each node $i \in \{1, \dots, N\}$ carries a state $x_i \in \mathbb{R}^d$, and its isolated (intrinsic) dynamics are given by

$$\dot{x}_i = f(x_i) \tag{3.1}$$

where $f : \mathbb{R}^d \to \mathbb{R}^d$ is a nonlinear vector field.

Coupled network dynamics. Interactions between nodes are assumed to be pairwise and are described by a coupling function $\phi : \mathbb{R}^d \times \mathbb{R}^d \to \mathbb{R}^d$. The resulting network dynamics take the form

$$\dot{x}_i = f(x_i) + \sum_{j=1}^{N} A_{ij}\, \phi(x_i, x_j), \qquad i = 1, \ldots, N. \tag{3.2}$$

The pairwise assumption is fundamental: each interaction involves only two nodes at a time, in contrast to the higher-order interactions considered in chapter 4.

Linear coupling. In this chapter, we focus on linear coupling functions of the form

$$\phi(u, v) = M(\alpha u + \beta v) \tag{3.3}$$

where $\alpha, \beta \in \mathbb{R}$ are coupling parameters and $M \in \mathbb{R}^{d\times d}$ is the *coupling channel matrix*, which specifies how interactions are transmitted between components of the state.

Compact formulation. Let $\mathbf{x} = (x_1, \ldots, x_N) \in \mathbb{R}^{Nd}$ denote the stacked state vector and define

$$\mathbf{f}(\mathbf{x}) = (f(x_1), \ldots, f(x_N))$$

Then the network dynamics (3.2) can be written compactly as

$$\dot{\mathbf{x}} = \mathbf{f}(\mathbf{x}) + (L_{\alpha\beta} \otimes M)\mathbf{x} \tag{3.4}$$

where $\otimes$ denotes the Kronecker product and

$$L_{\alpha\beta} = \alpha D_{\text{in}} + \beta A \tag{3.5}$$

is the *parametrized coupling Laplacian*, with

$$D_{\text{in}} = \text{diag}(A\mathbf{1}) \tag{3.6}$$

denoting the in-degree matrix.

Structural role of the coupling Laplacian. The matrix $L_{\alpha\beta}$ encodes both the network topology and the coupling parameters, and therefore constitutes the primary structural object governing the dynamics. In particular, the graph influences the system only through this operator, while the intrinsic node behavior is determined by f.

Special cases. Two important instances of (3.5) are:

$$L^{-} = D^{\text{in}} - A \tag{3.7}$$

corresponding to diffusive coupling ($\beta = -\alpha$), and

$$L^{+} = D^{\text{in}} + A \tag{3.8}$$

corresponding to signless-diffusive coupling ($\beta = \alpha$). This operator, unlike the former (3.7), does not frequently appear in the literature.

This formulation isolates the role of network structure in a transparent way, in the sense that the dynamics depend on the graph only through the coupling Laplacian, and different choices of coupling parameters lead to qualitatively different system behaviors. This observation will be central to the stability analysis developed in the remainder of this chapter.

3.3 Homogeneous Equilibrium and Linearization

3.3.1 Equilibria of the Dynamics

Definition 3.1. *The* synchronization manifold *of the network dynamics is defined as*

$$\mathcal{S} = \left\{ \mathbf{x} \in \mathbb{R}^{Nd} \;\middle|\; x_i = x_j,\ \forall i, j \right\} \tag{3.9}$$

This manifold represents the set of states in which all nodes share a common value. It plays a central role in the analysis of network dynamical systems, as it captures fully synchronized behavior.

Let $x_0 \in \mathbb{R}^d$ be an equilibrium of the isolated node dynamics, namely

$$f(x_0) = 0 \tag{3.10}$$

We have the following characterization of the equilibria of the dynamics depending on the structure of the coupling.

Proposition 3.2. *Let x_0 be an equilibrium of the isolated dynamics f.*

1. *If $\alpha = -\beta$, then the state $\mathbf{1} \otimes x_0$ is an equilibrium of the network dynamics.*

2. *If $x_0 = 0$, then the origin is an equilibrium of the network dynamics for any $\alpha, \beta \in \mathbb{R}$.*

Proof. The first assertion follows from the zero-row-sum property $L_{\alpha\beta}\mathbf{1} = 0$, which ensures that the coupling term vanishes on the synchronization manifold. The second assertion follows from the linearity of the coupling operator. ■

In particular, for diffusive coupling ($\alpha = -\beta$), the synchronization manifold is flow invariant, and homogeneous equilibria, nameley equilibria (3.2) that lie in (3.9), arise naturally.

3.3.2 Linearization and Variational Equation

Proposition 3.3. *Suppose we are given an* arbitrary *reference trajectory $\bar{\mathbf{x}}(t)$ of* (3.2)*, the variational equation describing the dynamics of infinitesimal perturbations is given by the following linear time-varying equation*

$$\dot{\delta\mathbf{x}} = \left(\sum_{i=1}^{N} \mathbf{E}_{ii} \otimes \frac{\partial f}{\partial x}(\bar{x}_i) + \sum_{i,j=1}^{N} A_{ij} \left\{ \mathbf{E}_{ii} \otimes \frac{\partial \phi}{\partial u}(\bar{x}_i, \bar{x}_j) + \mathbf{E}_{ij} \otimes \frac{\partial \phi}{\partial v}(\bar{x}_i, \bar{x}_j) \right\} \right) \delta\mathbf{x} \tag{3.11}$$

Proof. Let $\mathbf{x}$ be a $\delta\mathbf{x}$ perturbed trajectory away from $\bar{\mathbf{x}}$. Denote by $\{\mathbf{E}_{ij}\}_{1\leq i,j\leq N}$ the standard basis of the space $\mathrm{Mat}_N(\mathbb{R})$ of square matrices with coefficients in the field $\mathbb{R}$. A Taylor expansion yields the following

$$\begin{aligned}\dot{\bar{x}}_i + \dot{\delta x_i} &= f(\bar{x}_i + \delta x_i) + \sum_{j=1}^{N} A_{ij}\phi(\bar{x}_i + \delta x_i, \bar{x}_j + \delta x_j),\ 1 \leq i \leq N \\ &= f(\bar{x}_i) + \frac{\partial f}{\partial x}(\bar{x}_i)\delta x_i + f_{2+}(\delta x_i) + \sum_{j=1}^{N} A_{ij}\left\{\phi(\bar{x}_i, \bar{x}_j) + \right. \\ &\left. \frac{\partial \phi}{\partial u}(\bar{x}_i, \bar{x}_j)\delta x_i + \frac{\partial \phi}{\partial v}(\bar{x}_i, \bar{x}_j)\delta x_j + \phi_{2+}(\delta x_i, \delta x_j)\right\}\end{aligned} \tag{3.12}$$

Noting that $\bar{\mathbf{x}}$ is a solution of (3.2) and ignoring the higher order terms, we recover (3.11) as the compact version of (3.12). ■

Corollary 3.4. *If the reference trajectory $\bar{\mathbf{x}}$ described in Proposition 3.3 is constrained to lie in the synchronization manifold $\mathcal{S}$, then equation* (3.11) *simplifies to*

$$\dot{\delta\mathbf{x}} = \left(I_N \otimes \frac{\partial f}{\partial x}(\bar{x}) + D^{in} \otimes \frac{\partial \phi}{\partial u}(\bar{x}, \bar{x}) + A \otimes \frac{\partial \phi}{\partial v}(\bar{x}, \bar{x})\right)\delta\mathbf{x} \tag{3.13}$$

In particular, if the coupling ϕ is also constrained to be linear as in (3.3)*, then system* (3.13) *further simplifies to*

$$\dot{\delta\mathbf{x}} = \left(I_N \otimes \frac{\partial f}{\partial x}(\bar{x}) + L_{\alpha\beta} \otimes M\right)\delta\mathbf{x} \tag{3.14}$$

In the special case $M = I_d$, the Jacobian simplifies to

$$J = I_N \otimes F_0 + L_{\alpha\beta} \otimes I_d \tag{3.15}$$

where

$$F_0 = \frac{\partial f}{\partial x}(\bar{x}) \tag{3.16}$$

Remark 3.5. *While the general variational dynamics* (3.11) *define a linear time-varying*

system, linearization about a homogeneous equilibrium yields a linear time-invariant system, which admits a tractable spectral characterization of stability.

3.4 Spectral Decomposition of the Network Jacobian

We now characterize the spectrum of the linearized network dynamics at a homogeneous equilibrium.

Proposition 3.6 (Spectral decomposition of the network Jacobian)**.** *Let $x^* \in \mathbb{R}^d$ be a homogeneous equilibrium of the network dynamics, and assume that $M = I_d$. Let*

$$J = I_N \otimes F_0 + L_{\alpha\beta} \otimes I_d \tag{3.17}$$

where $F_0 = Df(x^*)$. Then the spectrum of J is given by

$$\sigma(J) = \sigma(F_0) + \sigma(L_{\alpha\beta}) \tag{3.18}$$

where

$$\sigma(F_0) + \sigma(L_{\alpha\beta}) = \{\nu + \lambda \mid \nu \in \sigma(F_0),\ \lambda \in \sigma(L_{\alpha\beta})\}$$

Proof. The result follows from standard properties of Kronecker sums. In particular, since J can be written as a Kronecker sum of the matrices F_0 and $L_{\alpha\beta}$, its spectrum is given by all pairwise sums of eigenvalues of F_0 and $L_{\alpha\beta}$. This can be established, for instance, via the Schur decomposition of the two matrices (see [26]). ■

Interpretation. Proposition 3.6 provides a precise characterization of how network structure influences stability. Each eigenvalue $\nu \in \sigma(F_0)$ of the isolated node dynamics is shifted by each eigenvalue $\lambda \in \sigma(L_{\alpha\beta})$ of the coupling Laplacian. As a result, the spectrum of the network Jacobian is obtained by translating the node spectrum along the spectral structure of the graph.

This decomposition highlights an operator-theoretic perspective, namely the coupling does not act as a simple additive perturbation, but rather as a structured operator that organizes how the network topology modifies the intrinsic dynamics. In the static setting considered here, the structural effect of the graph is entirely captured by the spectrum of the coupling Laplacian $L_{\alpha\beta}$. A useful summary of this result is

$$\text{node dynamics} + \text{network spectrum} = \text{network stability}. \tag{3.19}$$

Thus in the pairwise static regime, the spectrum of the coupling Laplacian constitutes the primary structural quantity governing stability.

This spectral mechanism admits a natural geometric interpretation illustrated in the conceptual diagram Figure 3.1.

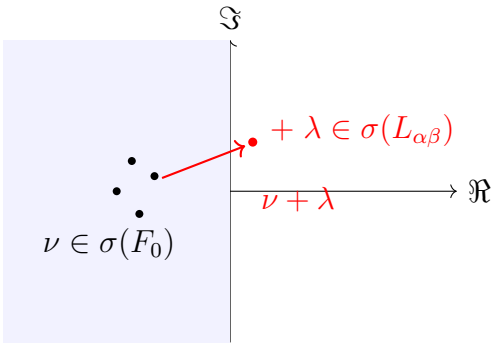

Figure 3.1: Spectral shift induced by network coupling. Eigenvalues of the isolated node dynamics (black) are translated by eigenvalues of the coupling Laplacian (red). If $\sigma(L_{\alpha\beta})$ extends into the right half-plane, then the shifted spectrum $\sigma(F_0) + \sigma(L_{\alpha\beta})$ may cross the stability boundary $\Re = 0$, leading to instability.

3.5 Stability Conditions

From this point onward, we assume that the equilibrium of the dynamics is located at the origin. This can always be achieved via an appropriate change of coordinates. Furthermore, all notions of stability considered in this section are local, unless otherwise specified.

Proposition 3.7. *Assume that the coupling Laplacian $L_{\alpha\beta}$ has at least one eigenvalue in the right half-plane (RHP). Then stability of the isolated node dynamics is a necessary condition for the stability of the network dynamics* (3.4).

Proof. Under the assumption, there exists $\lambda_0 \in \sigma(L_{\alpha\beta})$ such that $\mathrm{Re}(\lambda_0) > 0$. If the isolated node dynamics is not stable, then there exists $\nu_0 \in \sigma\big(Df(0)\big)$ such that $\mathrm{Re}(\nu_0) \geq 0$. By the spectral decomposition of the Jacobian (cf. (3.18)), it follows that $\nu_0 + \lambda_0 \in \sigma(J)$ satisfies

$$\mathrm{Re}(\nu_0 + \lambda_0) > 0$$

which implies that the spectrum of J intersects the right half-plane. Therefore, the network dynamics cannot be stable. ■

We now impose the condition $|\alpha| = |\beta|$ for the remainder of this section. Under this condition, the dynamics (3.4) depends effectively on a single scalar parameter, whose magnitude is referred to as the *coupling strength*. This parameter plays a central role in shaping the behavior of the network. In particular, the coupling strength can qualitatively alter stability. More specifically, it may destabilize a network of individually stable nodes, or conversely, it can stabilize a network of unstable node dynamics. This observation highlights that the condition in Proposition 3.7 is necessary but not sufficient in general. The coupling strength can act as a control parameter, and its variation may induce bifurcations in the network dynamics. A detailed analysis of such phenomena is not considered here, but it will be analyzed more carefully in the context of hypergraphs in Chapter 4.

Remark 3.8. *The case $\beta = -\alpha$ corresponds to* diffusive coupling*, while the case $\beta = \alpha$ corresponds to what we refer to as* signless-diffusive coupling*.*

Let $L^{\pm} = D_{\mathrm{in}} \pm A$ denote the coupling Laplacian, where $L^{-} = D_{\mathrm{in}} - A$ is the classical (diffusive) Laplacian and $L^{+} = D_{\mathrm{in}} + A$ is the signless Laplacian. While the former is standard in the literature, the latter has received comparatively less attention, with early work appearing in [18].

Let

$$\sigma(L^{\pm}) = \{\lambda_1^{\pm}, \ldots, \lambda_N^{\pm}\} \tag{3.20}$$

denote the spectrum of the coupling Laplacian. Then, from (3.18), the spectrum of the network Jacobian can be expressed as

$$\sigma(J) = \left\{\nu_i + \alpha\lambda_j^{\pm} \;\middle|\; 1 \le i \le d,\ 1 \le j \le N\right\} \tag{3.21}$$

Define

$$\nu_{\max} := \max_{1\le i\le d} \mathrm{Re}(\nu_i) \tag{3.22}$$

and similarly define $\lambda_{\min}^{\pm}$ and $\lambda_{\max}^{\pm}$ as the extremal real parts of the eigenvalues of $L^{\pm}$. Unless otherwise stated, we assume that $\nu_{\max} \neq 0$.

3.5.1 Coupling-Induced Destabilization

We now characterize how coupling can destabilize a network of otherwise stable dynamical units. Assume that the isolated node dynamics are asymptotically stable, meaning

$$\nu_{\max} < 0 \tag{3.23}$$

The following result shows that sufficiently strong coupling can nevertheless induce instability.

Proposition 3.9 (Coupling-induced destabilization)**.** *Suppose the isolated node dynamics are stable. Then there exists a critical coupling strength*

$$\alpha_c = -\frac{\nu_{\max}}{\lambda_{\max}^{\pm}} > 0 \tag{3.24}$$

such that the network dynamics (3.4) *satisfy:*

- *The network is exponentially stable for* $\alpha \in (-\infty, \alpha_c)$.

- *The network is unstable for* $\alpha \in (\alpha_c, \infty)$.

Proof. The spectrum of $L^{\pm}$ lies in the open right half plane union the origin, thus $\mathrm{Re}(\lambda_j^{\pm}) \geq 0$ for all j. If $\alpha \leq 0$, then $\mathrm{Re}(\nu_i + \alpha\lambda_j^{\pm}) < 0$ for all $1 \leq i \leq d$ and $1 \leq j \leq N$. Hence the network is stable for all $\alpha \in (-\infty, 0]$. If however $\alpha > 0$, then $\nu_{\max} + \alpha\lambda_{\max}^{\pm}$ is the top element of the bounded lattice $(\mathrm{Re}(\sigma(J)), \leq)$. Therefore for $\alpha_c := -\frac{\nu_{\max}}{\lambda_{\max}^{\pm}}$, it follows that the network is stable for all $\alpha \in (0, \alpha_c)$ and unstable for $\alpha \in (\alpha_c, \infty)$. Note that $\lambda_{\max}$ does not vanish since the network topology is connected. ■

Interpretation. Proposition 3.9 shows that coupling can destabilize a network even when all nodes are stable in isolation. The mechanism is purely spectral, in the sense that instability occurs when the coupling-induced shift $\alpha\lambda^{\pm}$ moves the rightmost eigenvalue of the node dynamics across the stability boundary $\mathrm{Re} = 0$ see Figure 3.1 for a conceptual illustration.

In particular, the largest eigenvalue of the coupling Laplacian determines how strongly the network amplifies perturbations. Once the coupling strength exceeds the critical threshold α_c, this amplification dominates the intrinsic stability of the nodes, leading to a loss of stability. This phenomenon highlights the central role of the interaction structure in this setting, namely stability is governed by the interplay between node dynamics and network topology through the spectral combination $\nu + \alpha\lambda^{\pm}$.

3.5.2 Coupling-Induced Stabilization

We now examine the converse question, namely can coupling stabilize a network of unstable dynamical units? Assume that the isolated node dynamics are unstable, meaning

$$\nu_{\max} := \max_{\nu \in \sigma(F_0)} \mathrm{Re}(\nu) > 0 \tag{3.25}$$

In contrast to the destabilization case, stabilization by coupling is not always possible. A necessary condition is that the coupling Laplacian does not admit a zero eigenvalue, thai

is $0 \notin \sigma(L^{\pm})$. Otherwise, there exists an unshifted mode that preserves the instability of the node dynamics. The following result characterizes when stabilization can occur.

Proposition 3.10 (Coupling-induced stabilization)**.** *Assume* $0 \notin \sigma(L^{\pm})$ *and that the isolated node dynamics are unstable. Then there exists a critical coupling strength*

$$\alpha_c = -\frac{\nu_{\max}}{\lambda^{\pm}_{\min}} < 0 \tag{3.26}$$

such that the network dynamics (3.4) *is*

- *Exponentially stable for* $\alpha \in (-\infty, \alpha_c)$*;*
- *Unstable for* $\alpha \in (\alpha_c, \infty)$*.*

Proof. The argument of the proof here is similar to that of Proposition 3.9, but noting that $\nu_{\max} + \alpha\lambda^{\pm}_{\min}$ is now the maximal element of the ordered set $(\mathrm{Re}(\sigma(J)), \leq)$. Here we have $\alpha_c := -\frac{\nu_{\max}}{\lambda^{\pm}_{\min}}$. Furthermore, note that $\lambda^{\pm}_{\min}$ does not vanish since the origin is excluded from the geometry of the spectrum of $L^{\pm}$. ■

The condition $0 \notin \sigma(L^{\pm})$ is essential. If the coupling Laplacian contains the origin in its spectrum, then stabilization by coupling alone is impossible.

Proposition 3.11. *Suppose the isolated node dynamics are unstable. If* $0 \in \sigma(L^{\pm})$*, then the network cannot be stabilized by coupling alone.*

Proof. If $0 \in \sigma(L^{\pm})$, then from (3.21) there exists an eigenvalue of J of the form $\nu \in \sigma(F_0)$ that is unaffected by the coupling. Since $\mathrm{Re}(\nu) > 0$, the instability persists for all values of the coupling parameter α. ■

Interpretation. Coupling-induced stabilization requires that all unstable modes of the node dynamics be shifted into the left half-plane. This is possible only if the coupling operator acts on every mode, which is precisely ensured by the condition $0 \notin \sigma(L^{\pm})$.

From a structural perspective, this result highlights a fundamental distinction between diffusive and signless-diffusive coupling. In the diffusive case, $0 \in \sigma(L^-)$ always holds, implying that coupling alone cannot stabilize an unstable network. In contrast, signless-diffusive coupling may admit a strictly positive spectrum, enabling stabilization through sufficiently strong negative coupling.

3.6 Obstructions to Stabilization

The stabilization results of Section 3.5.2 reveal a fundamental obstruction principle. Coupling can stabilize unstable node dynamics only if the coupling operator is able to shift *all* unstable modes into the left half-plane. Any mode that remains unaffected by the coupling constitutes an obstruction to stabilization.

This obstruction can arise from two distinct sources, namely the *functional* form of the coupling and the *structural* form of the underlying network.

3.6.1 Functional Obstruction: Diffusive Coupling

Consider the diffusive coupling Laplacian

$$L^- = D_{\text{in}} - A \tag{3.27}$$

It is well known that L^- has the zero-row-sum property, and therefore

$$0 \in \sigma(L^-) \tag{3.28}$$

This zero eigenvalue corresponds to the synchronization direction. As a result, there exists a mode of the dynamics that is unaffected by diffusive coupling. If the isolated node dynamics are unstable, this mode cannot be shifted into the left half-plane regardless of the choice of coupling strength. Therefore, diffusive coupling alone cannot stabilize a network

of unstable node dynamics. In this sense, diffusion constitutes a *functional obstruction* to coupling-induced stabilization.

3.6.2 Structural Obstruction: Bipartiteness

We now consider the signless Laplacian

$$L^+ = D_{\text{in}} + A \tag{3.29}$$

In contrast to the diffusive case, the spectrum of L^+ need not contain the origin. From Proposition 3.10, stabilization by coupling is feasible provided that

$$0 \notin \sigma(L^+) \tag{3.30}$$

The existence of a zero eigenvalue for L^+ is determined by the structure of the underlying graph as characterized by the following classical result.

Proposition 3.12. *The signless Laplacian L^+ is invertible if and only if the underlying graph is non-bipartite.*

Proof. This follows from Proposition 2.1 in [18]. ■

This result provides a direct structural criterion for the feasibility of coupling-induced stabilization. If the graph is bipartite, then

$$0 \in \sigma(L^+) \tag{3.31}$$

and an unshifted mode persists, preventing stabilization. Conversely, non-bipartite graphs admit a strictly positive spectrum, allowing all modes to be shifted by the coupling. Thus, bipartiteness constitutes a *structural obstruction* to coupling-induced stabilization.

3.6.3 Examples

The preceding results allow for a direct characterization of stabilizability for standard graph families.

Corollary 3.13. *Let P_n, S_n, and C_n denote the path, star, and cycle graphs on n nodes, respectively* [52]*. Then we have the following*

1. *A network of unstable node dynamics on the odd cycle C_{2n+1} can be stabilized by coupling alone.*

2. *A network of unstable node dynamics on P_n, S_n, or the even cycle C_{2n} cannot be stabilized by coupling alone.*

3.7 Summary of Static Stability Mechanisms

The preceding analysis provides a unified operator-theoretic perspective on stability in static pairwise network dynamical systems. When the isolated node dynamics are stable, coupling can induce instability by shifting eigenvalues of the linearized dynamics into the right half-plane. Conversely, when the node dynamics are unstable, stabilization through coupling is possible only if the coupling operator acts on all modes, that is if no zero eigenvalue obstructs the required spectral shift. These results highlight two complementary ways in which network structure influences stability, namely

- **Spectral geometry:** the eigenvalues of the coupling Laplacian $L_{\alpha\beta}$ determine how the spectrum of the node dynamics is shifted, thereby shaping the overall stability of the network.

- **Structural obstruction:** graph-theoretic properties, such as bipartiteness, determine whether certain stabilizing shifts are feasible by controlling the presence or absence of zero eigenvalues in the coupling spectrum.

These observations yield the first central insight of this chapter, namely

In static pairwise network systems, interaction structure manifests itself through the spectrum of the coupling operator.

3.8 Switching Network Dynamical Systems

The preceding sections considered network dynamical systems defined over a fixed interaction topology. In many applications however, the underlying graph evolves over time due to changing communication patterns, agent mobility, or network reconfiguration. This motivates the study of network dynamics under time-varying graph structures.

To model this behavior, we consider the system (3.4) under switching topology. Let

$$\mathcal{G} = \{\mathcal{G}_1, \ldots, \mathcal{G}_m\}$$

be a finite family of connected simple graphs defined over a common vertex set V. The interaction graph $\mathcal{G}(t)$ is assumed to take values in $\mathcal{G}$ according to a switching mechanism.

3.8.1 Formulation and Equilibrium structure.

A switched network dynamical system consists of two components:

1. A collection of vector fields $\{F_{\mathcal{G}} : \mathbb{R}^{Nd} \to \mathbb{R}^{Nd}\}_{\mathcal{G}\in\mathcal{G}}$, where each vector field is of the form

$$F_{\mathcal{G}}(\mathbf{x}) = \mathbf{f}(\mathbf{x}) + \left(L^{\mathcal{G}}_{\alpha\beta} \otimes M\right)\mathbf{x} \tag{3.32}$$

   These vector fields are referred to as the *modes* or *subsystems* of the switched system.

2. A *switching signal*

$$\sigma : [0, \infty) \to \mathcal{G} \tag{3.33}$$

which specifies the active graph $\mathcal{G}(t)$ at each time instant $t \in [0, \infty)$. We assume that σ is piecewise constant and exhibits only finitely many switches on any bounded time interval, preventing pathological behaviors such as chattering.

The resulting switched dynamics is given by

$$\begin{aligned} \dot{\mathbf{x}}(t) &= F_{\sigma(t)}(\mathbf{x}(t)) \\ &= \mathbf{f}(\mathbf{x}(t)) + \big(L_{\alpha\beta}^{\sigma(t)} \otimes M\big)\mathbf{x}(t) \end{aligned} \tag{3.34}$$

System (3.34) belongs to the broader class of switched systems for which there some available general conditions that guarantee stability under arbitrary switching (see, e.g., [39]).

Assume that the isolated node dynamics admit an equilibrium at the origin. Then, by Proposition 3.2, each subsystem $F_{\mathcal{G}}$ also admits the origin as an equilibrium. Consequently, the origin is a *common equilibrium* of the switched system (3.34).

3.8.2 Challenges of switching dynamics.

In contrast to the static case, the spectral decomposition of the Jacobian no longer provides a direct characterization of stability. Even if each subsystem corresponding to a fixed graph $\mathcal{G}_i$ is stable, arbitrary switching among these subsystems may lead to instability. This phenomenon is well known in the theory of switched systems [39, 17, 30]. A key difficulty arises from the fact that the Laplacians $\{L_{\alpha\beta}^{\mathcal{G}_i}\}$ generally do not commute. As a result, the spectral geometry that governs stability in the static setting does not extend directly to the time-varying case. This necessitates a shift away from eigenvalue-based analysis.

3.8.3 Stability objective.

Our objective is to characterize the asymptotic stability properties of the common equilibrium under arbitrary switching. A central notion in this context is that of *Global Uniform Asymptotic Stability* (GUAS). The system (3.34) is said to be GUAS if there exists a class

$\mathcal{KL}$ function β [30] such that, for all initial conditions and all admissible switching signals $\sigma(\cdot)$, the corresponding solutions satisfy

$$\|\mathbf{x}(t)\| \leq \beta\big(\|\mathbf{x}(0)\|, t\big), \quad \forall t \geq 0. \tag{3.35}$$

If in addition, β can be chosen of the form $\beta(r,t) = ce^{-st}r$ for some constants $c, s > 0$, then the system is said to be *Globally Uniformly Exponentially Stable* (GUES).

In many applications, one may relax the requirement of global stability and instead consider *local* uniform asymptotic or exponential stability, where the estimate (3.35) holds only in a neighborhood of the origin.

From spectral to Lyapunov analysis. The limitations of spectral methods in the switching setting motivate a different analytical approach. Rather than relying on eigenvalue-based arguments, we seek conditions that ensure stability uniformly across all admissible switching signals. This naturally leads to the use of Lyapunov methods, and in particular to the construction of common Lyapunov functions. In the remainder of this section, we develop such Lyapunov-based conditions and, we show how they reveal structural properties of the network that are not captured by spectral analysis alone.

3.9 Common Lyapunov Functions and Stability under Switching

In contrast to the static case, stability of switched network systems cannot in general be characterized through spectral arguments. Instead, one may seek conditions that guarantee stability uniformly across all admissible switching signals. A central tool for this purpose is the notion of a *common Lyapunov function*. A common Lyapunov function is a scalar function that decreases along the trajectories of every subsystem in the switching family. The existence of such a function ensures stability independently of the switching signal, and

in particular guarantees stability under arbitrary switching.

3.9.1 Separable Lyapunov Structure

Assume that the isolated node dynamics admit a Lyapunov function

$$V : \mathbb{R}^d \to \mathbb{R}_{\geq 0}.$$

A natural candidate for the network dynamics is the separable Lyapunov function

$$V_{\text{net}}(\mathbf{x}) = \sum_{i=1}^{N} V(x_i). \tag{3.36}$$

This structure is particularly appealing because it is independent of the underlying graph. Consequently, if V_{net} decreases along the trajectories of each subsystem, it defines a common Lyapunov function for the switched network system. The central question is therefore:

Under what structural conditions on the coupling Laplacians does V_{net} decrease for all modes?

3.9.2 Existence of a Common Quadratic Lyapunov Function

We now provide a sufficient condition for the existence of a common Lyapunov function in the case of quadratic node dynamics and undirected switching graphs.

Theorem 3.14. *Suppose the node dynamics admit a quadratic Lyapunov function. If the coupling Laplacian $L_{\alpha\beta}^{\sigma(t)}$ satisfies $\alpha < 0$ and $|\alpha| \geq |\beta|$ for all $t \geq 0$, then the switched network system admits a common quadratic Lyapunov function.*

Proof. Note that for a fixed $t \geq 0$, if $\alpha < 0$ and $|\alpha| \geq |\beta|$ then the spectrum of the coupling Laplacian $L_{\alpha\beta}$ is contained in the left half-plane $\mathbb{C}_-$. In particular, if the underlying graph is undirected then $L_{\alpha\beta}$ is negative semi-definite. Now, let $v(x) = x^T P x$ be a quadratic

Lyapunov function for the node dynamics, where $x \in \mathbb{R}^d$ and P is a positive definite. The quadratic form $\mathcal{V}(\mathbf{x}) = \mathbf{x}^T(I_N \otimes P)\mathbf{x}$ is a common Lyapunov function for the switched network system. In fact, $\mathcal{V}$ is evidently a positive definite function. Its Lie derivative along (3.34) is given by $\dot{\mathcal{V}}(\mathbf{x}) = 2\mathbf{x}^T I_N \otimes P(\mathbf{f}(\mathbf{x}) + L^\sigma_{\alpha\beta} \otimes M)\mathbf{x} = 2\sum_{i=1}^N \dot{v}(x_i) + 2\mathbf{x}^T(L^\sigma_{\alpha\beta} \otimes PM)\mathbf{x} < 2\mathbf{x}^T(L^\sigma_{\alpha\beta} \otimes PM)\mathbf{x}$. In particular, if M is chosen such that the product PM is positive semi-definite (e.g. $M = I_d$), then we have the following uniform estimate: $\dot{\mathcal{V}}(\mathbf{x}) < \sup_\sigma\{2\lambda_{\max}(L^\sigma_{\alpha\beta} \otimes PM)\}\mathbf{x}^T\mathbf{x}$. The result follows from compactness of the index set $\mathcal{G}$.

■

Corollary 3.15. *If the node dynamics admit a quadratic Lyapunov function and $\alpha < 0$, then both diffusive and signless-diffusive switched network systems are globally uniformly exponentially stable (GUES).*

3.10 A Network-Only Stability Condition for Switching

In the previous section, stability under arbitrary switching was established through the existence of a common Lyapunov function, relying on structural properties of the coupling Laplacians. In this section, we further refine this analysis by deriving a *network-only* sufficient condition for stability that depends solely on local degree information rather than spectral properties.

3.10.1 Quadratic-Type Lyapunov Functions

To extend the scope beyond strictly quadratic Lyapunov functions, we consider a broader class of Lyapunov functions.

Definition 3.16. *A function $\gamma : [0, a) \to \mathbb{R}_+$ is said to be of class $\mathcal{K}$ if it is continuous, strictly increasing, and satisfies $\gamma(0) = 0$. It is said to be of class $\mathcal{K}_\infty$ if, in addition, $a = \infty$*

and $\gamma(r) \to \infty$ *as* $r \to \infty$.

Definition 3.17. *Let* $x = 0$ *be an equilibrium of* $\dot{x} = f(x)$. *A Lyapunov function* V *is said to be of* quadratic-type *if there exist class* $\mathcal{K}$ *functions* $\lambda_1, \lambda_2, \gamma$ *and constants* $c_1, c_2 > 0$ *such that, for all* x *in a neighborhood of the origin,*

$$\begin{aligned} \lambda_1(\|x\|) \leq V(x) \leq \lambda_2(\|x\|) \\ \frac{\partial V}{\partial x} f(x) \leq -c_1 \gamma^2(\|x\|) \\ \left\| \frac{\partial V}{\partial x} \right\| \leq c_2 \gamma(\|x\|) \end{aligned} \tag{3.37}$$

These conditions generalize quadratic Lyapunov functions while preserving sufficient structure to derive stability results.

3.10.2 Degree-Based Switching Stability Condition

We now present the main result of this section.

Theorem 3.18. *Consider the switched system* (3.34). *Suppose the node dynamics admit a quadratic-type Lyapunov function satisfying* $\gamma(r) \leq \delta r$ *on* $[0, a)$ *for some* $\delta > 0$. *Let* $k_{\sigma,i}^{in}$ *and* $k_{\sigma,i}^{out}$ *denote the in-degree and out-degree of node* i *in the graph* $\sigma(t)$. *If the coupling parameters satisfy* $\alpha < 0$ *and*

$$2|\alpha|\, k_{\sigma,i}^{in} \;\geq\; |\beta| \big(k_{\sigma,i}^{in} + k_{\sigma,i}^{out} \big) \quad \forall i,\ \forall \sigma(t) \in \mathcal{G} \tag{3.38}$$

then the switched network system admits the common Lyapunov function

$$V_{net}(\mathbf{x}) = \sum_{i=1}^{N} V(x_i) \tag{3.39}$$

and is uniformly asymptotically stable. Furthermore, if λ_1 *is of class* $\mathcal{K}_\infty$ *and* $a = \infty$, *then the result holds globally.*

Proof. define $\mathcal{V}(\mathbf{x}) := \sum_{i=1}^{N} V(x_i)$ for $\mathbf{x} \in D^N$, where D is the domain in $\mathbb{R}^d$ containing the origin and supporting V. The estimate $\mathcal{V}(\mathbf{x}) \geq \lambda_1\big(\max\{\|x_i\|,\ 1 \leq i \leq N\}\big) = \lambda_1(\|\mathbf{x}\|)$ ensures positive definiteness of $\mathcal{V}$ since the function λ_1 is of class $\mathcal{K}$. The Lie derivative of $\mathcal{V}$ along (3.34) is given by the expression: $\dot{\mathcal{V}}(\mathbf{x}) = \sum_{i=1}^{N} \dot{V}(x_i) + \sum_{i,j=1}^{N} \frac{\partial V}{\partial x_i} L_{\alpha\beta}^{\sigma,ij} M x_j$, where $L_{\alpha\beta}^{\sigma,ij}$ is the ij-entry of the coupling Laplacian $L_{\alpha\beta}^{\sigma}$ associated with the σ-subsystem. Taking into account (3.37) and the fact that the matrix M is diagonal with boolean entries, we have the following estimate on the Lie derivative: $\dot{\mathcal{V}}(\mathbf{x}) \leq -\sum_{i=1}^{N} c_1 \gamma^2(\|x_i\|) + \sum_{i,j=1}^{N} c_2 |L_{\alpha\beta}^{\sigma,ij}| \gamma(\|x_i\|)\, \|x_j\|$. Using the sublinearity of γ on the interval $[0, a)$, we obtain the following quadratic upper-bound on the Lie derivative:

$$\dot{\mathcal{V}}(\mathbf{x}) \leq \sum_{i=1}^{N} \big(\sum_{j=1}^{N} c_2 |L_{\alpha\beta}^{\sigma,ij}|\, \|x_i\|\, \|x_j\| - c_1 \|x_i\|^2 \big).$$

Define the matrix $B_\sigma := c_1 I_N - c_2 L_{\alpha\beta}^{\sigma}$ where I_N is the identity matrix of size N. We get the following estimate: $\dot{\mathcal{V}}(\mathbf{x}) \leq -\frac{1}{2}\tilde{\mathbf{x}}^T \big(B_\sigma + B_\sigma^T\big)\tilde{\mathbf{x}}$, where $\tilde{\mathbf{x}} = [\|x_1\|, \cdots, \|x_N\|]^T$. Since the index set $\mathcal{G}$ is compact, it suffices to establish positive definiteness of the matrix $B_\sigma + B_\sigma^T$. This in turn follows from establishing negative semidefiniteness of the matrix $L_{\alpha\beta}^{\sigma} + \big(L_{\alpha\beta}^{\sigma}\big)^T$ which owing to the Gershgorin circle theorem, is guaranteed whenever $\alpha < 0$ and $2|\alpha| k_{in}^{\sigma,i} \geq |\beta|(k_{in}^{\sigma,i} + k_{out}^{\sigma,i})$. Furthermore, if the function λ_1 is of class $\mathcal{K}_\infty$, it follows that $\mathcal{V}$ must be radially unbounded, and the result holds globally. ■

3.10.3 Interpretation and Structural Implications

Theorem 3.18 is conceptually distinct from the static spectral results. It provides a sufficient condition for stability that

- does not rely on eigenvalues of the coupling Laplacians
- does not require commutativity of the Laplacians
- does not impose dwell-time or switching constraints

- depends only on local degree information.

The condition (3.38) states that, at each node and for each switching mode, *the stabilizing effect of incoming coupling must dominate the combined effect of incoming and outgoing interactions*. In the special case of diffusive or signless-diffusive coupling where $|\alpha| = |\beta|$, the condition simplifies to

$$k^{\text{in}}_{\sigma,i} \;\geq\; k^{\text{out}}_{\sigma,i}, \quad \forall i,\ \forall \sigma(t) \tag{3.40}$$

This motivates our introduction of the class of *non-positive divergence graphs*, defined by the condition that each node has in-degree greater than or equal to its out-degree. Fig. 3.8 shows a random sample of of such graphs.

Proposition 3.19. *Assume the node dynamics possesses a quadratic-type Lyapunov function such that $\gamma(r) \leq \delta r$ on the interval $[0, a)$ for some positive constants $a, \delta > 0$. If $\alpha < 0$ and $k^{\sigma,i}_{in} \geq k^{\sigma,i}_{out}$, for all graphs $\sigma(t) \in \mathcal{G}$, and for all nodes $i \in \{1, \cdots, N\}$, then the diffusive and signless-diffusive coupled switched network system are uniformly asymptotically stable. Moreover, if the function λ_1 in (3.37) is of class $\mathcal{K}_\infty$ and $a = \infty$, then the result holds globally.*

Proof. It follows from the proof of Theorem 3.18. ■

3.11 Spectral and Lyapunov Structural Perspectives on Network Dynamical Systems

The results developed in this chapter reveal a fundamental shift in how interaction structure manifests itself in network dynamical systems. Depending on the analytical framework, the same underlying network topology gives rise to distinct structural representations.

Static spectral perspective. In the case of fixed interaction graphs, stability is governed by the spectral structure of the coupling operator. The network Jacobian satisfies

$$\sigma(J) = \sigma(F_0) + \sigma(L_{\alpha\beta}) \tag{3.41}$$

so that the effect of the network is to shift the spectrum of the node dynamics according to the eigenvalues of the coupling Laplacian. In this setting, structure enters the analysis through global spectral properties, yielding an operator-theoretic characterization of stability.

Switching Lyapunov perspective. In contrast, when the interaction topology varies in time, spectral methods no longer provide a direct characterization of stability. Instead, stability is established through the construction of common Lyapunov functions. In this framework, structural information appears through local, combinatorial quantities such as node degrees via conditions of the form

$$2|\alpha|\, k_{\sigma,i}^{\text{in}} \geq |\beta|\big(k_{\sigma,i}^{\text{in}} + k_{\sigma,i}^{\text{out}}\big) \tag{3.42}$$

These conditions ensure that the Lyapunov function decreases uniformly across all switching modes.

3.12 Numerical Simulation

In this section, we present numerical simulations to illustrate and validate the theoretical results. First, we consider a static network of four Sprott systems [64] under stable ($\mu = 0.55$) and unstable ($\mu = 0$) regimes and coupled over the bidirectional network shown in Fig. 3.7. The Sprott system is a ubiquitous dynamical system whose dynamical and controllability properties have been studied in [45, 36] building from the work in [9]. It is a simplified and tractable version of the repressilator [21], a well-known model of synthetic genetic regulatory

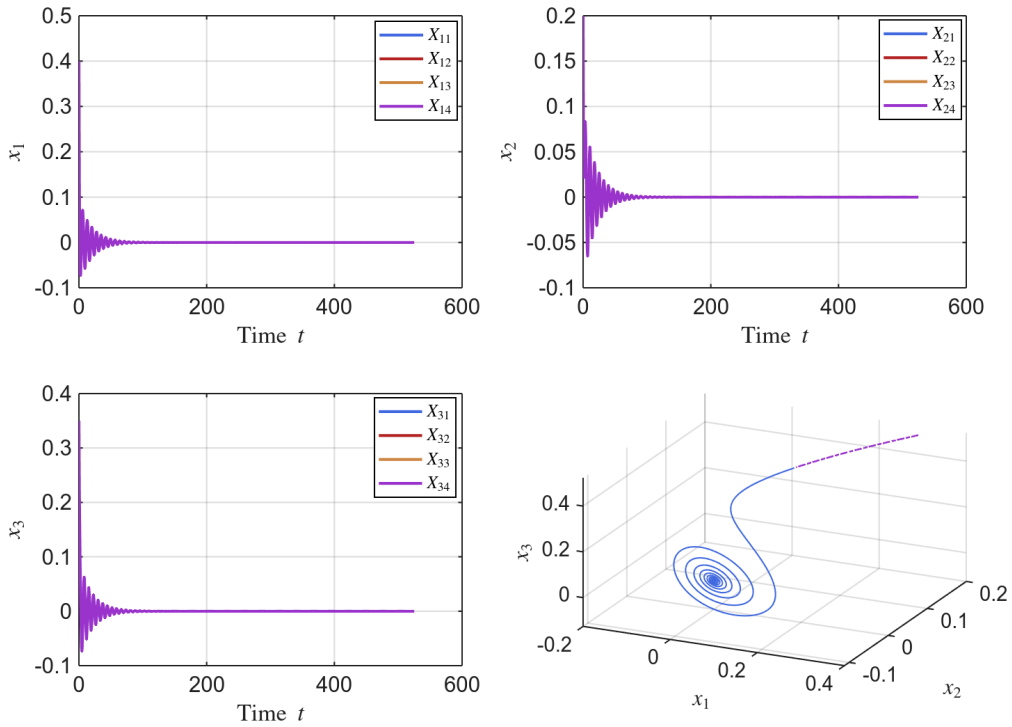

Figure 3.2: Four diffusively coupled *stable* Sprott systems [64] with parameter $\mu = 0.55$ on the bidirectional graph shown in Fig. 3.7. The coupling strength is set to $\alpha = \alpha_c - \frac{1}{1000} = 0.0115$, where $\alpha_c = 0.0125$. The resulting network system is *stable* as predicted by Proposition 3.9. The top left, top right and bottom left plots show trajectories of the 1st, 2nd and 3rd channel respectively of each of the 4 nodes. The bottom right plot shows the trajectory of the node dynamics in 3D space. The purple dash-dotted line shows the beginning segment of the trajectory to give a sense of orientation. The join state space is 12-dimensional.

networks that is ubiquitous in biology. In the stable regime, we compute the critical coupling parameter to be $\alpha_c = 0.0125$, and both Fig. 3.2. and Fig. 3.3. confirm that a deviation as small as $\epsilon = \frac{1}{1000}$ from this critical value can destabilize the network system, thus verifying the validity of Proposition 3.9. Likewise in the unstable regime which in fact is chaotic [64], we compute $\alpha_c = -0.6545$, and both Fig. 3.4. and Fig. 3.5. show that it is indeed possible to stabilize a network of signless-diffusively coupled unstable node dynamics, in agreement with our theoretical predictions.

Next, we consider a switched network of four copies of the globally asymptotically stable node dynamics $\dot{x} = -x^3$, coupled via signless-diffusive over the *non-positive divergence* graphs shown in Fig. 3.8. These are directed graphs in which the out-degree of each node is no greater than its in-degree. The network system is allowed to randomly switch its

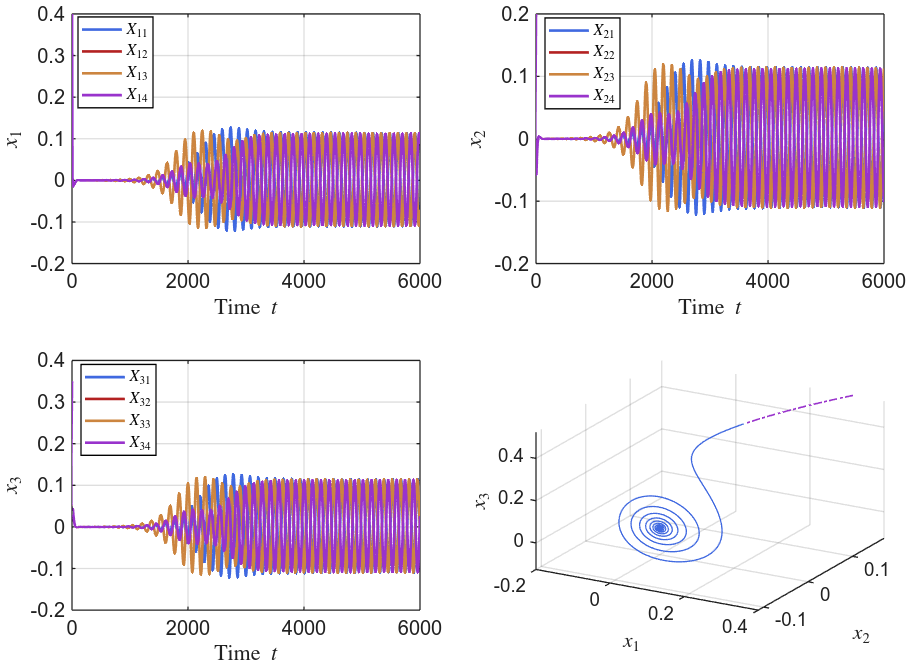

Figure 3.3: Same setup as in Fig. 3.2., but here the coupling strength is set to $\alpha = \alpha_c + \frac{1}{1000} = 0.0135$. The resulting network system is *unstable* as predicted by Proposition 3.9.

connectivity topology at regular time interval for a total of seven times over the course of the experiment. For coupling parameters $\alpha = -1 = \beta$, the hypothesis of Proposition 3.19 are satisfied, and Fig. 3.6 shows that the network remains stable under switching, thereby confirming the theoretical predictions.

Finally, we repeated the experiment above, but now changing the coupling parameters to $\alpha = 1$ and $\beta = -1$. Under these conditions, the hypotheses of Proposition 3.19 are not met. Consequently, stability of the switched system is *not guaranteed*. Indeed, as shown in Fig. 3.9, the switched network system becomes unstable, confirming that violation of the stated conditions can lead to loss of stability.

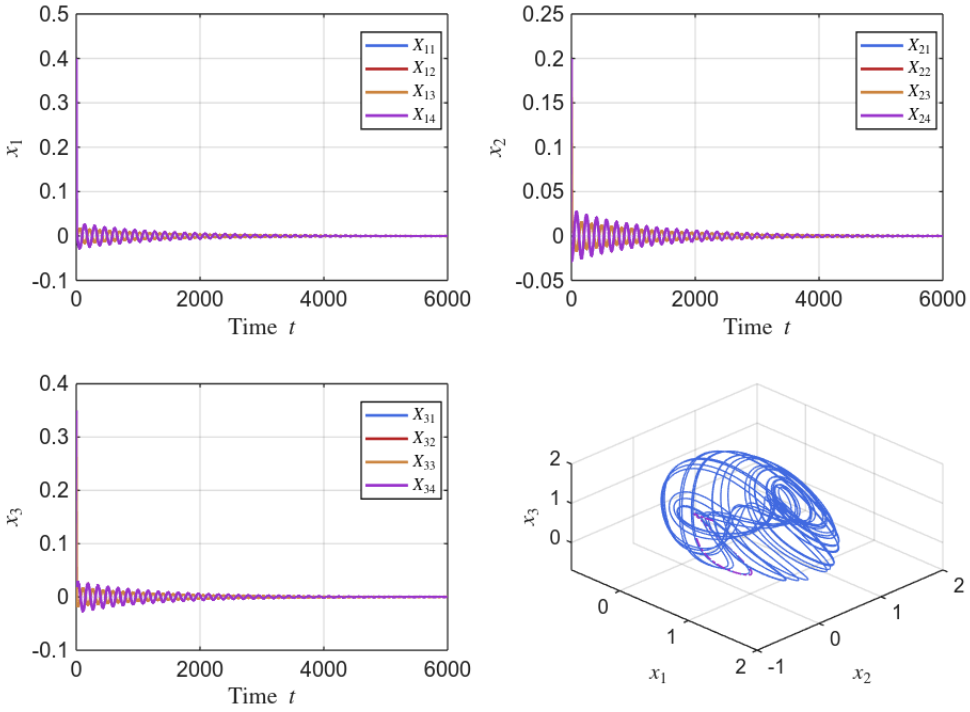

Figure 3.4: Four *signless-diffusively* coupled *unstable* Sprott systems [64] with parameter $\mu = 0$ on the bidirectional graph shown in Fig. 3.7. The coupling parameter is set to $\alpha = \alpha_c - \frac{1}{1000} = -0.6555$, where $\alpha_c = -0.6545$. The resulting network system is *stable* as predicted by Proposition 3.10. The top left, top right and bottom left plots show trajectories of the 1st, 2nd and 3rd channel respectively of each of the 4 nodes. The bottom right plot shows the trajectory of the node dynamics in 3D space. The purple dash-dotted line shows the beginning segment of the trajectory to give a sense of orientation. The join state space is 12-dimensional. Note that the node dynamics in this regime (i.e. frictionless Sprott system with $\mu = 0$) is in fact *chaotic* [64], yet with the *right coupling* we're able to tame it down and effectively *stabilize* the whole network system.

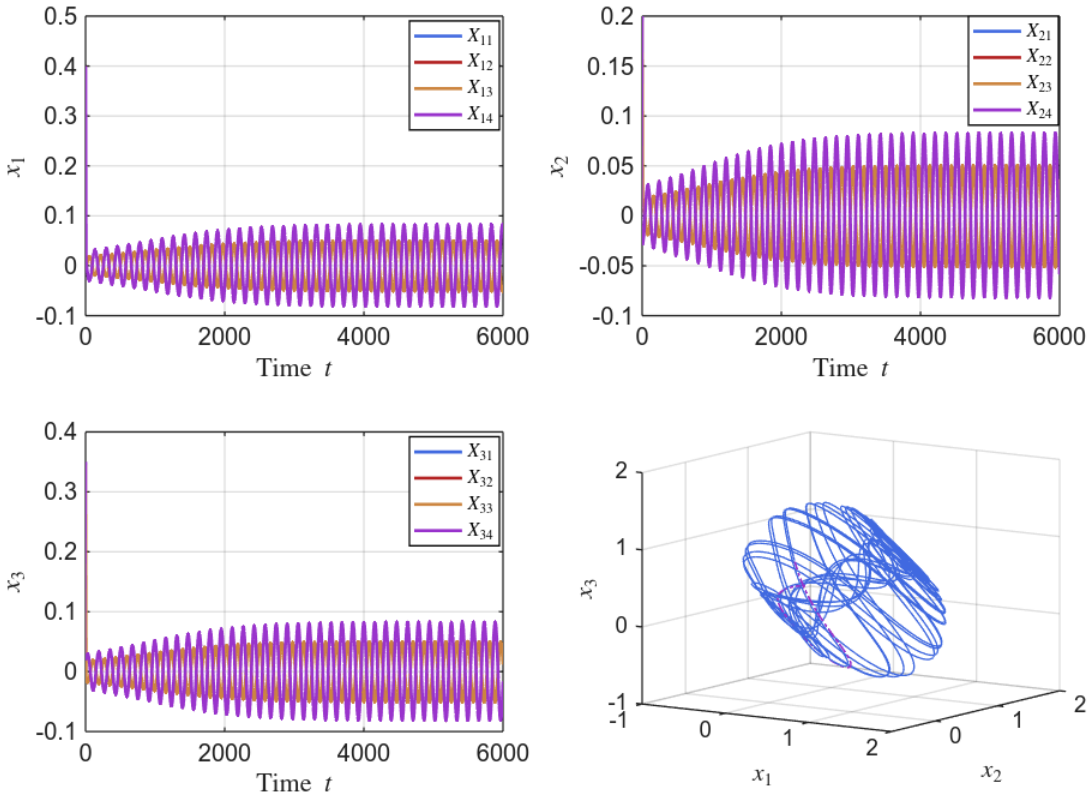

Figure 3.5: Same setup as in Fig. 3.4. Here however, the coupling parameter is set to $\alpha = \alpha_c + \frac{1}{1000} = -0.6535$. The resulting network system is *unstable* as predicted by Proposition 3.10. The trajectories are hinting that the dynamics of each channel is evolving on a toroidal manifold, so it's either *periodic* or *quasi-periodic*.

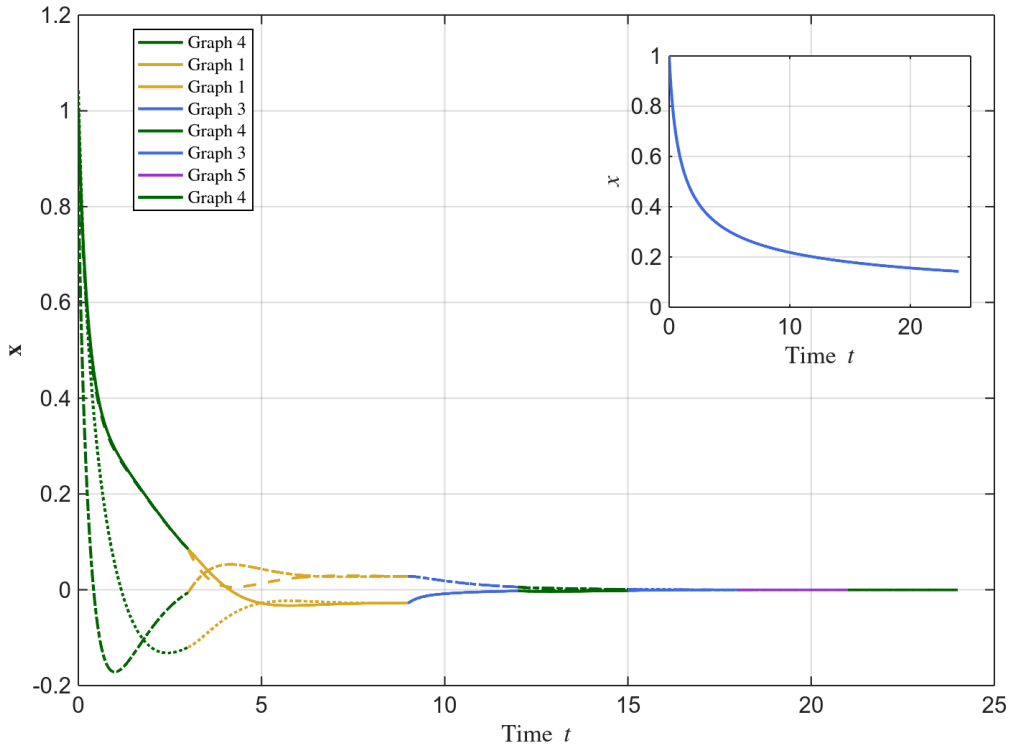

Figure 3.6: Switched network system with modes made of scalar node dynamics $\dot{x} = -x^3$ (see inset plot) *signless-diffusively* coupled over the network topologies shown in Fig. 3.8. $\alpha = -1 = \beta$. Solid lines indicate the dynamics of Node 1, dashed lines that of Node 2, dotted lines indicate Node 3, and finally dash-dotted lines indicate Node 4. The hypothesis of Proposition 3.19 are met, and the switched network is indeed asymptotically stable.

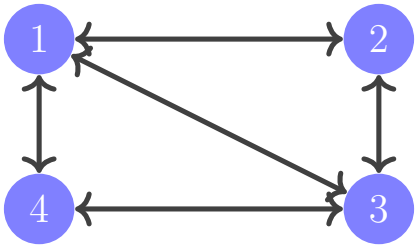

Figure 3.7: Bidirectional graph on a set of four nodes.

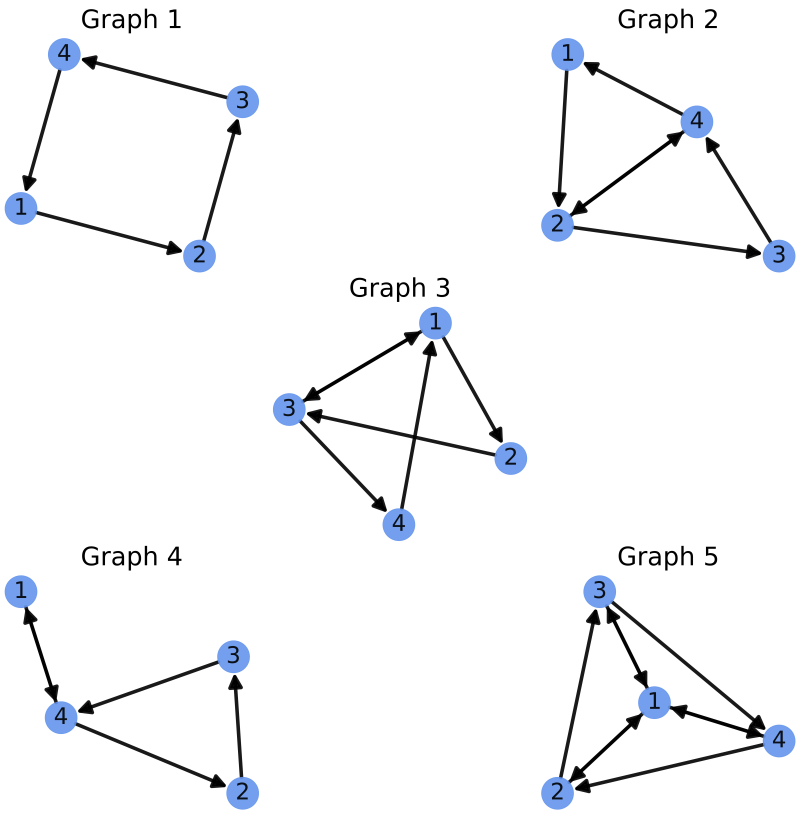

Figure 3.8: Randomly selected set of 5 *non-positive divergence* graphs on 4 nodes. These are directed graphs for which the out-degree of each node is no greater than the in-degree. This class of graphs is narrower than that of strongly connected graphs, but it's larger than that of undirected graphs. According to Proposition 3.19, this is the most conducive class of network topologies for asymptotic stability under arbitrary switching of signless-diffusively coupled network systems.

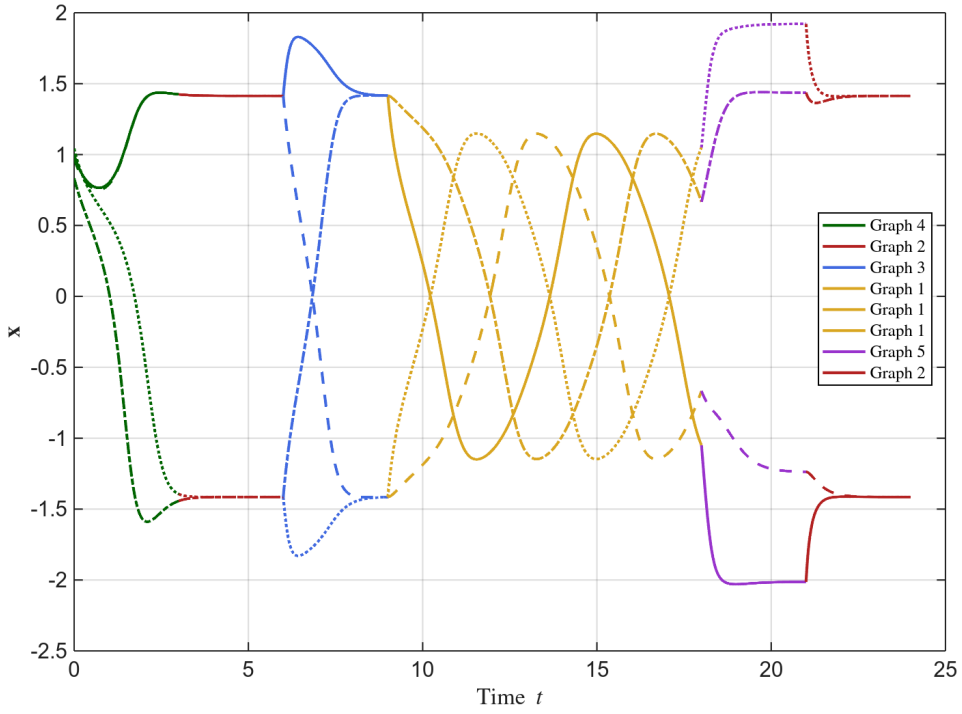

Figure 3.9: Switched network system with modes made of scalar node dynamics $\dot{x} = -x^3$ *diffusively* coupled over the network topologies shown in Fig. 3.8. $\alpha = 1$ and $\beta = -1$. The line style convention is the same as in Fig. 3.6. Here, the hypothesis of Proposition 3.19 are *violated*, so the stability of the resulting switched system under arbitrary switching is *not guaranteed* . In particular, the switching signal used in this plot shows that the switched network system is in fact not stable.

3.13 Chapter Summary

This chapter developed a dynamical perspective on pairwise network structure, with a particular emphasis on how interaction topology influences stability properties in both static and time-varying settings. The main conclusions can be summarized as follows.

- **Static pairwise networks admit a spectral characterization of stability.** When the coupling channel is the identity, the network Jacobian decomposes as

$$\sigma(J) = \sigma(F_0) + \sigma(L_{\alpha\beta}) \tag{3.43}$$

  so that the effect of the network is to shift the spectrum of the node dynamics according to the eigenvalues of the coupling Laplacian. In this regime, graph structure influences stability through its spectral geometry.

- **Coupling can both stabilize and destabilize network dynamics.** Even when all nodes are stable in isolation, coupling may induce instability by shifting eigenvalues into the right half-plane. Conversely, unstable node dynamics may be stabilized if the coupling operator is capable of shifting all unstable modes into the stable region.

- **Stabilization may be obstructed by structural and functional constraints.** *Diffusive coupling introduces a functional obstruction* through the presence of a zero eigenvalue in L_-, preventing full stabilization. Similarly, *bipartite graphs create a structural obstruction* for signless coupling via the zero eigenvalue of L_+. These phenomena highlight *intrinsic limitations of coupling-based stabilization.*

- **Switching dynamics require a distinct analytical framework.** In the presence of time-varying topology, spectral methods no longer yield direct stability criteria. Instead, Lyapunov-based approaches provide sufficient conditions for stability under

arbitrary switching, leading to network-only conditions expressed in terms of local degree information.

These results establish that pairwise network structure manifests itself through different mathematical objects depending on the dynamical regime and analytical method. In particular, *spectral geometry* and *degree-based conditions* provide *complementary perspectives* on *how structure influences stability*.

This analysis prepares the transition to Chapter 4. While the present chapter is restricted to pairwise interactions, the next chapter considers directed hypergraph systems in which interactions may involve more than two nodes simultaneously. In that setting, the central question becomes

Which aspects of higher-order structure are dynamically observable under nonlinear reduction?

As we will show, addressing this question requires distinguishing between *exposure* and *packing*, which constitute the relevant structural information driving the dynamics.

Chapter 4

Pattern Formation in Hypergraphs: Linear and Nonlinear Structural Effects

4.1 From Reconstruction to Pattern Formation

The preceding chapters developed two complementary perspectives on structural effects in network dynamical systems. Chapter 2 established that higher-order interaction structure cannot in general be uniquely recovered from static pairwise observations. A single graph may be consistent with multiple distinct hypergraphs, and the reconstruction procedures necessarily produce candidate structures rather than a uniquely determined ground truth. Chapter 3 then shifted from reconstruction to dynamics showing that in pairwise network systems, structure influences behavior through operator-level representations such as Laplacian spectra and degree-based Lyapunov conditions.

This chapter brings these perspectives together in the context of reaction-diffusion dynamics on directed hypergraphs. Rather than asking whether the full higher-order structure can be reconstructed, we instead adopt a dynamical viewpoint and ask the following question

Which components of higher-order structure are observable through pattern-forming dynamics?

This question is intrinsically weaker than full reconstruction, yet it is more closely aligned with the objectives of dynamical systems theory. Pattern formation is governed not by the entirety of the interaction structure, but by those aspects that enter the operators and coefficients controlling instability onset and nonlinear saturation.

The main result of this chapter is a *structural separation principle*: At the *linear level*, the hypergraph reduces to *exposure* information. Only first-order tail-moment statistics contribute to the linearized operator and the associated Turing instability condition. Consequently, hypergraphs that differ in their higher-order organization but agree in exposure are linearly indistinguishable. *Beyond onset* however, this degeneracy is lifted. A weakly nonlinear reduction reveals that nonlinear saturation depends on higher-order co-occurrence statistics of tail nodes within hyperedges. These quantities enter the reduced amplitude equation only through projections onto the critical eigendirections. We refer to these dynamically relevant projections as *packing effects*.

The chapter therefore completes the conceptual progression of the dissertation, namely from reconstruction to pattern formation. While static reconstruction seeks the full hypergraph and encounters fundamental non-uniqueness, pattern-forming dynamics identifies those components of higher-order structure that influence observable behavior. The central conclusion developed here is that *linear onset is governed by exposure*, whereas *nonlinear pattern selection is governed by packing effects*.

4.2 Introduction

Diffusion-driven instability and spontaneous pattern formation are foundational themes in applied mathematics, with classical roots in Turing's theory of morphogenesis [70], and an extensive development in the reaction-diffusion literature [49, 16, 27, 41]. In many contempo-

rary systems however, interactions occur not on continuous spatial domains but on discrete relational structures. In these settings, the geometry underlying diffusion is replaced by interaction networks, and the structure of these interactions directly shapes both instability onset and the nonlinear states that emerge beyond it [50].

Recently, a growing body of work has emphasized that many interactions in biological, ecological, and social systems are fundamentally higher-order in nature [5, 28, 13]. These interactions involve joint dependencies among multiple agents, and they cannot in general be accurately reduced to pairwise couplings. Directed hypergraphs provide a natural representation of these systems by allowing groups of tail nodes to mutually influence a designated head node. Motivated by these developments, classical diffusion and pattern formation theory is increasingly been extended to higher-order settings such as hypergraphs and simplicial complexes [5, 61, 43].

Existing work on hypergraph dynamical systems has primarily focused on developing higher-order interaction models and characterizing their collective behavior, including synchronization, diffusion, contagion, and pattern formation [47, 48, 20]. While these studies demonstrate that higher-order interactions can qualitatively alter dynamics, they do not address the question of which aspects of that structure are actually visible through the dynamics. In particular, it still remains unclear whether linear and nonlinear dynamical reductions retain the same structural information or reveal different projections of the underlying hypergraph.

The present work addresses this question by developing a structural visibility framework for nonlinear diffusion on directed hypergraphs, showing that linear onset depends only on exposure information, whereas nonlinear saturation progressively reveals additional packing information.

We address this question for a broad class of nonlinear multiway diffusion operators on directed hypergraphs. Our framework is inspired by the DeepSet construction [73], which characterizes permutation-invariant aggregation through symmetric pooling followed by non-

linear activation. While originally developed in the machine learning context [73, 37], the DeepSet viewpoint provides a natural and analytically tractable mechanism for defining genuinely multiway diffusion operators without reducing interactions to pairwise form. In our setting, each directed hyperedge aggregates the states of its tail nodes through a nonlinear activation applied to their mean state, hence preserving both directionality and higher-order coupling structure.

Our first main result shows that the linearized dynamics depends only on first-tail-moment statistics, termed exposure, which yields an induced operator reminiscent of the graph Laplacian. Consequently, hypergraphs that agree in their exposure statistics are linearly indistinguishable: they exhibit identical dispersion relations, critical eigenmodes, and instability thresholds. In particular, all higher-order co-occurrence information inside hyperedges disappears at linear order. This provides a precise explanation for why graph-based surrogates can remarkably well reproduce instability onset despite neglecting higher-order interactions.

Beyond onset however, the weakly nonlinear analysis reveals a fundamentally different picture. Expanding the nonlinear multiway interactions generates higher-order co-occurrence effects associated with joint participation of tail nodes within hyperedges. These effects are encoded structurally through pair and triple packing tensors, but the reduced dynamics does not depend directly on these raw tensors themselves, rather on projected packing effects obtained through contraction with the critical left and right eigenvectors. These projected quantities constitute the dynamically visible part of higher-order hypergraph structure near onset, and they govern nonlinear saturation, branch selection, and pattern morphology.

This reveals a new mechanism absent in purely pairwise systems, namely higher-order interactions can remain completely invisible at linear onset while re-emerging through nonlinear saturation. Consequently, exposure-equivalent systems may become distinguishable only beyond onset despite exhibiting identical linear instability behavior. Building on this principle, we introduce the notion of weak packing-equivalence, which compares only the

higher-order information visible in the reduced dynamics, and we establish nonlinear distinguishability results based on differences in packing effects.

The analysis also leads naturally to a characterization of dynamical graph surrogacy near onset. We show that a hypergraph-coupled system may remain dynamically equivalent to a graph-based system despite the presence of genuine higher-order interactions, provided the corresponding packing effects vanish.

Finally, the weakly nonlinear reduction reveals that the resulting amplitude equations are generically not of Stuart-Landau type. In the generic resonant regime, quadratic nonlinearities survive projection onto the critical mode and dominate saturation near onset. In the nonresonant regime, quadratic contributions vanish, and the leading nonlinear balance is cubic, thus recovering classical Stuart-Landau scaling. These regimes determine the order at which higher-order structure first becomes dynamically observable.

4.3 Hypergraph Background and Directionality

In this section we recall basic notions from hypergraph theory and introduce the directed hypergraph formalism used throughout this chapter. This section establishes the hypergraph objects used throughout, and it fixes notation. We work with directed hypergraphs in which a set of "tail" vertices jointly influences a "head" vertex. This setting captures genuinely higher-order interactions while retaining a notion of directionality that is essential in many applications. Our goal is not to provide a comprehensive survey, but to establish a minimal and consistent set of definitions sufficient to formulate and analyze dynamical systems with higher-order interactions. We also describe a directification procedure that allows undirected hypergraphs to be embedded into the directed framework, ensuring that the theory developed here applies to both settings.

4.3.1 Hypergraphs

A hypergraph (undirected) is a generalization of a graph in which edges can connect more than two vertices simultaneously. Formally, a hypergraph is a pair $\mathcal{H} = (V, E)$, where $V = \{v_1, \ldots, v_N\}$ is a finite set of vertices and $E \subseteq 2^V$ is a collection of hyperedges, each of which is a nonempty subset of vertices. The size of a hyperedge is the number of vertices it contains. Its *rank* $r(\mathcal{H}) := \max_{e \in E} |e|$ is the size of the largest hyperedge, meanwhile the *corank* $c(\mathcal{H}) := \min_{e \in E} |e|$ is the size of its smallest hyperedge.

An undirected hypergraph is said to be k-*uniform* if all its hyperedges are of size k, or equivalently if $r(\mathcal{H}) = c(\mathcal{H}) = k$. In particular, when $k = 2$, the hypergraph reduces to a standard graph.

Allowing hyperedges of arbitrary size enables the modeling of multiway interactions that cannot be decomposed into pairwise effects.

4.3.2 Directed hypergraphs and B-hypergraphs

To describe asymmetric interaction, we work with directed hypergraphs.

Definition 4.1 (Directed hyperedge)**.** *A directed hyperedge (or* hyperarc*) on V is an ordered pair $e = (T(e), H(e))$ of disjoint nonempty subsets of V, where $T(e) \subset V$ is the* tail *set and $H(e) \subset V$ is the* head *set. We assume $T(e) \cap H(e) = \emptyset$ to avoid loops.*

We focus on a particular class known as B-hypergraphs [23] which are sufficient for modeling the dynamics considered here.

Definition 4.2 (B-arc and B-hypergraph)**.** *A hyperarc $e = (T(e), H(e))$ is called a* B-arc *if $|H(e)| = 1$. In this case we write $H(e) = \{v_i\}$ and denote the hyperarc as $e = (T \to v_i)$. A directed hypergraph $\mathcal{H} = (V, E)$ is a* B-hypergraph *if every $e \in E$ is a B-arc.*

Definition 4.3 (k-uniform B-hypergraph)**.** *A B-hypergraph $\mathcal{H} = (V, E)$ is said to be k-uniform if all of its B-arcs have tail size k.*

Oftentimes, it is useful to assign *weights* to each hyperedge in order to encode heterogeneous interaction strengths. This gives rise to notion of *weighted (directed) hypergraph*, namely a triple $\mathcal{H} = (V, E, w)$ where (V, E) is a (directed) hypergraph and $w : E \to \mathbb{R}_{>0}$ assigns a positive weight to each hyperarc.

Note that we will sometimes refer to a node only by its index whenever the context is clear. For instance, $e = (T \to v_i)$ will be sometimes denoted as $e = (T \to i)$.

4.3.3 Order decomposition and uniform B-components

In a B-hypergraph, hyperarcs may have varying tail cardinalities. Since the dynamics will sum over interaction orders, it is convenient to group hyperarcs by order.

Definition 4.4 (Order-k component)**.** *Let $\mathcal{H} = (V, E, w)$ be a B-hypergraph. For each $k \in \{1, \dots, r(\mathcal{H}) - 1\}$, define*

$$E_k := \{e = (T \to i) \in E : \ |T| = k\}, \qquad \mathcal{H}_k := (V, E_k, w|_{E_k}). \tag{4.1}$$

If $E_k \neq \emptyset$, then $\mathcal{H}_k$ is a k-uniform B-hypergraph called the k-uniform B-component of $\mathcal{H}$. Furthermore, the $\mathcal{H}_k$ form a partition of $\mathcal{H}$.

Throughtout this chapter, we sometimes use ρ to denote the hypergraph rank, namely the maximal hyperedge *size* (tail+head), so tails have size at most $\rho - 1$.

4.3.4 Adjacency tensors for uniform B-hypergraphs

Definition 4.5 (Adjacency tensor)**.** *Let $\mathcal{H}_k = (V, E_k, w)$ be a k-uniform B-hypergraph. The adjacency tensor of $\mathcal{H}_k$ is the order-$(k+1)$ tensor $\mathsf{A} \in \mathbb{R}^{N \times N \times \cdots \times N}$ defined as follows*

$$\mathsf{A}^{(k)}_{ij_1\cdots j_k} = \begin{cases} \frac{w(e)}{k!} & \text{if } \; e = (\{v_{j_1}, \cdots, v_{j_k}\}, v_i) \in E \\ \\ 0 & \text{otherwise} \end{cases} \tag{4.2}$$

Remark 4.6. *The normalization used in* (4.2) *is convenient when summing over ordered tuples* $(v_{j_1}, \ldots, v_{j_k})$ *in the dynamical equations. Each unordered tail set* $\{v_{j_1}, \ldots, v_{j_k}\}$ *appears* $k!$ *times under permutations, and the factor* $1/k!$ *exactly cancels this multiplicity. This makes expressions invariant to tail ordering while allowing us to use standard tensor-index summations.*

Furthermore, we note that in general adjacency tensor $\mathsf{A}^{(k)}$ *of a B-hypergraph is not* symmetric. *However by construction, it is symmetric in the tail indices* $j_1, \ldots, j_k$*, namely the* k*-order slices* $\mathsf{A}^{(k)}_{i:\cdots:}$ *are symmetric.*

4.3.5 Degrees for directed B-hypergraphs

For directed graphs, *in-degree* and *out-degree* distinguish incoming from outgoing interactions. In a B-hypergraph, the analogous quantities count incoming and outgoing hyperarcs adjusted for their weights.

Definition 4.7 (in-degree and out-degree)**.** *Let* $\mathcal{H}_k = (V, E_k, w)$ *be a* k*-uniform B-hypergraph. The (weighted)* in-degree *and* out-degree *of vertex* v_i *and are defined as follows:*

$$d^{(k)}_{\text{in}}(v_i) \coloneqq \sum_{e=(T\to v_i)\in E_k} w(e) \tag{4.3}$$

$$d^{(k)}_{\text{out}}(v_i) \coloneqq \sum_{e=(T\to v_h)\in E_k:\, v_i\in T} w(e) \tag{4.4}$$

The intuitive interpretation is that $d^{(k)}_{\text{in}}(v_i)$ measures the total incoming order-k interac-

tion strength into head vertex v_i, whereas $d^{(k)}_{\text{out}}(v_i)$ measures how strongly vertex v_i participates in tails of order-k interactions.

4.3.6 Directification

Our theory is developed for directed B-hypergraphs. To ensure that it also applies to undirected hypergraphs, we introduce a canonical procedure that embeds an undirected hypergraph into the space of B-hypergraphs by replacing each undirected hyperedge by a set of B-arcs.

Definition 4.8 (B-arc set associated with an undirected hyperedge)**.** *Let $\mathcal{H} = (V, E, w)$ be an undirected weighted hypergraph and let $e = \{v_1, \dots, v_p\} \in E$ be a hyperedge of size $p \geq 2$. For each $v_i \in e$, define $e_{\hat{i}} := e \setminus \{v_i\}$ and set*

$$B_{\text{arc}}(e) := \{(e_{\hat{i}} \to v_i) : \ v_i \in e\} \tag{4.5}$$

Definition 4.9 (B-embedding / Directification)**.** *Let $\mathcal{H} = (V, E, w)$ be an undirected weighted hypergraph. Its* B-embedding *(or* directification*) is the weighted B-hypergraph*

$$\widetilde{\mathcal{H}} := (V, \widetilde{E}, \widetilde{w}), \qquad \widetilde{E} := \bigcup_{e \in E} B_{\text{arc}}(e) \tag{4.6}$$

with weights inherited from $\mathcal{H}$ via

$$\widetilde{w}\big(e \setminus \{v\} \to v\big) := w(e) \quad \textit{for each } e \in E, \quad \textit{and} \ \ v \in e \tag{4.7}$$

The B-embedding replaces an undirected group interaction among p vertices by the p directed influences in which each vertex acts as a head receiving influence from the remaining $p - 1$ vertices. This choice preserves the permutation symmetry of the original undirected hyperedge while producing a directed structure compatible with our theory.

Directification example

Let $V = \{1, 2, 3, 4\}$, and consider the undirected 3-uniform hypergraph with hypergraphs $e_1 = \{2, 3, 4\}$ and $e_2 = \{1, 2, 4\}$ with weight $w(e_1) = \omega = w(e_2)$ shown in Figure 4.1. Then the B-arc set associated with e_1 is $B_{\text{arc}}(e_1) = \{(\{3, 4\} \to 2), (\{2, 4\} \to 3), (\{2, 3\} \to 4)\}$ and each resulting B-arc has weight ω as shown in Figure 4.2. Similarly we have $B_{\text{arc}}(e_2) = \{(\{2, 4\} \to 1), (\{1, 4\} \to 2), (\{1, 2\} \to 4)\}$.



Figure 4.1: A 3-uniform hypergraph on four nodes with hyperedges $e_1 = \{2, 3, 4\}$ and $e_2 = \{1, 2, 4\}$.

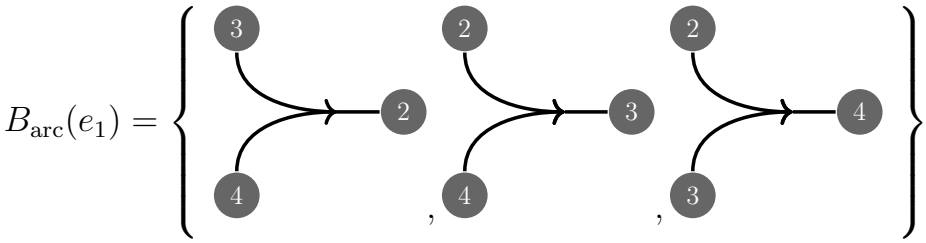

Figure 4.2: The B-arc set associated with the hyperedge $e_1 = \{2, 3, 4\}$, obtained by selecting each node in turn as the head node while the remaining nodes form the tail set.

Remark 4.10 (Relevance of directification)**.** *All results proved for directed B-hypergraphs apply to undirected hypergraphs by first applying the B-embedding and then interpreting the resulting directed dynamics as the natural directed representation of the original undirected group interactions.*

4.3.7 Symmetric B-hypergraphs

Definition 4.11 (Complement B-arc set)**.** *Let $\mathcal{H} = (V, E, w)$ be a uniform B-hypergraph, and consider the B-arc $e = (T(e), h) \in E$. We define the* complement B-arc set $\bar{B}_{arc}(e)$ *of e as follows:*

$$\bar{B}_{arc}(e) = \{(T_{\hat{v}}(e) \cup \{h\}, v) \mid v \in T(e)\} \tag{4.8}$$

where $T_{\hat{v}}(e) = T(e) \setminus \{v\}$

The notion of *complement arc set* defined above allows us to give precise definition of *symmetric B-hypergraphs* which generalizes the notion of *bidirectional graphs*.

Definition 4.12 (Symmetric Uniform B-hypergraph)**.** *Let $\mathcal{H} = (V, E, w)$ be a uniform B-hypergraph. $\mathcal{H}$ is said to be* symmetric *if its hyperarc set E is* closed under B-arc set complementation. *More specifically, $\mathcal{H}$ is symmetric if the following holds:*

$$\bar{B}_{arc}(e) \subset E \quad \textit{whenever } e \in E \tag{4.9}$$

Proposition 4.13. *Let $\mathcal{H} = (V, E, w)$ be a symmetric uniform B-hypergraph. The adjacency tensor (see 4.2) of $\mathcal{H}$ is symmetric.*

Proof. It follows by construction. ■

Proposition 4.14. *Let $\mathcal{H} = (V, E, w)$ be a uniform undirected hypergraph. Its B-embedding $\tilde{\mathcal{H}}$ is a symmetric B-hypergraph.*

Proof. The map

$$\imath\colon \{\text{Undirected Hypergraphs}\} \hookrightarrow \{\text{Symmetric B-hypergraphs}\}$$

that sends an undirected hypergraph $\mathcal{H}$ to its B-embedding $\tilde{\mathcal{H}} = \imath(\mathcal{H})$ is an injection that preserves symmetry. ■

Remark 4.15. *Let $\mathcal{H}$ be a B-hypergraph of rank $\rho = r(\mathcal{H}) \geq 2$. It is fairly straightforward to see that $\mathcal{H}$ can be partitioned into its* uniform components*, say $\mathcal{H}_k$. Each of which is a $(k+1)$-uniform B-hypergraph. More specifically we have*

$$\mathcal{H} = \cup_{k=1}^{\rho-1} \mathcal{H}_k \tag{4.10}$$

4.4 A Unifying Framework for Dynamical Systems on Directed Hypergraphs

We now introduce a general framework for defining and analyzing dynamical systems on directed B-hypergraphs. The framework accommodates higher-order directed interactions between groups of nodes, supports multi-dimensional node states, and it includes a wide and flexible class of coupling mechanisms. It is sufficiently general to recover many classical network dynamical systems as special cases, while providing a systematic extension to directed hypergraph settings.

4.4.1 Dynamical systems on hypergraphs

We consider a system of N identical dynamical units (nodes or agents), indexed by $i \in \{1, \ldots, N\}$. The state of node i is denoted by $x_i(t) \in \mathbb{R}^d$, where $d \geq 1$ is the dimension of the local state space. In isolation, each node evolves according to the same intrinsic dynamics

$$\dot{x}_i = f(x_i) \tag{4.11}$$

where $f : \mathbb{R}^d \to \mathbb{R}^d$ is assumed to be sufficiently smooth. The joint state of the system is

$$\mathbf{x} = (x_1, \ldots, x_N) \in (\mathbb{R}^d)^N \cong \mathbb{R}^{Nd}$$

Let $\mathcal{H} = (V, E, w)$ be a B-hypergraph of rank $\rho \geq 2$ modeling the interaction of these N agents. As discussed in Definition 4.4, $\mathcal{H}$ can be partitioned into uniform B-components $\{\mathcal{H}_k\}_{k=1}^{\rho-1}$ collecting all hyperarcs of tail size k. Each uniform component $\mathcal{H}_k$ is encoded by an order-$(k+1)$ adjacency tensor $\mathsf{A}^{(k)}$ with entries $\mathsf{A}^{(k)}_{ij_1\cdots j_k}$ as defined in Definition 4.5. The first mode corresponds to the head index, while the remaining k modes correspond to the tail indices.

Definition 4.16 (Dynamical system on directed hypergraphs)**.** *A* dynamical system on a directed hypergraph $\mathcal{H}$ *is a system of ordinary differential equations of the form*

$$\dot{x}_i = f(x_i) + \sum_{k=1}^{\rho-1} \sum_{j_1,\ldots,j_k} \mathsf{A}^{(k)}_{ij_1\cdots j_k}\, \phi_k(x_{j_1}, \ldots, x_{j_k}, x_i), \qquad i = 1, \ldots, N \tag{4.12}$$

where for each k, the coupling function

$$\phi_k : (\mathbb{R}^d)^k \times \mathbb{R}^d \to \mathbb{R}^d$$

is a sufficiently smooth function that specifies how the states of the k tail nodes jointly influence the head node.

The following proposition gives an equivalent formulation of the dynamical system (4.12) under additional symmetry assumption. This formulation turns out to be more for computationally tractable.

Proposition 4.17 (Hyperedge formulation)**.** *Assume that for each order k, the coupling function ϕ_k is symmetric in its k tail arguments. Then the tensor formulation given in* (4.12) *is equivalent to the hyperedge-sum formulation*

$$\dot{x}_i = f(x_i) + \sum_{k=1}^{\rho-1} \sum_{e=(T\to i)\in E_k} w(e)\, \phi_k\big((x_j)_{j\in T}, x_i\big) \tag{4.13}$$

where E_k denotes the set of k-hyperedges.

Proof. Fix i and k. For any hyperedge $e = (T \to i)$ with $|T| = k$, the unordered tail set T appears in (4.12) through all $k!$ permutations of its elements. Since $A^{(k)}_{ij_1\cdots j_k} = \frac{w(e)}{k!}$ for each such ordering, the contribution of e to (4.12) is $\frac{w(e)}{k!}\sum_{\pi\in S_k}\phi_k(x_{j_{\pi(1)}},\ldots,x_{j_{\pi(k)}},x_i)$, where $\pi \in S_k$ is a permutation on k symbols. By symmetry of ϕ_k in the tail arguments, each term in the sum is identical, so this reduces to $\frac{w(e)}{k!}\cdot k!\,\phi_k\big((x_j)_{j\in T},x_i\big) = w(e)\,\phi_k\big((x_j)_{j\in T},x_i\big)$. Summing over all k-hyperedges with head i yields (4.13). ■

4.5 Aggregator-Mixer coupling structure

Although there is a lot of flexibility in choosing the coupling functions ϕ_k in (4.12), many applications share a common structure in which the states of the tail nodes are first aggregated into a collective signal, then mixed into the head node dynamics. To capture this structure, we propose the following flexible class of coupling functions

$$\phi_k(x_{j_1},\cdots,x_{j_k},x_i) = M_k\Theta_k\big(\alpha_k\psi_k(x_{j_1},\cdots,x_{j_k}) + \beta_k h_k(x_i)\big) \tag{4.14}$$

where:

- $\psi_k : (\mathbb{R}^d)^k \to \mathbb{R}^d$ is a permutation-invariant function termed *aggregator* or *tail function*.
- $\Theta_k : \mathbb{R}^d \to \mathbb{R}^d$ is the *mixer*. This function could be linear or nonlinear.
- $h_k : \mathbb{R}^d \to \mathbb{R}^d$ is the *head function*.
- $M_k \in \mathbb{R}^{d\times d}$ is the mixing matrix.
- $\alpha_k, \beta_k \in [-1, 1]$ are *gates*.

From a modeling standpoint, there is a lot of versatility in the use of the mixing matrix M_k. For instance,

1. It can encode the *coupling strength parameter* whenever it is a multiple of the identity matrix, namely $M_k = \lambda_k I_d$, for some $\lambda_k \in \mathbb{R}$.

2. It can model a *channel-wise selector operator* that controls cross-channel coupling as in [46].

3. It can encode the *species diffusion matrix* in reaction-diffusion systems. *This is the point of view we will adopt throughout this chapter, where M_k will be the diagonal matrix of diffusion coefficients.*

4. Lastly, it can be factored into a product of relevant matrices to encode any combination of the above accordingly.

4.5.1 Relation to existing models and unifying perspective

The framework (4.12)–(4.14) subsumes a variety of classical dynamical systems as special cases while providing a systematic mechanism for extending them to directed hypergraph interactions.

In the rank-2 case (i.e. $\rho = 2$), the adjacency tensor reduces to the standard adjacency matrix associated with directed graphs. Choosing linear aggregator and mixing functions,

$$\psi(x) = x, \qquad \Theta = \mathrm{Id} \tag{4.15}$$

the framework recovers classical diffusive or consensus-type coupling on directed networks [55, 59, 3].

For scalar phase variables, suitable choices of linear aggregator, head function, and trigonometric mixer recover Kuramoto-type dynamics [34, 1, 66]. For example, taking

$$\Theta(x) = \sin(x) \tag{4.16}$$

in the rank-2 setting yields the classical Kuramoto model on directed graphs, while the case $\rho > 2$ produces higher-order generalizations of Kuramoto dynamics on directed hypergraphs. More details are provided in section A.4 in the appendix.

The framework also encompasses tensor-based multilinear hypergraph systems previously studied in [14]. In particular, choosing

$$\Theta_k = \mathrm{Id}, \qquad h_k \equiv 0 \tag{4.17}$$

together with the multiplicative (Hadamard product) aggregator

$$\psi_k(x_{j_1}, \ldots, x_{j_k}) = x_{j_1} \odot x_{j_2} \odot \cdots \odot x_{j_k} \tag{4.18}$$

recovers and extends multilinear tensor interactions to directed hypergraphs.

When combined with local reaction terms f, diagonal mixing matrices M_k, linear mixers $\Theta_k = \mathrm{Id}$, and diagonal head functions, the framework also recovers reaction-diffusion systems on network structures [50, 47].

In general, the proposed aggregator-mixer formulation provides a flexible architecture for modeling nonlinear multiway interactions. Appropriate choices of aggregator, mixer, and head functions allow the framework to capture threshold effects, saturation phenomena, cooperative interactions, and other nonlinear mechanisms arising in biological, social, and physical systems. The few examples given above illustrate that the proposed framework is not tied to a single dynamical model, but instead it provides a unifying perspective on higher-order dynamical systems. See Appendix A for additional information.

4.6 Reaction-Diffusion on B-hypergraphs and Laplacian dynamics

We now specialize the general framework above to the diffusive coupling regime, and we show how a natural Laplacian-type structure emerges at the tensorial level. This case provides the direct higher-order analogue of classical Laplacian-driven dynamics on graphs. It plays a central role in pattern formation analysis, and it clarifies the structural origin of the operators

appearing in the subsequent linear and weakly nonlinear analyses.

4.6.1 Diffusive coupling

We say that the coupling function in (4.12) is *diffusive* if for each interaction order k, it takes the form

$$\phi_k(x_{j_1}, \ldots, x_{j_k}, x_i) = M_k\Big(\psi_k(x_{j_1}, \ldots, x_{j_k}) - \psi_k^{\Delta}(x_i)\Big). \tag{4.19}$$

This corresponds to choosing $\Theta_k = \mathrm{Id}$, and a *diagonal head function* $h_k(x_i) = \psi_k^{\Delta}(x_i) \coloneqq \psi_k(x_i, \cdots, x_i)$ in (4.14) for some smooth and permutation-invariant aggregator ψ_k. The defining feature of (4.19) is that the coupling depends only on differences between aggregated tail states and the head state, ensuring that the interaction vanishes identically on homogeneous configurations (4.20).

Definition 4.18. *The synchronization manifold $\mathcal{S}$ of system* (4.12) *is the subspace of the joint state space along which the states of all agents coincide. More specifically,*

$$\mathcal{S} \coloneqq \big\{(x_1, \cdots, x_N) \in \mathbb{R}^{Nd} \mid x_i = x_j,\ \forall\ i, j = 1, \cdots, N\big\} \tag{4.20}$$

Note that coupling (4.19) vanishes on the synchronization manifold (4.20). In fact, this is one of the most important properties of *diffusive coupling*.

4.6.2 Laplacian tensor formulation

Substituting (4.19) into (4.12), we get a higher-order reaction-diffusion dynamics involving the Laplacian tensor as follows

$$
\begin{aligned}
\dot{x}_i &= f(x_i) + \sum_{k=1}^{\rho-1} \sum_{j_1,\cdots,j_k} \mathsf{A}^{(k)}_{ij_1\cdots j_k} M_k \left(\psi_k(x_{j_1},\cdots,x_{j_k}) - \psi_k^{\Delta}(x_i)\right) \\
&= f(x_i) - \sum_{k=1}^{\rho-1} \sum_{j_1,\cdots,j_k} \left(d^{(k)}_{\text{in}}(v_i)\delta_{ij_1\cdots j_k} - \mathsf{A}^{(k)}_{ij_1\cdots j_k}\right) M_k \psi_k(x_{j_1},\cdots,x_{j_k}) \\
&= f(x_i) - \sum_{k=1}^{\rho-1} \sum_{j_1,\cdots,j_k} \mathsf{L}^{(k)}_{ij_1\cdots j_k} M_k \psi_k(x_{j_1},\cdots,x_{j_k})
\end{aligned} \tag{4.21}
$$

where, $d^{(k)}_{in}(v_i)$ is the in-degree of the head node v_i as in Definition 4.7, δ is the order-$(k+1)$ Kronecker diagonal tensor defined as follows

$$
\delta_{ij_1\cdots j_k} := \begin{cases} 1 & \text{if } j_1 = \cdots = j_k = i, \\ 0 & \text{otherwise.} \end{cases} \tag{4.22}
$$

and, $\mathsf{L}^{(k)} = \mathsf{D}^{(k)} - \mathsf{A}^{(k)}$ is the order-$(k+1)$ *Laplacian tensor* associated with the uniform B-component $\mathcal{H}_k$ at interaction order k. $\mathsf{D}^{(k)}$ is the order-$(k+1)$ diagonal *in-degree tensor* at interaction order k defined as follows

$$
\mathsf{D}^{(k)}_{ij_1\cdots j_k} := \begin{cases} d^{(k)}_{\text{in}}(v_i) & \text{if } j_1 = \cdots = j_k = i, \\ 0 & \text{otherwise.} \end{cases} \tag{4.23}
$$

4.7 Model specification

DeepSet models [73] provide a natural framework for modeling permutation-invariant multiway interactions through a combination of elementwise transformations and symmetric pooling operations. The general structure of such aggregators takes the form

$$
\psi_k = \sigma_k \circ \text{mean} \circ \lambda_k \tag{4.24}
$$

where $\lambda_k : \mathbb{R}^d \to \mathbb{R}^d$ denotes an embedding transformation and $\sigma_k : \mathbb{R}^d \to \mathbb{R}^d$ represents an elementwise activation.

Throughout this work, we set the embedding map to the identity transformation, $\lambda_k = \mathrm{Id}$, and we concentrate on the simplified mean-pooling followed by an elementwise activation structure as follows

$$\psi_k(x_{j_1}, \ldots, x_{j_k}) = \sigma_k \left(\frac{1}{k} \sum_{r=1}^{k} x_{j_r} \right) \tag{4.25}$$

with σ_k chosen as a *sigmoid*, *tanh*, *Hill-type* nonlinearity, or any other sufficiently smooth *nonlinear* saturating activation. This particular choice preserves the core permutation-invariant properties characteristic of DeepSet-type models, while isolating the role of nonlinear activation in shaping diffusion and pattern formation, which is the focus of our subsequent analysis. Under this specification, the coupling term takes the form

$$\phi_k(x_{j_1}, \ldots, x_{j_k}, x_i) = M_k \left[\sigma_k \left(\frac{1}{k} \sum_{r=1}^{k} x_{j_r} \right) - \sigma_k(x_i) \right] \tag{4.26}$$

which will be the form used for the analysis throughout the remainder of this work. We note that the activation σ and the mixing matrix M are fixed and independent of the interaction order k, and all k-dependence enter only through the hypergraph structure.

The framework introduced in this section separates structure (encoded by the tensors $\mathsf{A}^{(k)}$) from dynamics (encoded by f, σ, and M). This separation will allow us to identify which contractions of $\mathsf{A}^{(k)}$ control linearized dynamics near homogeneous equilibria in (4.20), and which higher-order contractions enter nonlinear saturation. In particular, in Section 4.8 and Section 4.10 we will show that different dynamical regimes are associated with different tensorial marginals of the same underlying hypergraph structure.

4.8 Linear Dynamics and Pattern Onset

In this section, we derive the linearization of the hypergraph reaction-diffusion system (4.21) about a homogeneous equilibrium, namely one that belongs to the synchronization manifold (4.20), and we show that it depends only on the *first-moment* (exposure) statistics of the underlying hypergraph structure. This yields a Laplacian operator governing linear stability and reminiscent of graph settings. It also establishes a rigorous validity boundary for graph-based surrogates, and provides a rigorous justification for why clique-expansion reductions are quite successful at the level of pattern formation onset. This result forms the basis for all subsequent analysis.

We start with the following useful definition and lemma. The choice of the adjective "canonical" in Definition 4.19 is justified by the fact the object therein described "naturally" arises from the dynamics as we will see later.

Definition 4.19 (Canonical Higher Order Matrix)**.** *Let $\mathsf{T} \in I_0 \times I_1 \times \cdots \times I_k$ be an order-$(k+1)$ tensor, where $I_r = \mathbb{R}^N$. For $l \in \{1, \cdots, k\}$, we define the k-th order l-pointed Canonical Higher Order Matrix or $\hat{l}$-CHOM of T as the following tensor contraction using tensor notation in* [33]

$$T^{\hat{l}} = \langle \mathsf{T}, \mathsf{1}_{k-1} \rangle_{\{1,\cdots,l-1,l+1,\cdots,k\}} \tag{4.27}$$

$$= \mathsf{T} \bar{\times}_{-\{0,l\}} \{\mathbf{1}\} \tag{4.28}$$

where $\mathbf{1}$ is the N-dimensional vector of all-ones , and $\mathsf{1}_{k-1} = \mathbf{1}^{\otimes(k-1)}$ is the order-(k-1) tensor of all-ones.

Lemma 4.20 (Symmetry and Contraction Invariance)**.** *Let $\mathsf{T} \in \mathbb{R}^{n_0 \times n^k}$ be an order-$(k+1)$ tensor written as $\mathsf{T}_{ij_1\cdots j_k}$ in coordinates, where $i \in \{1, \cdots, n_0\}$ and $j_l \in \{1, \cdots, n\}$ for all $1 \le l \le k$. Assume T is symmetric in the last k tail indices, namely for every permutation $\tau \in S_k$, we have $\mathsf{T}_{ij_1\cdots j_k} = \mathsf{T}_{ij_{\tau(1)}\cdots j_{\tau(k)}}$. Then the $\hat{l}$-CHOM of T is independent of l. More*

specifically, for any $l, l' \in \{1, \cdots, k\}$, we have $T^{\hat{l}}_{ij} = T^{\hat{l}'}_{ij}$ for all i, j.

Proof. See Appendix B.1 ■

Lemma 4.20 above allows us to unambiguously define the notion of *tail moments* of tail-symmetric tensors. As we will see in this section and the next, these tail moments play a fundamental role in the mechanism of pattern formation, both at instability onset and in the subsequent nonlinear regime.

4.8.1 Structural visibility hierarchy

Definition 4.21 (p-th tail moment tensor)**.** *Let $\mathcal{H}_k = (V, E_k, w)$ be a k-uniform B-hypergraph. For an interger $p \in \{0, 1, \cdots, k\}$, the p-th tail moment tensor is the order-$(p+1)$ tensor*

$$\mathsf{T}^{(k,p)}_{ij_1\cdots j_p} \coloneqq \sum_{\substack{e=(T\to v_i)\in E_k,\\ \{j_1,\cdots,j_p\}\in T}} \frac{w(e)}{k^p} \tag{4.29}$$

Structural Dictionary: The tensors $\mathsf{T}^{(k,p)}$ define a hierarchy of tail co-occurrence moments associated with order-k directed hyperedges. The first few tail moments recover familiar structural quantities:

$$\mathsf{T}^{(k,0)} = d^{(k)}_{\text{in}}, \qquad \text{(in-degree vector, see 4.3)} \tag{4.30}$$

$$\mathsf{T}^{(k,1)}_{ij} = A^{(k)}_{ij}, \qquad \text{(exposure matrix/}k\text{-th order CHOM, see 4.45)} \tag{4.31}$$

$$\mathsf{T}^{(k,2)}_{ij\ell} = \mathsf{P}^{(k)}_{ij\ell}, \qquad \text{(pair packing tensor, see 4.70)} \tag{4.32}$$

$$\mathsf{T}^{(k,3)}_{ij\ell m} = \mathsf{T}^{(k)}_{ij\ell m}, \qquad \text{(triple packing tensor, see 4.70)} \tag{4.33}$$

More generally, $\mathsf{T}^{(k,p)}$ encodes p-fold tail co-occurrence statistics for order-k hyperedges pointing to node v_i. Note that only the off-diagonal (i.e. distinct tail indices) elements capture genuine p-way interactions.

The tail moments are related to contractions of the adjacency tensor as follows

Proposition 4.22 (p-th tail moments as tensor contraction)**.** *Let* $\mathsf{A}^{(k)}$ *denote the order-*$(k+1)$ *adjacency tensor of the* k*-uniform B-component* $\mathcal{H}_k$*. For an integer* $p \in \{0, 1, \ldots, k\}$ *and distinct tail indices* $j_1, \ldots, j_p$*, define the order-*$(p+1)$ *tensor*

$$\mathsf{A}^{(k,p)} = \frac{(k)_p}{k^p} \left\langle \mathsf{A}^{(k)}, 1_{k-p} \right\rangle_{\{p+2,\ldots,k+1\}}, \tag{4.34}$$

where $(k)_p = k(k-1)\cdots(k-p+1)$ *is the falling factorial and* 1_{k-p} *is the all-ones tensor of order* $k-p$*.*

Then the p*-th tail moment tensor satisfies*

$$\mathsf{T}^{(k,p)}_{ij_1\cdots j_p} = \mathsf{A}^{(k,p)}_{ij_1\cdots j_p}. \tag{4.35}$$

Equivalently, letting $\mathbf{1} \in \mathbb{R}^N$ *denote the all-ones vector and* $\times_n$ *the mode-n product,*

$$\mathsf{T}^{(k,p)} = \frac{(k)_p}{k^p} \mathsf{A}^{(k)} \times_{p+2} \mathbf{1}^\top \times_{p+3} \mathbf{1}^\top \times \cdots \times_{k+1} \mathbf{1}^\top. \tag{4.36}$$

Proof. See Appendix B.2 ■

Structural Visibility: One of the main take away of the the present work is establishing that *different asymptotic orders of the dynamical reduction reveal different tail moments.* Figure 4.3 summarizes this principle.

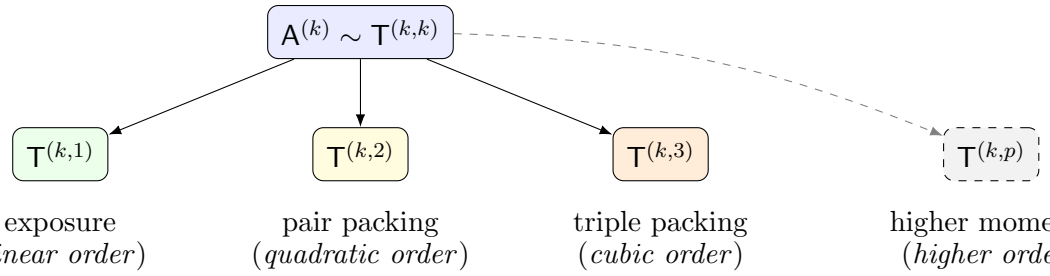

Figure 4.3: Visibility hierarchy structure illustrating the principle by which *different asymptotic orders of the dynamical reduction reveal different tails moments*. This is one of the main take away of the present work. We show that at *linear order*, the only structural information visible to the dynamics is *exposure*, and everything else is discarded. Higher-order interactions only become relevant in the nonlinear regime. More specifically, at *quadratic order*, the dynamics sources *pair packing* structural information encoded in the tail moment tensor $\mathsf{T}^{(k,2)}$, then contracts it with the critical directions to build the *second* order coefficient β of the reduced dynamics (see (4.61)). At *cubic order*, the dynamics probes *triple packing* structural information encoded in the tensor $\mathsf{T}^{(k,3)}$ in addition to pair packing information in $\mathsf{T}^{(k,2)}$ to build the *cubic* order coefficient γ through contraction with the critical directions as well. The process can be continued accordingly.

4.8.2 Linearization about a reference trajectory

We linearize (4.21) about a reference trajectory $\bar{\mathbf{x}}(t) = (\bar{x}_1(t), \cdots, \bar{x}_N(t))$, this leads to the linear dynamics describing the evolution of small perturbations around $\bar{\mathbf{x}}(t)$ as follows:

$$\dot{\delta\mathbf{x}} = J(\bar{\mathbf{x}})\delta\mathbf{x} \tag{4.37}$$

where

$$J(\bar{\mathbf{x}}) = \big(J_{i,\lambda}(\bar{\mathbf{x}})\big)_{i,\lambda} \tag{4.38}$$

is the $Nd \times Nd$ block-matrix whose $d \times d$ block entry $J_{i,\lambda}$ represents the *sensitivity* of the right hand side ($RHS(i)$) of (4.21) with respect to the state x_λ. More specifically, for any $1 \leq \lambda \leq N$ we have

$$J_{i,\lambda}(\bar{\mathbf{x}}) = \frac{\partial RHS(i)}{\partial x_\lambda}\Big|_{(\bar{\mathbf{x}})} \tag{4.39}$$

where,

$$\begin{aligned}\frac{\partial RHS(i)}{\partial x_\lambda}\Big|_{(\bar{\mathbf{x}})} &= \frac{\partial f}{\partial x}(\bar{x}_i)\frac{\partial x_i}{x_\lambda} - \sum_{k=1}^{\rho-1}\sum_{j_1,\cdots,j_k} \mathsf{L}^{(k)}_{ij_1\cdots j_k} M_k \sum_{l=1}^{k} \frac{\partial \psi_k}{\partial x_l}(\bar{x}_{j_1},\cdots,\bar{x}_{j_k})\frac{\partial x_{j_l}}{x_\lambda} \\ &= \frac{\partial f}{\partial x}(\bar{x}_i)\delta_{i\lambda} - \sum_{k=1}^{\rho-1}\sum_{l=1}^{k}\sum_{j_l=1}^{N}\left(\sum_{\hat{j}_l} \mathsf{L}^{(k)}_{ij_1\cdots j_k} M_k \frac{\partial \psi_k}{\partial x_l}(\bar{x}_{j_1},\cdots,\bar{x}_{j_k})\delta_{j_l\lambda}\right)\end{aligned} \tag{4.40}$$

The summation over $\hat{j}_l$ means that we are summing over all the indices j_r *except* j_l, and δ_{ij} is the usual Kronecker delta.

We now constrain the reference trajectory $\bar{\mathbf{x}}(t)$ to lie in the *synchronization manifold* $\mathcal{S}$ (4.20), thus (4.40) becomes

$$\frac{\partial RHS(i)}{\partial x_\lambda}\Big|_{(\bar{\mathbf{x}})} = \frac{\partial f}{\partial x}(\bar{x})\delta_{i\lambda} - \sum_{k=1}^{\rho-1}\sum_{l=1}^{k}\sum_{j_l=1}^{N} \mathsf{L}^{(k),\hat{l}}_{ij_l} M_k \frac{\partial \psi_k}{\partial x_l}(\bar{x},\cdots,\bar{x})\delta_{j_l\lambda} \tag{4.41}$$

where $\mathsf{L}^{(k),\hat{l}}$ is the k-th order $\hat{l}$-CHOM of the Laplacian tensor defined in section 4.6.2. In fact using Lemma 4.20, one can show that this operator is *independent of* l. So, we refer to it as the k-th order CHOL (Canonical Higher Order Laplacian).

The λ-th column of the block Jacobian matrix $J(\bar{\mathbf{x}})$ on $\mathcal{S}$ therefore reads:

$$\mathbf{e}_\lambda \otimes \frac{\partial f}{\partial x}(\bar{x}) - \sum_{k=1}^{\rho-1}\sum_{l=1}^{k}\left(\mathsf{L}^{(k),\hat{l}} \otimes M_k\right)\left(\mathbf{e}_\lambda \otimes \frac{\partial \psi_k}{\partial x_l}(\bar{x},\cdots,\bar{x})\right) \tag{4.42}$$

where $\{\mathbf{e}\}_{1\le i\le N}$ is the canonical basis of $\mathbb{R}^N$. Putting everything together, we get the final form of the Jacobian matrix $J(\bar{\mathbf{x}})$ as follows:

$$\begin{aligned}J(\bar{\mathbf{x}}) &= I_N \otimes \frac{\partial f}{\partial x}(\bar{x}) - \sum_{k=1}^{\rho-1}\sum_{l=1}^{k}\left(\mathsf{L}^{(k),\hat{l}} \otimes M_k\right)\left(I_N \otimes \frac{\partial \psi_k}{\partial x_l}(\bar{x},\cdots,\bar{x})\right) \\ &= I_N \otimes \frac{\partial f}{\partial x}(\bar{x}) - \sum_{k=1}^{\rho-1}\left(L^{(k)} \otimes M_k \sum_{l=1}^{k}\frac{\partial \psi_k}{\partial x_l}(\bar{x},\cdots,\bar{x})\right)\end{aligned} \tag{4.43}$$

where by Lemma 4.20, the k-th order CHOL matrix $L^{(k)}$ satisfies

$$L^{(k)} = \mathsf{L}^{(k),\hat{l}^*} \, for \; any \; l^* \in \{1, \dots, k\} \tag{4.44}$$

It is worth pointing out that this operator is *not symmetric* in general. In the undirected setting however, it is closely related to the *Laplacian of the clique-expansion* of the k-uniform component of the underlying hypergraph. We will not develop this connection further here, and leave it for future communications.

From tensor contraction of the decomposition $\mathsf{L}^{(k)} = \mathsf{D}^{(k)} - \mathsf{A}^{(k)}$, together with tail index symmetry in Lemma 4.20 we get

$$L^{(k)} = D_{\text{in}}^{(k)} - A^{(k)} \qquad 1 \leq k \leq N \tag{4.45}$$

where $D_{\text{in}}^{(k)}$ is the diagonal matrix of node in-degrees at interaction order k, and $A^{(k)}$ is the k-th order CHOM of the adjacency tensor $\mathsf{A}^{(k)}$. Therefore, the vector $d_{\text{in}}^{(k)} = \text{diag}\left(D_{\text{in}}^{(k)}\right)$ and the matrix $A^{(k)}$ can be viewed respectively as the *zeroth* and *first tail moments* of the tensor $\mathsf{A}^{(k)}$ by Definition 4.21.

4.9 Working assumptions

Although the linearization derived above applies to general multiway coupling functions in (4.19), we now focus attention on a regime in which the *mechanism governing pattern onset and saturation* can be clearly isolated.

Order-independent coupling: From now onward, we fix the aggregator in the class (4.25) defined in section 4.7, and we assume that it is independent of the interaction order k. This is equivalent to fixing the same activation function σ across all the interaction layers. In addition, we also fix the mixing matrix M. Order dependence enters only through the directed hypergraph structure and its relevant tensors.

Regularity: The reaction term f and activation function σ are assumed to be sufficiently smooth to admit a Taylor expansion about the homogeneous equilibrium $\bar{\mathbf{x}} \in \mathcal{S}$ up to at least third order, as required for the weakly nonlinear analysis in the next section.

Codimension-1 steady bifurcation: For clarity of the presentation, we focus only on *steady instability* in the present work. More specifically, we assume there exists a critical parameter value p_c (e.g. inhibitor diffusion coefficient) at which the linearized operator $J(\bar{\mathbf{x}})$ has a simple eigenvalue at zero, while all remaining eigenvalues have strictly negative real parts. Equivalently,

$$\dim \ker J(\bar{\mathbf{x}}) = 1 = \dim \ker (J(\bar{\mathbf{x}}))^\dagger \tag{4.46}$$

where $(J(\bar{\mathbf{x}}))^\dagger$ denotes the adjoint of the operator $J(\bar{\mathbf{x}})$ with respect to the standard Euclidean inner product.

Oscillatory (Hopf) instabilities and higher-codimension bifurcations are not considered here and are left for future work.

4.9.1 Linearization theorem

Under the nonlinear mean-aggregator (4.25), the Jacobian (4.43) simplifies drastically. In particular, the matrix multiplying each operator $L^{(k)}$ is independent of the interaction order k. As a result, the Jacobian depends on the hypergraph only through its zeroth and first tail moments.

Theorem 4.23 (First tail-moment reduction)**.** *Let $\bar{\mathbf{x}}$ be a homogeneous equilibrium of* (4.12) *under nonlinear mean coupling* (4.26)*. Then the linearized dynamics about $\bar{\mathbf{x}}$ reads*

$$\dot{\delta\mathbf{x}} = \left(I_N \otimes J_f - \sum_{k=1}^{\rho-1} L^{(k)} \otimes D_{\text{eff}} \right) \delta\mathbf{x} \tag{4.47}$$

or equivalently,

$$\dot{\delta\mathbf{x}} = \big(I_N \otimes J_f - L_{\text{tot}} \otimes D_{\text{eff}}\big)\delta\mathbf{x} \tag{4.48}$$

where $J_f = Df(\bar{x})$, $D_{\text{eff}} = MD\sigma(\bar{x})$ *and* $L_{\text{tot}} = \sum_{k=1}^{\rho-1} L^{(k)}$.

In particular, the hypergraph influences the Jacobian only through its zeroth and first tail moments, namely the exposure information.

Proof. It follows from (4.43) under the working assumptions (4.9) and (4.9). ■

The theorem above shows that linear stability and Turing onset depend only on the zeroth and first tail moments of the adjacency tensor. The linearized operator is fully determined by these moments. Higher-order tail moments are invisible at linear level, and they reappear only through nonlinear terms. This separation underlies the mechanism developed in the Section 4.10.

4.9.2 Directed dispersion relation

We start with the following Lemma 4.24 which characterizes the spectrum of the Jacobian in (4.48).

Lemma 4.24. *Let* $\bar{\mathbf{x}} \in \mathcal{S}$ *be a homogeneous equilibrium of* (4.12) *under nonlinear mean coupling* (4.26), $J_f = Df(\bar{x})$, $L_{\text{tot}} \in \mathbb{R}^{N\times N}$ *and* $D_{\text{eff}} \in \mathbb{R}^{d\times d}$. *The spectrum* $\sigma(J)$ *of the jacobian* $J = I_N \otimes J_f - L_{\text{tot}} \otimes D_{\text{eff}}$ *of the system is given by*

$$\sigma(J) = \bigcup_{\lambda\in\sigma(L_{\text{tot}})} \sigma\left(J_f - \lambda\, D_{\text{eff}}\right) \tag{4.49}$$

Proof. It relies on the Schur decomposition (see, e.g., [26, 24, 69]) as follows: Let $U^* L_{\text{tot}} U = T$ for some unitary matrix U and upper triangular matrix T. Then we have $(U^* \otimes I_d)\, L_{\text{tot}}\, (U \otimes$

$I_d) = I_N \otimes J_f - T \otimes D_{\text{eff}}$. The latter matrix is block upper triangular with diagonal blocks $J_f - \lambda_i D_{\text{eff}}$, where the λ_i's are the eigenvalues of L_{tot} along the diagonal of T. ■

Definition 4.25 (Generalized dispersion relation)**.** *For each $\lambda \in \mathbb{C}$, define the linear operator $A(\lambda) := J_f - \lambda D_{\text{eff}} \in \mathbb{R}^{d\times d}$. The associated* generalized dispersion relation *is the function*

$$\omega(\lambda) := \max\left\{\Re(\nu) \,:\, \nu \in \sigma\big(A(\lambda)\big)\right\} \tag{4.50}$$

By Lemma 4.24, the spectrum of the Jacobian $J = I_N \otimes J_f - L_{\text{tot}} \otimes D_{\text{eff}}$ is obtained by evaluating the spectra $\sigma(A(\lambda))$ over all $\lambda \in \sigma(L_{\text{tot}})$. Thus, the homogeneous equilibrium is linearly stable if and only if $\omega(\lambda) < 0, \quad \forall \lambda \in \sigma(L_{\text{tot}})$. Instability onset occurs when

$$\max_{\lambda\in\sigma(L_{\text{tot}})} \omega(\lambda) = 0. \tag{4.51}$$

In the undirected case, L_{tot} has a real spectrum and $\omega(\lambda)$ reduces to the classical real-valued dispersion relation. In contrast, directed interaction structures may yield a complex-valued spectrum, and this will require the dispersion relation to be evaluated over the complex plane. Moreover, since L_{tot} may also be non-normal, transient amplification can occur even when $\omega(\lambda) < 0$ for all $\lambda \in \sigma(L_{\text{tot}})$.

4.9.3 Linear indistinguishability

Since the linearized operator in Theorem 4.23 depends only on exposure structural information, hypergraphs that agree on their first tail moments are indistinguishable at linear level. We formalize this observation below.

Definition 4.26 (Exposure-equivalence)**.** *Two directed hypergraphs $\mathcal{H}_A$ and $\mathcal{H}_B$ are said to be exposure-equivalent or first-tail-moment equivalent if for every interaction order k, their*

first tail moments are equal:

$$A^{(k)}(\mathcal{H}_A) = A^{(k)}(\mathcal{H}_B), \quad \textit{for all } k. \tag{4.52}$$

Since $d_{in}^{(k)} = A^{(k)}\mathbf{1}$, then exposure-equivalence also implies equality of the zeroth tail moments.

Corollary 4.27 (Linear indistinguishability)**.** *If two directed hypergraphs $\mathcal{H}_A$ and $\mathcal{H}_B$ are exposure-equivalent, then they induce identical linear operators. In particular, they have identical spectra, dispersion relations, and Turing onset thresholds.*

4.9.4 Interpretation

Theorem 4.23 reveals a strict hierarchy in the structural information encoded by the hypergraph. At linear level, the dynamics depends only on the first tail moment, and all higher-order tail moments are suppressed. Hypergraphs that coincide at this level are therefore indistinguishable with respect to stability and Turing onset. The distinctions between such hypergraphs emerge only beyond onset, where nonlinear interactions reintroduce higher-order tail moments into the dynamics. Understanding how this mechanism occurs is the focus of the next section.

4.10 Nonlinear Analysis and Pattern Saturation

From this point onward, we develop a weakly nonlinear theory describing pattern formation near a steady (Turing) instability. Our goal is to identify the structural quantities that determine pattern saturation beyond the instability threshold. We show that while instability onset is fully determined by the first tail moment (exposure) tensor, the quadratic and cubic normal-form coefficients governing nonlinear saturation depend on higher-order tail moment (packing) tensors that are completely invisible to linear theory. This reveals a

deep hierarchy of structural information and establishes a clear separation between linear and nonlinear structural mechanisms (see Figure 4.3). More specifically, we establish that exposure statistics suffice to determine the onset of instability, but packing statistics are required to determine post-onset pattern saturation.

4.10.1 Spectral setup

Throughout this section, we assume (4.9), namely a codimension-one steady instability at a control parameter p (e.g. inhibitor diffusion coefficient), and set $p = p_c$ at criticality. It will be more convenient in subsequent analysis to use the detuning parameter $\epsilon = p - p_c$, which measures the distance from onset. Let us denote by $\dot{\mathbf{x}} = F(\mathbf{x}; p_c + \epsilon)$ the dynamical system given by (4.12) under nonlinear mean coupling (4.26), and let $\delta\mathbf{x} = \mathbf{x} - \bar{\mathbf{x}}$ denote the perturbation from the homogeneous equilibrium $\bar{\mathbf{x}} \in \mathcal{S}$. The third-order Taylor expansion (4.9) of the vector field at $\bar{\mathbf{x}}$ reads

$$F(\bar{\mathbf{x}} + \delta\mathbf{x}; p_c + \epsilon) = J(\epsilon)\delta\mathbf{x} + B(\delta\mathbf{x}, \delta\mathbf{x}) + C(\delta\mathbf{x}, \delta\mathbf{x}, \delta\mathbf{x}) + O(\|\delta\mathbf{x}\|^4) \tag{4.53}$$

where, $J(\epsilon) = D_{\mathbf{x}}F(\bar{\mathbf{x}}; p_c + \epsilon)$ is the Jacobian, and

$$B = \frac{1}{2}D^2_{\mathbf{x}}F(\bar{\mathbf{x}}; p_c), \qquad C = \frac{1}{6}D^3_{\mathbf{x}}F(\bar{\mathbf{x}}; p_c) \tag{4.54}$$

are the scaled symmetric bilinear and trilinear maps corresponding to the second and third derivatives of the vector field F at onset.

Since F depends smoothly on ϵ, the Jacobian admits the following expansion

$$J(\epsilon) = J_0 + \epsilon J_1 + O(\epsilon^2) \tag{4.55}$$

where, $J_0 = I_N \otimes J_f - L_{\text{tot}} \otimes D_{\text{eff}}$ is the Jacobian in the linearization (4.48) at onset ($\epsilon = 0$),

and

$$J_1 = \frac{\partial J(\epsilon)}{\partial \epsilon}\Big|_{\epsilon=0} \tag{4.56}$$

Remark 4.28. *Analogous expansions also hold for the maps B and C. However, their ϵ-dependence contributes terms of order $O(\epsilon\|\delta\mathbf{x}\|^2)$ and higher which are absorbed into the remainder in the weakly nonlinear analysis considered below.*

The codimension-one assumption implies that J_0 has a simple eigenvalue at 0 while all the remaining eigenvalues have strictly negative real part.

Using Lemma 4.24, there exists a critical eigenvalue λ_c of L_{tot} with right and left normalized eigenvectors $r, l \in \mathbb{R}^N$ satisfying

$$L_{\text{tot}}\, r = \lambda_c\, r, \qquad l^\top L_{\text{tot}} = \lambda_c\, l^\top, \qquad l^\top r = 1 \tag{4.57}$$

Let $\xi, \eta \in \mathbb{R}^d$ denote the normalized right and left eigenvectors associated with the zero eigenvalue of the linear operator $J_f - \lambda_c D_{\text{eff}}$, so that

$$(J_f - \lambda_c D_{\text{eff}})\, \xi = 0, \qquad \eta^\top (J_f - \lambda_c D_{\text{eff}}) = 0, \qquad \eta^\top \xi = 1 \tag{4.58}$$

Using the Kronecker product structure of J_0, its critical right and left eigenvectors associated with the zero eigenvalue can be written in the following form

$$v = r \otimes \xi, \qquad w = l \otimes \eta \tag{4.59}$$

These critical eigenvectors are normalized since $w^\top v = (l^\top r)(\eta^\top \xi) = 1$.

4.10.2 Weakly nonlinear reduction

Standard weakly nonlinear theory [12, 25, 35, 71] implies that near the codimension-one steady instability described above, the dynamics reduces to a one-dimensional center manifold tangent to the right eigenvector v. The evolution on this manifold is governed by a scalar amplitude equation describing the growth and nonlinear saturation of the critical mode. The following proposition states this reduction, and it provides generic expressions for the resulting coefficients. A detailed derivation is given in Appendix B.3.

Proposition 4.29 (Center manifold reduction and amplitude equation)**.** *Under the above assumption* (4.9)*, there exists a one-dimensional, locally invariant center manifold tangent to* $\mathrm{span}\{v\}$ *at* $\delta\mathbf{x} = 0$*, on which the system dynamics can be parametrized by a scalar amplitude* $A(t)$ *whose dynamics satisfies the following amplitude equation*

$$\dot{A} = \epsilon\alpha A + \beta A^2 + \gamma A^3 + O(A^4) \tag{4.60}$$

where,

$$\alpha = w^\top J_1 v, \qquad \beta = w^\top B(v, v), \qquad \gamma = w^\top \Big(2B(v, u) + C(v, v, v)\Big) \tag{4.61}$$

and u *is the unique solution of the equation* $J_0 u = -QB(v, v)$*, where* $Q = I - vw^\top$ *is the complementary projection onto the stable subspace.*

Proof. The result follows from standard center manifold reduction for a codimension-one steady bifurcation. A detailed derivation is provided in Appendix B.3 ■

4.10.3 Linear growth rate coefficient

We now specialize the linear growth rate coefficient α appearing in the amplitude equation (4.60) to our hypergraph setting. By leveraging the Kronecker product structure of the

linearized operator, we derive an explicit expression for α in terms of the critical eigenvalue λ_c of L_{tot} and the "species" eigenvectors p and q. The resulting formula reveals that the linear growth rate depends solely on the first-tail moment (exposure) information of the hypergraph, and it does not involve higher-order tails moments (packing) information. This is consistent with the linear analysis findings from the preceding section.

Let's recall from (4.61) that $\alpha = w^\top J_1 v$, where J_1 is given by (4.56). Equivalently, using the relation $p = p_c + \epsilon$ and the fact that the control parameter p enters the Jacobian only through D_{eff}, the chain rule yields

$$J_1 = -L_{\text{tot}} \otimes \frac{\partial D_{\text{eff}}}{\partial p}\Big|_{p=p_c} \tag{4.62}$$

Altogether, using (4.57) and (4.59) we get

$$\begin{aligned} \alpha &= -\left(l^\top \otimes \eta^\top\right) L_{\text{tot}} \otimes \frac{\partial D_{\text{eff}}}{\partial p}\,(r \otimes \xi) \\ &= -\lambda_c\, \eta^\top \left(\frac{\partial D_{\text{eff}}}{\partial p}\right) \xi \end{aligned} \tag{4.63}$$

where the derivative is evaluated at the critical parameter value $p = p_c$.

For clarity of presentation, we specialize expression (4.63) to the classical two-species setting $d = 2$. In this case, the state variable is $x = (u, v)$, where u and v represent the activator and inhibitor species respectively. The resulting formula for the growth-rate coefficient α is stated in the following proposition.

Proposition 4.30 (Linear growth rate coefficient in the two-species case)**.** *Consider the hypergraph reaction–diffusion system* (4.12) *with nonlinear mean coupling* (4.26)*. Assume $d = 2$, corresponding to the classical two-species setting $x = (u, v)$, where u and v denote the activator and inhibitor species respectively. Let the effective diffusion matrix be $D_{\text{eff}} = MD\sigma(\bar{x})$, as defined in* (4.48)*, where $M = \operatorname{diag}(d_u, d_v)$ and d_u, d_v are the activator and inhibitor diffusion coefficients. Using the notation introduced in Section 4.10.1, the linear*

growth-rate coefficient in the amplitude equation (4.60) *is given by*

$$\alpha = -\lambda_c \, \sigma_v'(\bar{v}) \, \eta_v \, \xi_v \tag{4.64}$$

where λ_c is the critical eigenvalue of the operator L_{tot}, and ξ_v, η_v denote the v-components of the corresponding right and left species eigenvectors.

Proof. It follows from (4.63) by taking $p = d_v$ as the control parameter, and using the fact that the activation σ acts componentwise. ■

The expression for α shows that the onset growth rate depends on the hypergraph structure only through the critical eigenvalue λ_c of the operator L_{tot} (i.e. *exposure Laplacian*). The remaining factors are determined by the local kinetics and the activation function σ. In particular, no higher-order tail moment (*packing*) information appears. Therefore, exposure-equivalent hypergraphs exhibit identical linear growth rates. This mirrors the *Linear distinguishability* result 4.27 established in the linear analysis section.

4.10.4 Nonlinear saturation coefficients

To understand how the hypergraph structure influences pattern saturation, we leverage the natural decomposition of the vector field F into its reaction and diffusion components. Under nonlinear mean coupling (4.26), the diffusion term can be further separated into contributions from the head node and contributions from multiway tail interactions. This separation induces a corresponding split of the quadratic and cubic multilinear maps B and C (4.54), and hence of the amplitude equation coefficients β and γ given in (4.61).

Using the equivalent hyperedge formulation of the dynamics stated in Proposition 4.17, the multilinear operators decompose as

$$B = B^{\mathrm{react}} + B^{\mathrm{head}} + B^{\mathrm{tail}}, \qquad C = C^{\mathrm{react}} + C^{\mathrm{head}} + C^{\mathrm{tail}} \tag{4.65}$$

where, for arbitrary perturbation $\delta\mathbf{x}, \delta\mathbf{y}$ and $\delta\mathbf{z}$ of the homegeneous equilibrium $\bar{\mathbf{x}} \in \mathcal{S}$, and $i \in \{1, \cdots, N\}$, we have

$$B_i^{\text{react}}(\delta\mathbf{x}, \delta\mathbf{y}) = \frac{1}{2} D^2 f(\bar{x})(\delta x_i, \delta y_i) \tag{4.66}$$

$$B_i^{\text{head}}(\delta\mathbf{x}, \delta\mathbf{y}) = -\frac{1}{2} \left(\sum_{k=1}^{\rho-1} d_{\text{in}}^{(k)}(v_i) \right) M D^2 \sigma(\bar{x})(\delta x_i, \delta y_i) \tag{4.67}$$

and the following tail piece from which the second-order tail moment (*pair packing*) tensor emerges

$$B_i^{\text{tail}}(\delta\mathbf{x}, \delta\mathbf{y}) = \frac{1}{2} \sum_{k=1}^{\rho-1} \sum_{e=(T\to i)\in E_k} \sum_{j,l\in T} \frac{w(e)}{k^2} M D^2 \sigma(\bar{x})(\delta x_j, \delta y_l) \tag{4.68}$$

Similarly, one can derive the expressions for C^{react} and C^{head}, with the latter involving only the zeroth tail moment tensor $d_{\text{in}}^{(k)}$ as in (4.67). For the sake of completeness, we give below the expression for C^{tail} since as in (4.68), it reveals the origin of the third tail moment (*triple packing*) tensor.

$$C_i^{\text{tail}}(\delta\mathbf{x}, \delta\mathbf{y}, \delta\mathbf{z}) = \frac{1}{6} \sum_{k=1}^{\rho-1} \sum_{e=(T\to i)\in E_k} \sum_{j,l,t\in T} \frac{w(e)}{k^3} M D^3 \sigma(\bar{x})(\delta x_j, \delta y_l, \delta z_t) \tag{4.69}$$

Pair and triple packing tensors: $k \geq 2$

The expressions for B^{tail} and C^{tail} above show how the higher-order tail moments arise naturally from the dynamics. Using Definition 4.21, we now introduce the *pair* and *triple* packing tensors, which correspond to the second and third tail-moment tensors, respectively.

$$\mathsf{P}_{ij_1j_2}^{(k)} \coloneqq \sum_{\substack{e=(T\to i)\in E_k,\\ j_1,j_2\in T}} \frac{w(e)}{k^2}, \qquad \mathsf{Q}_{ij_1j_2j_3}^{(k)} \coloneqq \sum_{\substack{e=(T\to i)\in E_k,\\ j_1,j_2,j_3\in T}} \frac{w(e)}{k^3} \tag{4.70}$$

A few observations are in order here. First, the tensor $\mathsf{P}^{(k)}$ measures pairwise co-occurrence of nodes within B-hyperedges of tail size k pointing to a given head node in $\mathcal{H}_k$, while $\mathsf{Q}^{(k)}$ measures triple co-occurrence. Next, these quantities capture hyperedge "packing" patterns, and they contain structural information that *cannot* be inferred from the first tail moment (exposure) tensor alone when $k \geq 2$. Finally, Proposition 4.22 shows that these *packing tensors* arise as *contractions* of the *adjacency tensor*. More specifically, we have

$$\mathsf{P}^{(k)}_{ij_1j_2} = \mathsf{A}^{(k,2)}, \qquad \mathsf{Q}^{(k)}_{ij_1j_2j_3} = \mathsf{A}^{(k,3)} \tag{4.71}$$

The structure of the packing tensors is determined by k. At $k = 1$, tails are singletons, so all nonzero entries occur when indices are equal. Both tensors reduce to diagonal tensors with entries given by the exposure matrix $A^{(1)}$ (see (4.45)) and therefore carry no nontrivial co-occurrence information. More specifically, we have

$$\mathsf{P}^{(1)}_{ij_1j_2} = \delta_{j_1j_2}\, A^{(1)}_{ij_1}, \qquad \mathsf{Q}^{(1)}_{ij_1j_2j_3} = \delta_{j_1j_2}\delta_{j_2j_3}\, A^{(1)}_{ij_1} \tag{4.72}$$

For $k \geq 2$, $\mathsf{P}^{(k)}$ has support on distinct index pairs and is genuinely pair-packing-driven. Meanwhile, The tensor $\mathsf{Q}^{(2)}$ has no support on triples of distinct indices and reduces to pairwise co-occurrence structure via repeated indices. Genuine triple packing appears only for $k \geq 3$, where $\mathsf{Q}^{(k)}$ admits nonzero entries on triples of distinct indices and is not reducible to lower-order statistics.

Summary of Packing Types

$$\mathsf{P}^{(k)} = \begin{cases} \text{exposure}, & k = 1, \\ \text{pair-packing}, & k \geq 2, \end{cases} \qquad \mathsf{Q}^{(k)} = \begin{cases} \text{exposure}, & k = 1, \\ \text{pair-packing}, & k = 2, \\ \text{triple-packing}, & k \geq 3. \end{cases} \tag{4.73}$$

In particular, *genuine* r-way packing requires tails of size at least r, which is reflected in the tensor contractions (4.71) and more generally in (4.35).

Decomposition of the saturation coefficients

It follows from (4.61) that the nonlinear coefficients β and γ are obtained by projecting the quadratic and cubic nonlinear forcing terms onto the critical left eigenvector w. As a result, the decomposition of the multilinear maps in (4.65) induces a corresponding decomposition of the nonlinear coefficients as follows.

$$\beta = \beta_{\text{react}} + \beta_{\text{head}} + \beta_{\text{tail}}, \qquad \gamma = \gamma^B + \gamma^C_{\text{react}} + \gamma^C_{\text{head}} + \gamma^C_{\text{tail}} \tag{4.74}$$

where, $\beta_{\text{react}}, \beta_{\text{head}}$ and $\gamma^C_{\text{react}}, \gamma^C_{\text{head}}$ are obtained by projecting the appropriate component of the quadratic and cubic maps respectively onto the critical left eigenvector. The component γ^B is given by

$$\gamma^B = 2w^\top B(v, u) \tag{4.75}$$

The tail contribution to the quadratic saturation coefficient β, and the tail contribution of the trilinear map C to the cubic saturation coefficient γ are given by

$$\beta_{\text{tail}} = w^\top B^{\text{tail}}(v, v), \qquad \text{and} \qquad \gamma^C_{\text{tail}} = w^\top C^{\text{tail}}(v, v, v) \tag{4.76}$$

How packing tensors enter the saturation coefficients

We now explicitly show how packing tensors contribute to the nonlinear saturation coefficients. We first consider the quadratic forcing term. Substituting the critical right eigenvec-

tor $v = r \otimes \xi$ into (4.68), we get

$$\begin{aligned} B_i^{\text{tail}}(v,v) &= \frac{1}{2}\left(\sum_{k=1}^{\rho-1} \Pi_i^{(k)}\right) MD^2\sigma(\bar{x})(\xi,\xi) \\ &= \frac{1}{2}\left(\Pi_i^{(1)} + \Pi_i^{\mathsf{P}}\right) MD^2\sigma(\bar{x})(\xi,\xi) \end{aligned} \tag{4.77}$$

where the order-k pair-packing scalars obtained by contraction with the right eigenvector r of L_{tot}, and their tail sum, are defined by

$$\Pi_i^{(k)} = \sum_{j_1,j_2=1}^{N} \mathsf{P}_{ij_1j_2}^{(k)} r_{j_1} r_{j_2}, \qquad \text{and} \qquad \Pi_i^{\mathsf{P}} = \sum_{k=2}^{\rho-1} \Pi_i^{(k)} \tag{4.78}$$

Collecting these scalars into N-dimensional vectors $\Pi^{(k)}$ and Π^{tot}, we get

$$B^{\text{tail}}(v,v) = \frac{1}{2}\left(\Pi^{(1)} + \Pi^{\mathsf{P}}\right) \otimes MD^2\sigma(\bar{x})(\xi,\xi) \tag{4.79}$$

where the order-k contracted pair-packing vector, and their tail sum, are defined by

$$\Pi^{(k)} \coloneqq \mathsf{P}^{(k)} \times_2 r \times_3 r, \qquad \text{and} \qquad \Pi^{\mathsf{P}} \coloneqq \sum_{k=2}^{\rho-1} \Pi^{(k)} \tag{4.80}$$

Projecting (4.79) onto the critical left eigenvector w, we get the following decomposition of the tail piece of the quadratic saturation coefficient into its *diagonal* component associated with $\Pi^{(1)}$ and its *pair-packing* component which is associated with Π^{P}

$$\beta_{\text{tail}} = \beta_{\text{diag}} + \beta_{\mathsf{P}} \tag{4.81}$$

Altogether, the quadratic saturation coefficient decomposes as follows

$$\beta = (\beta_{\text{react}} + \beta_{\text{head}} + \beta_{\text{diag}}) + \beta_{\mathsf{P}} \tag{4.82}$$

A similar argument shows that the cubic tail forcing term can be written in the following compact form

$$C^{\text{tail}}(v,v,v) = \frac{1}{6}\left(\Gamma^{(1)} + \Gamma^{(2)} + \Gamma^{\mathsf{Q}}\right) \otimes MD^3\sigma(\bar{x})(\xi,\xi,\xi) \tag{4.83}$$

where the order-k contracted triple-packing vector, and their tail sum, are defined by

$$\Gamma^{(k)} \coloneqq \mathsf{Q}^{(k)} \times_2 r \times_3 r \times_4 r, \qquad \text{and} \qquad \Gamma^{\mathsf{Q}} \coloneqq \sum_{k=3}^{\rho-1} \Gamma^{(k)} \tag{4.84}$$

The tail contribution of the trilinear map to the cubic saturation coefficient decomposes into its *diagonal* component driven by $\Gamma^{(1)}$, its *pair-packing* component driven by $\Gamma^{(2)}$ and its *triple-packing* component driven by Γ^{Q}

$$\gamma^C_{\text{tail}} = \gamma^C_{\text{diag}} + \gamma^C_{\mathsf{P}} + \gamma_{\mathsf{Q}} \tag{4.85}$$

Hence, we get the complete decomposition of the cubic saturation coefficient as follows

$$\gamma = \gamma^C_{\text{react}} + \gamma^C_{\text{head}} + \gamma^C_{\text{diag}} + \gamma^B + \gamma^C_{\mathsf{P}} + \gamma_{\mathsf{Q}} \tag{4.86}$$

The following proposition summarizes the derivation above, and it gives explicit expressions for the nonlinear saturation coefficients in our hypergraph setting

Proposition 4.31 (Nonlinear saturation coefficients)**.** *Consider the reaction–diffusion system on hypergraph given by* (4.12) *with nonlinear mean coupling* (4.26)*. Let $v = r \otimes \xi$ and $w = l \otimes \eta$ denote the critical right and left eigenvectors at onset as defined in Section 4.10.1. The nonlinear saturation coefficients in the amplitude equation* (4.60) *are given by*

$$\begin{aligned} \beta &= \beta_{\text{react}} + \beta_{\text{head}} + \beta_{\text{diag}} + \beta_{\mathsf{P}} \\ \gamma &= \gamma^C_{\text{react}} + \gamma^C_{\text{head}} + \gamma^C_{\text{diag}} + \gamma^B + \gamma^C_{\mathsf{P}} + \gamma_{\mathsf{Q}} \end{aligned} \tag{4.87}$$

where, the reaction and head components are defined as follows

$$\beta_{\text{react}} = \frac{1}{2}\left(l^\top r^{\odot 2}\right)\left(\eta^\top f_2\right), \qquad \gamma^C_{\text{react}} = \frac{1}{6}\left(l^\top r^{\odot 3}\right)\left(\eta^\top f_3\right) \tag{4.88}$$

$$\begin{aligned} \beta_{\text{head}} &= -\frac{1}{2}\left(l^\top \left(d^{\text{tot}}_{\text{in}} \odot r^{\odot 2}\right)\right)\left(\eta^\top s_2\right) \\ \gamma^C_{\text{head}} &= -\frac{1}{6}\left(l^\top \left(d^{\text{tot}}_{\text{in}} \odot r^{\odot 3}\right)\right)\left(\eta^\top s_3\right). \end{aligned} \tag{4.89}$$

The diagonal components of the saturation coefficients are given by

$$\beta_{\text{diag}} = \frac{1}{2}\left(l^\top \Pi^{(1)}\right)\left(\eta^\top s_2\right), \qquad \gamma^C_{\text{diag}} = \frac{1}{6}\left(l^\top \Pi^{(1)}\right)\left(\eta^\top s_3\right). \tag{4.90}$$

The direct pair-packing components to both coefficients are given by

$$\beta_{\mathsf{P}} = \frac{1}{2}\left(l^\top \Pi^{\mathsf{P}}\right)\left(\eta^\top s_2\right), \qquad \gamma^C_{\mathsf{P}} = \frac{1}{6}\left(l^\top \Gamma^{(2)}\right)\left(\eta^\top s_3\right). \tag{4.91}$$

The direct triple-packing component to the cubic saturation coefficient reads

$$\gamma_{\mathsf{Q}} = \frac{1}{6}\left(l^\top \Gamma^{\mathsf{Q}}\right)\left(\eta^\top s_3\right). \tag{4.92}$$

For convenience, we denote the quadratic and cubic reaction responses along the critical mode by

$$f_2 \coloneqq D^2 f(\bar{x})(\xi,\xi), \qquad \textit{and} \qquad f_3 \coloneqq D^3 f(\bar{x})(\xi,\xi,\xi).$$

Similarly, the species-side responses of the activation function along the critical mode is denoted by

$$s_2 \coloneqq M D^2 \sigma(\bar{x})(\xi,\xi), \qquad \textit{and} \qquad s_3 \coloneqq M D^3 \sigma(\bar{x})(\xi,\xi,\xi).$$

We denote the m-th elementwise power of r by $r^{\odot m}$, namely $\left(r^{\odot m}\right)_i = r_i^m$. The total in-degree

vector $d_{\text{in}}^{\text{tot}}$ *is defined as follows*

$$d_{\text{in}}^{(k)} \coloneqq \left(d_{\text{in}}^{(k)}(v_1), \cdots, d_{\text{in}}^{(k)}(v_N)\right)^\top, \qquad \textit{and} \qquad d_{\text{in}}^{\text{tot}} \coloneqq \sum_{k=1}^{\rho-1} d_{\text{in}}^{(k)}.$$

Finally, Π^{P} *and* Γ^{Q} *are the contracted intrinsic pair and triple-packing vectors defined in* (4.80) *and* (4.84).

Proof. The proof leverages the Kronecker product structure of the equations, and it follows from (4.74)–(4.86). ■

Remark 4.32. *The cubic saturation coefficient* γ *also contains the indirect contribution* $\gamma^B = 2w^\top B(v,u)$*, where* u *is the unique solution to the equation* $J_0 u = -QB(v,v)$*, and the operator* $Q = I - vw^\top$ *is the projection onto the stable subspace. The term* γ^B *inherits pair-packing dependence through the "feedback" term* u*, but it does not reduce to a direct contraction formula of the same form as* $\beta_{\mathsf{P}}, \gamma_{\mathsf{P}}^C$ *and* γ_{Q}*.*

The key implication of Proposition 4.31 is that the zeroth tail moment (exposure) information contributes to both saturation coefficients through their head and diagonal terms (4.89)–(4.90), whereas higher-order tail moment (packing) information enter through the tail terms. In particular, only pair packing contributes to the quadratic coefficient β via its component β_{P}. Meanwhile the cubic coefficient γ receives pair-packing effect through γ^B and γ_{P}^C, and triple packing effect through γ_{Q}. Therefore, *exposure* information alone is *insufficient* to determine pattern saturation, *packing* information is *required*.

4.10.5 Normal form regimes

The amplitude equation derived in (4.60) includes both quadratic and cubic nonlinear terms, leading to two distinct normal form regimes based on whether the quadratic coefficient β vanishes. In the *resonant case* ($\beta \neq 0$), the quadratic term governs the leading nonlinear dynamics, whereas in the *non-resonant case* ($\beta = 0$), the cubic term determines the leading nonlinear saturation, thus leading to the classical Stuart-Landau equation.

In contrast to classical reaction–diffusion systems, where symmetry often forces quadratic terms to cancel out [51, 16, 27, 15], no such cancellation mechanism exists a priori in hypergraph-coupled settings. This reflects a structural feature of our framework, namely nonlinear mean aggregation produces intrinsic quadratic contributions that generically persist under projection onto the critical mode. As a result, the condition $\beta = 0$ is non-generic and would require specific parameter tuning to achieve. The simple example provided below illustrates this mechanism explicitly.

Example 4.33 (Genericity of the resonant case)**.** *We consider three scalar dynamical units* $\{v_1, v_2, v_3\}$ *interacting over the hypergraph whose hyperedges are* $e_1 = (\{v_2, v_3\} \to v_1)$, $e_2 = (v_1 \to v_2)$ *and* $e_3 = (v_1 \to v_3)$*. The weight function* ω *assigns positive weights to each hyperedge as follows:* $\omega(e_1) = \omega_h$ *and* $\omega(e_2) = \omega_e = \omega(e_3)$*. The interaction is mediated by a nonlinear mean-aggregation activation function* σ *as in* (4.26) *and satisfying* $\sigma(0) = 0$, $\sigma'(0) > 0$ *and* $\sigma''(0) \neq 0$*. We set* $M = -d$*, where* $d > 0$ *is the control parameter. Each unit evolves according to the same intrinsic dynamics* $f(x) = c_1 x + c_2 x^2$*, where* $c_1 < -\omega_0 d\sigma'(0)$*. In fact, any sufficiently smooth* f *satisfying* $f(0) = 0$ *with appropriately bounded first derivative will do. The dynamics of the resulting higher-order network system reads*

$$\begin{aligned} \dot{x}_1 &= f(x_1) - \omega_h d \left(\sigma \left(\frac{x_2 + x_3}{2} \right) - \sigma(x_1) \right) \\ \dot{x}_2 &= f(x_2) - \omega_e d \left(\sigma(x_1) - \sigma(x_2) \right) \\ \dot{x}_3 &= f(x_3) - \omega_e d \left(\sigma(x_1) - \sigma(x_3) \right) \end{aligned} \tag{4.93}$$

The homogeneous equilibrium is $\bar{\mathbf{x}} = (0, 0, 0)^\top$*, and the Jacobian matrix* $J = I_3 \otimes J_f - L_{\text{tot}} \otimes D_{\text{eff}}(d)$ *has eigenvalues* $\lambda_1 = c_1 + (\omega_e + \omega_h) d\sigma'(0)$, $\lambda_2 = c_1 + \omega_e d\sigma'(0)$ *and* $\lambda_3 = c_1$*. So, a codimension-*1 *steady bifurcation occurs at*

$$d_c = -\frac{c_1}{(\omega_e + \omega_h)\sigma'(0)} \tag{4.94}$$

At onset ($d = d_c$), the normalized critical right and left eigenvectors are given by

$$v = (\omega_h, -\omega_e, -\omega_e)^\top, \qquad \textit{and} \qquad w = \frac{1}{\omega_e + \omega_h}\left(1, -\frac{1}{2}, -\frac{1}{2}\right)^\top \tag{4.95}$$

A Taylor expansion of the vector field in (4.93) *yields the following quadratic forcing vector*

$$B(v,v) = \begin{pmatrix} c_2\omega_h^2 + \frac{1}{2}(\omega_h^2 - \omega_e^2)\omega_h d_c\sigma''(0) \\ c_2\omega_e^2 + \frac{1}{2}(\omega_e^2 - \omega_h^2)\omega_e d_c\sigma''(0) \\ c_2\omega_e^2 + \frac{1}{2}(\omega_e^2 - \omega_h^2)\omega_e d_c\sigma''(0) \end{pmatrix} \tag{4.96}$$

The quadratic nonlinear saturation coefficient is obtained by projection onto the critical left eigenvector w, and it reads

$$\beta = (\omega_h - \omega_e)\left(c_2 - \frac{\sigma''(0)}{2\sigma'(0)}c_1\right) \tag{4.97}$$

Thus, if we assume $\omega_e \neq \omega_h$, the condition $\beta = 0$ requires fine-tuning the system parameters to lie exactly on the hypersurface defined by setting the right-hand side of (4.97) *to zero, and it is therefore non-generic.*

Since the condition $\beta = 0$ is non-generic, the weakly nonlinear dynamics falls into two normal form regimes depending on whether the quadratic saturation coefficient vanishes. We will make use of the time rescaling $T = \epsilon t$ to derive the resulting *slow-time* dynamics in both cases.

Resonant case $\beta \neq 0$

The amplitude equation (4.60) retains its form $\dot{A} = \epsilon\alpha A + \beta A^2 + \gamma A^3 + O(A^4)$.

Balancing the linear and quadratic terms yields $A = O(\epsilon)$. Thus introducing the amplitude rescaling $A = \epsilon a$, we arrive at the *slow-time* dynamics

$$a_T = \alpha a + \beta a^2 + \epsilon\gamma a^3 + O(a^4) \tag{4.98}$$

which to leading order, gives the following *transcritical-type* normal form

$$a_T = \alpha a + \beta a^2 \tag{4.99}$$

In this regime, the quadratic coefficient β determines the orientation of the bifurcating branch, while the linear growth rate coefficient α controls its stability. This reflects the exchange-of-stability mechanism characteristic of transcritical bifurcations.

When the nontrivial branch is stable, namely $\alpha\epsilon > 0$, the amplitude saturates at

$$A_\infty(\epsilon) = -\frac{\alpha}{\beta}\epsilon + O(\epsilon^2) \tag{4.100}$$

Non-resonant case $\beta = 0$

Here, the amplitude equation (4.60) takes the form $\dot{A} = \epsilon\alpha A + \gamma A^3 + O(A^4)$.

Balancing the linear and cubic terms yields $A = O(\epsilon^{\frac{1}{2}})$ so that the amplitude rescaling $A = \epsilon^{\frac{1}{2}} a$ gives the following *slow-time* dynamics

$$a_T = \alpha a + \gamma a^3 + O(a^4) \tag{4.101}$$

To leading order, we get the following *pitchfork-type* normal form characteristic of the steady Stuart-Landau equation

$$a_T = \alpha a + \gamma a^3 \tag{4.102}$$

In this regime, the linear growth rate coefficient α determines the side of onset on which the homogeneous state loses stability, while the cubic coefficient γ controls the criticality of the bifurcation. More specifically, the bifurcation is supercritical for $\gamma < 0$, and it is subcritical for $\gamma > 0$.

When the nontrivial branch is stable, which occurs whenever $\gamma < 0$ and $\alpha\epsilon > 0$ hold

simultaneously, the amplitude saturates at

$$A_\infty(\epsilon) = \pm\sqrt{-\frac{\alpha}{\gamma}\epsilon} + O(\epsilon) \tag{4.103}$$

Remark 4.34. *In both the resonant and non-resonant regimes, packing terms enter the leading nonlinear saturation coefficient. Although these terms may vanish in special cases, such as when the critical mode does not probe the tail directions as in Example 4.35 below, they are generically present. Therefore, outside such degenerate configurations, the post-onset dynamics is intrinsically shaped by packing effects, thus emphasizing the robustness of the mechanism.*

4.10.6 Nonlinear distinguishability and structural effects

Up to this point, we have established that packing statistics is the structural information controlling the nonlinear saturation of the dynamics. In this section, we take a step further to highlight a core subtlety of this mechanism. In particular, we show that structural presence alone is not sufficient for packing tensors to be *dynamically relevant*, even though these tensors naturally arise whenever non-trivial hyperedges are present. Rather, packing must be "*seen by the critical mode*", in the sense that its *contribution* to the relevant saturation coefficients is nonzero.

Example 4.35 (Vanishing of quadratic packing effect β_{P})**.** *Beyond providing a template for the* genericity of the resonant case *in hypergraph setting, Example 4.33 reveals an important subtlety in the system dynamics. It follows from* (4.97) *that*

$$\begin{aligned}\beta &= \beta_{\text{react}} + \beta_{\text{head}} + \beta_{\text{diag}} + \beta_{\mathsf{P}} \\ &= c_2(\omega_h - \omega_e) - \kappa(\omega_h^3 - \omega_e^3) - \kappa\,\omega_e\omega_h^2 + \kappa\,\omega_h\omega_e^2\end{aligned} \tag{4.104}$$

where,

$$\kappa \coloneqq \frac{1}{(\omega_e + \omega_h)^2}\frac{\sigma''(0)}{2\sigma'(0)}c_1 \tag{4.105}$$

This matches the decomposition predicted by (4.87).

Now, observe that if we set $\omega_e = 0$*, meaning removing all pairwise interactions, then the tail contribution* (4.81) *disappears from* (4.104)*. In particular, the quadratic packing effect vanishes* (i.e. $\beta_{\mathsf{P}} = 0$)*, despite the persistence of the nontrivial hyperedge* e_1*. This should not be interpreted as the system being intrinsically pairwise, rather it indicates that higher-order interactions are dynamically inactive at quadratic order. This reflects the structure of the critical mode* v (see (4.95))*, which in this case has no support on the tail nodes when* $\omega_e = 0$*.*

This example highlights a key insight about the mechanism governing post-onset dynamics. The dynamical relevance of packing tensors is not determined solely by the presence of higher-order hyperedges, but by how they interact with the critical mode. In particular, packing tensors enter the reduced dynamics (i.e. amplitude equation) only through their contraction with the critical eigendirections, as seen in (4.80) and (4.84). Consequently, *higher-order interactions may be structurally present, yet dynamically invisible at leading order.*

Packing tensors encode node co-occurrence within hyperedges in a combinatorial sense, but only the portion that projects onto the critical eigendirections influences the reduced dynamics. We call this portion *packing effect*, as it represents the part of packing that actually enters the saturation coefficients in the amplitude equation, and it should be distinguished from packing as a purely structural feature (i.e packing tensor). At quadratic order, the packing effect is simply

$$\beta_{\text{pack}} = \beta_{\mathsf{P}} \tag{4.106}$$

while at cubic order it takes the form

$$\gamma_{\text{pack}} = \gamma^B_{\text{pack}} + \gamma^C_{\mathsf{P}} + \gamma_{\mathsf{Q}} \tag{4.107}$$

where the terms represent direct second and third-order contributions together with indirect (feedback) effects arising through the center-manifold correction γ^B.

We can now state the following important theorem.

Theorem 4.36 (Nonlinear structural decomposition)**.** *The amplitude saturation coefficients decompose as*

$$\beta = \beta_{\mathrm{exp}} + \beta_{\mathrm{pack}}, \qquad \textit{and} \qquad \gamma = \gamma_{\mathrm{exp}} + \gamma_{\mathrm{pack}} \tag{4.108}$$

where the exposure-driven parts β_{exp} and γ_{exp} collect contributions from the reaction, head, and diagonal components, while the packing-driven parts β_{pack} and γ_{pack} are simply the packing effects given in (4.106) *and* (4.107)

Proof. It follows from (4.74) through (4.86). ■

This motivates the following definition of weak packing-equivalence

Definition 4.37 (Weak packing-equivalence)**.** *Consider two hypergraph reaction–diffusion systems $\mathcal{H}_A$ and $\mathcal{H}_B$ with dynamics* ((4.12) + (4.26)) *under the same local reaction and activation functions, and admitting reduced amplitude equations of the form*

$$\dot{A} = \mu A + \beta A^2 + \gamma A^3 + O(A^4).$$

For $m \in \{2, 3\}$, we say that the hypergraphs $\mathcal{H}_A$ and $\mathcal{H}_B$ are weakly packing-equivalent to order m if their packing effects agree up to order m. In particular, for $m = 2$, we have

$$\beta_{\mathrm{pack}}(\mathcal{H}_A) = \beta_{\mathrm{pack}}(\mathcal{H}_B) \tag{4.109}$$

while for $m = 3$ we have

$$\beta_{\mathrm{pack}}(\mathcal{H}_A) = \beta_{\mathrm{pack}}(\mathcal{H}_B), \qquad \textit{and} \qquad \gamma_{\mathrm{pack}}(\mathcal{H}_A) = \gamma_{\mathrm{pack}}(\mathcal{H}_B) \tag{4.110}$$

Remark 4.38. *The qualifier "weak" in Definition 4.37 indicates that only the packing effects appearing in the saturation coefficients are compared, rather than the full packing tensors or the underlying hypergraph structure.*

The following theorem characterizes the condition under which two hypergraph-coupled systems are indistinguishable at the level of the amplitude equation, thus identifying the structural features that govern this dynamics.

Theorem 4.39 (Reduced dynamics equivalence)**.** *Fix $m \in \{2, 3\}$, and consider two hypergraph reaction–diffusion systems $\mathcal{H}_A$ and $\mathcal{H}_B$ with dynamics* ((4.12) + (4.26)) *under the same local reaction and activation functions, and admitting reduced amplitude equations of the form*

$$\dot{A} = \mu A + \beta A^2 + \gamma A^3 + O(A^4).$$

If the two systems are exposure-equivalent (see Definition 4.26) *and weakly packing-equivalent to order m* (see Definition 4.37)*, then their reduced dynamics agree up to order m. In particular, for $m = 2$, we have*

$$\mu(\mathcal{H}_A) = \mu(\mathcal{H}_B) \qquad \textit{and} \qquad \beta(\mathcal{H}_A) = \beta(\mathcal{H}_B) \tag{4.111}$$

while for $m = 3$ we have

$$\mu(\mathcal{H}_A) = \mu(\mathcal{H}_B), \qquad \beta(\mathcal{H}_A) = \beta(\mathcal{H}_B), \qquad \textit{and} \qquad \gamma(\mathcal{H}_A) = \gamma(\mathcal{H}_B) \tag{4.112}$$

Proof. First, note that the linear coefficient $\mu = \epsilon\alpha$ depends only on exposure information (see (4.63)). Next, exposure-equivalence implies equality of μ, β_{exp} and γ_{exp}, while weak packing-equivalence implies equality of β_{pack} and γ_{pack}. Finally, conclude using Theorem 4.36. ■

The following corollary characterizes nonlinear distinguishability.

Corollary 4.40 (Nonlinear distinguishability)**.** *Fix an integer $m \in \{2, 3\}$. If two hypergraph-coupled systems are exposure-equivalent, but not weakly packing-equivalent to order m, then their reduced dynamics must differ at some order $1 < p \leq m$.*

Proof. The proof follows from Theorem 4.39. ■

The dependence of the reduced dynamics on exposure and packing effects leads naturally to the concept of *dynamical graph surrogacy*, which identifies the conditions under which a hypergraph-coupled system can be represented by an equivalent graph at the level of its reduced dynamics.

Corollary 4.41 (Dynamical graph surrogacy)**.** *Fix $m \in \{2, 3\}$. A hypergraph-coupled system admits a* dynamical graph surrogate *up to order m if and only if its packing effects vanish up to order m. In this case, the system is dynamically indistinguishable from a graph-based system at the level of the reduced dynamics up to order m.*

Proof. The result follows from Theorem 4.39, and noting that packing effects (4.106)–(4.107) quantify the "obstruction" to representing hypergraph dynamics by an exposure-driven (i.e. graph) model at the level of the reduced dynamics. ■

It is important to emphasize that *dynamical graph surrogacy* does not imply the absence of higher-order interactions in the hypergraph. Rather, it reflects the *absence of their net contribution* to the reduced dynamics up to the specified order.

Remark 4.42 (Quadratic surrogacy and curvature-free activation)**.** *The quadratic packing effect coefficient β_{P} depends jointly on the higher-order hypergraph structure and on the local geometry of the activation function* (see (4.91))*. In particular, if the activation has vanishing second derivative* (i.e. $D^2\sigma(\bar{x}) \coloneqq \sigma''(\bar{x})$, which we call curvature since the activation acts componentwise) *at the homogeneous equilibrium, then the quadratic packing effect necessarily vanishes. More specifically*

$$D^2\sigma(\bar{x}) = 0 \qquad \Longrightarrow \qquad \beta_{\mathsf{P}} = 0. \tag{4.113}$$

Thus, even in the presence of nontrivial higher-order interactions, quadratic packing effects become dynamically invisible whenever the activation is locally curvature-free around

equilibrium.

Typical examples include

$$\sigma(x) = a + b\tanh(x - \bar{x}), \qquad \sigma(x) = x + (x - \bar{x})^p, \quad p > 2. \tag{4.114}$$

For such activations, the weakly nonlinear reduction eliminates the quadratic packing term entirely.

This reveals two distinct mechanisms by which higher-order effects may fail to appear in the reduced dynamics. The first is structural invisibility*, arising when the relevant packing effects vanish because of the hypergraph organization itself. The second is* functional invisibility*, arising when the local curvature of the interaction nonlinearity suppresses higher-order effects independently of the underlying topology.*

Consequently, the dynamical visibility of higher-order interactions depends not only on combinatorial structure, but also on the local differential geometry of the nonlinear response.

4.11 Interpretation

The nonlinear analysis shows that higher-order interactions affect the dynamics solely through their contributions to the saturation coefficients. These contributions are therefore the only features of higher-order structure that are reflected in the reduced dynamics, and differences in them lead to distinguishable nonlinear behavior. This observation motivates the notion of graph surrogacy. A hypergraph-coupled system may be dynamically equivalent to a graph despite the presence of higher-order interactions, provided that their net contribution to the reduced dynamics vanishes.

4.12 Numerical Validation

4.12.1 Overview

We now validate the theoretical predictions on finite hypergraph-coupled reaction-diffusion systems. Since exposure-equivalence guarantees identical linearized dynamics by construction, the numerical experiments focus primarily on the nonlinear regime, where differences in packing effects become dynamically observable.

The main objective is to test two theoretical predictions developed in the previous sections. More specifically, we ascertain that exposure-equivalence alone does not determine nonlinear behavior beyond instability onset, and dynamic graph surrogacy is obstructed by nonzero packing effects. This latter statement simply means that a graph surrogate reproduces the hypergraph dynamics only when the relevant packing effects vanish.

4.12.2 Numerical setup

We consider finite directed hypergraph-coupled reaction-diffusion systems with Schnakenberg [?] local kinetics. Each node carries state variables (u_i, v_i) satisfying

$$\dot{u}_i = a - u_i + u_i^2 v_i \tag{4.115}$$

$$\dot{v}_i = b - u_i^2 v_i \tag{4.116}$$

Throughout the numerical experiments, the local kinetic parameters are fixed at $a = 0.2$ and $b = 1.3$. The corresponding homogeneous equilibrium is

$$u^* = a + b = 1.5, \qquad v^* = \frac{b}{(a+b)^2} \approx 0.57778. \tag{4.117}$$

For all interaction orders, the mixing matrices are taken to be $M = \mathrm{diag}(d_u, d_v)$, where $d_u = 0.25$, and the inhibitor diffusion coefficient d_v serving as the bifurcation parameter.

To generate nonlinear higher-order effects, we use polynomial activation functions of the form

$$\sigma(z) = c_1 z + c_2 z^2 + c_3 z^3. \tag{4.118}$$

Separate activation functions are used for the activator and inhibitor components:

$$\sigma_u(z) = c_{1,u} z + c_{2,u} z^2 + c_{3,u} z^3, \qquad \sigma_v(z) = c_{1,v} z + c_{2,v} z^2 + c_{3,v} z^3. \tag{4.119}$$

Unless otherwise specified, the coefficients are chosen as $c_{1,u} = 1.1,\ c_{2,u} = 0.2,\ c_{3,u} = 0.05$, and $c_{1,v} = 5.9,\ c_{2,v} = -0.15,\ c_{3,v} = 0.4$. These choices generate nontrivial quadratic and cubic nonlinearities and allow controlled suppression of the pair packing effect in the dynamical graph-surrogacy experiments through the condition $\sigma''(\bar{x}) = 0$.

First, we consider the pair of hypergraphs whose complete description is given in Table C.1. This pair is exposure-equivalent but not weakly packing-equivalent. This pair is used to validate nonlinear distinguishability under exposure-equivalence shown in Figure 4.4. Then we use the hypergraph described in Table C.2 for all subsequent experiments.

All simulations are performed near the instability threshold,

$$d_v = d_v^c + \varepsilon, \qquad \varepsilon > 0, \tag{4.120}$$

where d_v^c denotes the critical value predicted by the linear theory.

The modal amplitude is extracted by projection onto the critical left eigenvector w as follows

$$A_{\text{num}}(t) = w^\top \left(X(t) - \bar{X} \right), \tag{4.121}$$

where $X(t)$ denotes the full system state, $\bar{X}$ is the homogeneous equilibrium, and the critical eigenvectors are normalized by $w^\top v = 1$.

The saturated amplitude A_{sat} is estimated by averaging $|A_{\text{num}}(t)|$ over the terminal portion of the trajectory after convergence. Additional diagnostics include the relative standard

deviation and relative drift over the averaging window to ensure proper convergence.

4.12.3 Nonlinear Distinguishability under Exposure-Equivalence

Figure 4.4 shows the saturated amplitudes near onset for the pair in Table C.1.

Although the two systems possess identical exposure operators and therefore identical linear instability thresholds, their post-onset amplitudes differ substantially as one moves farther away from onset. This demonstrates that exposure-equivalence alone is insufficient to determine nonlinear dynamics beyond onset.

The observed discrepancy is consistent with the theory developed earlier. While the two systems agree at linear order, their packing effects differ, thus leading to different reduced coefficients in the amplitude equation and therefore different nonlinear saturation behavior.

Table 4.1 reports the corresponding coefficient data for the pair in Table C.1, including the common instability threshold d_v^c, the packing effects β_{pack} and γ_{pack}, and the measured saturation amplitudes. The table makes explicit that the two systems are linearly indistinguishable but nonlinearly distinguishable.

Table 4.1: Coefficient comparison for the pair of hypergraphs in Table C.1. The two systems are exposure-equivalent and therefore share the same linear instability threshold d_v^c, but they differ in their packing effects and nonlinear reduced coefficients. The resulting saturated amplitudes $|A_{\text{sat}}|$ confirms nonlinear distinguishability beyond the linear regime. See Figure 4.4 for the corresponding numerical comparison.

System	d_v^c	β	β_{pack}	γ	γ_{pack}	$\lvert A_{\text{sat}}\rvert$
$\mathcal{H}_A$	1.30079	0.17014	-0.01313	0.15544	0.06949	0.00189
$\mathcal{H}_B$	1.30079	0.19713	0.0	0.00603	0.0	0.00162

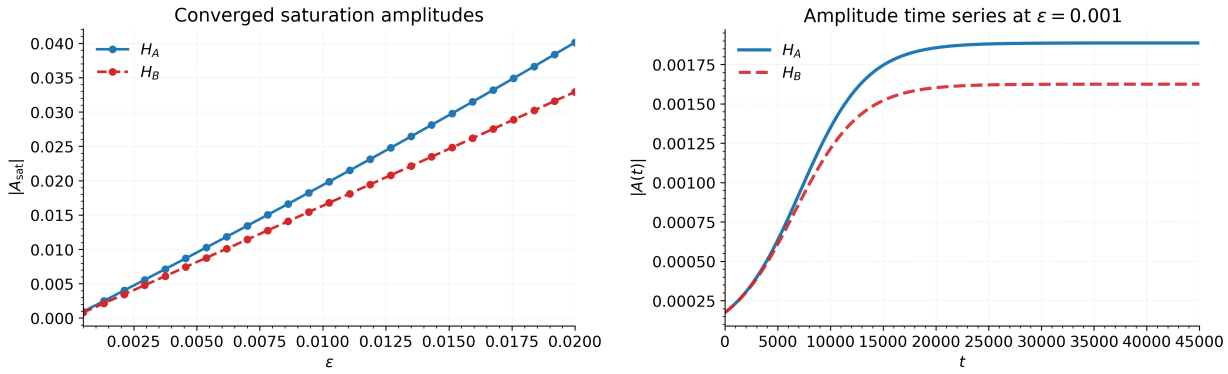

Figure 4.4: Nonlinear distinguishability for the pair of hypergraphs in Table C.1. **Left:** Saturated amplitudes as a function of $\varepsilon = d_v - d_v^c$. Although $\mathcal{H}_A$ and $\mathcal{H}_B$ are exposure-equivalent and therefore share an identical linear instability threshold, their nonlinear saturation amplitudes differ due to distinct packing effects. The discrepency is more pronounced the further away from onset (i.e larger ε). Moreover, the plots are consistent with the asymptotic prediction in (4.100). **Right:** Representative amplitude trajectories $A(t)$ at fixed $\varepsilon = 0.001$. Both systems exhibit similar early-time growth near onset consistent with exposure-equivalence, but they eventually converge to distinct saturated states. This demonstrates nonlinear distinguishability beyond the linear regime.

4.12.4 Dynamical Graph Surrogacy

We next test the graph-surrogacy prediction.

Given the hypergraph $\mathcal{H}$ described in Table C.2, we construct an exposure-preserving graph surrogate $\mathcal{G}$ by replacing each hyperedge $e := \{j_1, \dots, j_k\} \to i$ of weight $w(e)$ by the edges $j_m \to i$ of weight $\frac{w(e)}{k}$ for each $m = 1, \dots, k$. This construction preserves the exposure operator exactly, and therefore preserves the linearized dynamics.

We compare the projected amplitudes

$$\begin{aligned} A_{\mathcal{H}}(t) &= w^\top \left(X_{\mathcal{H}}(t) - \bar{X} \right) \\ A_{\mathcal{G}}(t) &= w^\top \left(X_{\mathcal{G}}(t) - \bar{X} \right) \end{aligned} \tag{4.122}$$

Two activation regimes are considered.

Case 1: Vanishing quadratic packing effect. When $\sigma''(\bar{x}) = 0$, the quadratic packing effect vanishes (see Remark 4.42). The graph surrogate reproduces the hypergraph dynamics

to quadratic order near onset. Numerically, the trajectories remain close, and since cubic packing effect is also small, the amplitudes nearly coincide. Figure 4.5 (Left panel) illustrates this behavior

Case 2: Nonzero quadratic packing effect. When $\sigma''(\bar{x}) \neq 0$, quadratic packing effects become active. In this regime, the exposure-preserving graph surrogate no longer reproduces the hypergraph dynamics. Although the two systems initially agree due to their identical linearization, they separate at nonlinear order and saturate at different amplitudes.

Figure 4.5 (Right panel) illustrates this behavior. The result demonstrates that packing effects provide an obstruction to graph surrogacy, in the sense that preserving exposure is sufficient to reproduce linear onset, but it is insufficient to reproduce nonlinear hypergraph dynamics.

Table 4.2 summarizes the graph-surrogacy experiments, including the common instability threshold, the packing effects β_{pack} and γ_{pack}, the final saturated amplitudes, and the saturation discrepancy

$$\Delta A_{\text{sat}} = |A_{\mathcal{H},\text{sat}} - A_{\mathcal{G},\text{sat}}|. \tag{4.123}$$

Table 4.2: Summary of the graph-surrogacy experiments. For each activation regime, the table reports the packing effects and the resulting saturated amplitudes for the hypergraph $\mathcal{H}$ and its exposure-preserving graph surrogate $\mathcal{G}$. Agreement is recovered when the relevant packing effects vanish, while nonzero packing effects produce observable nonlinear discrepancies despite identical linear dynamics. See Figure 4.5 for the corresponding visual comparison where we set $\varepsilon = 0.001$.

Case	d_v^c	$\beta_{\text{pack},\mathcal{H}}$	$\beta_{\text{pack},\mathcal{G}}$	$\gamma_{\text{pack},\mathcal{H}}$	$\gamma_{\text{pack},\mathcal{G}}$	$A_{\mathcal{H},\text{sat}}$	$A_{\mathcal{G},\text{sat}}$	ΔA_{sat}
$\sigma''(\bar{x}) = 0$	1.11	0.0	0.0	2.29e-4	0.0	6.82e-4	6.82e-4	7.68e-9
$\sigma''(\bar{x}) \neq 0$	1.11	7.86e-4	0.0	1.10e-3	0.0	1.80e-3	1.80e-3	6.41e-5

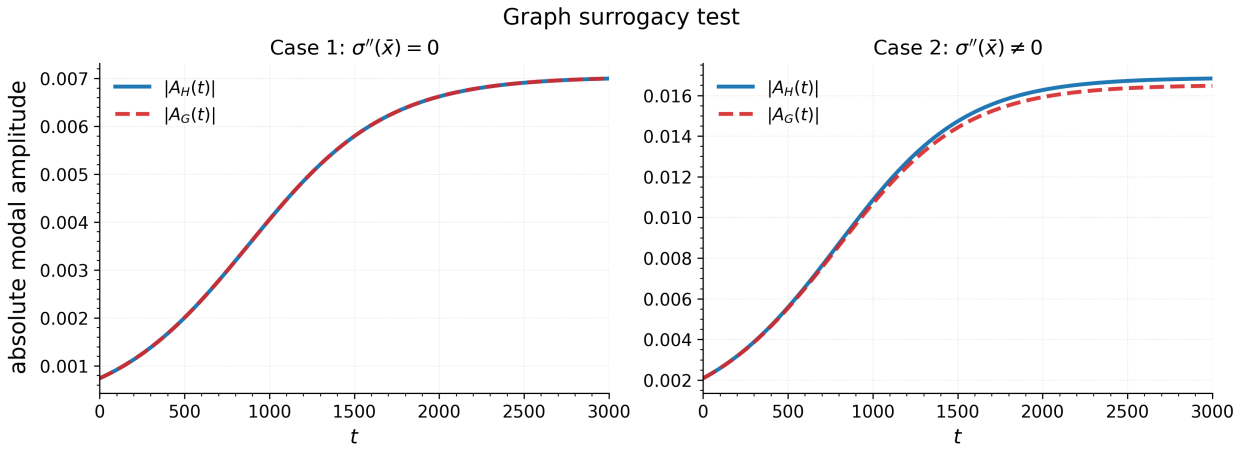

Figure 4.5: Graph-surrogacy test for a hypergraph $\mathcal{H}$ and its exposure-preserving graph surrogate $\mathcal{G}$. **Left:** Activation regime satisfying $\sigma''(\bar{x}) = 0$. In this regime, the quadratic packing effect vanishes, suppressing the leading nonlinear obstruction to graph surrogacy. The projected amplitudes $A_{\mathcal{H}}(t)$ and $A_{\mathcal{G}}(t)$ remain very close throughout the evolution, with only small deviations attributable to higher-order packing effects. **Right:** Activation regime satisfying $\sigma''(\bar{x}) \neq 0$. Quadratic packing effects are active, and the hypergraph and graph surrogate exhibit visibly different nonlinear dynamics despite identical linear onset. The systems initially evolve similarly but saturate at different amplitudes, demonstrating that exposure-equivalence alone is insufficient to guarantee nonlinear equivalence.

4.12.5 Reduced Dynamics versus the Full System

As an additional validation of the weakly nonlinear reduction, we compare the full projected amplitude $A_{\text{num}}(t)$ with the solution of the reduced amplitude equation

$$\dot{A} = \mu A + \beta A^2 + \gamma A^3,$$

A representative comparison is shown in Figure C.1. The close agreement near onset confirms that the reduced model accurately captures both the transient evolution and the nonlinear saturation of the critical mode in the weakly nonlinear regime.

Chapter 5

Conclusion and Outlook

5.1 Summary of Results

This dissertation studied how interaction structure influences the behavior of network dynamical systems, and more fundamentally which aspects of that structure are observable under different analytical frameworks. The central object of study throughout this work is the relationship

$$\text{interaction structure} \longrightarrow \text{observable dynamics}$$

A recurring theme has been that this relationship is not direct. Interaction structure does not appear uniformly across all dynamical or analytical settings. Rather, it becomes visible only through specific projections determined by the analytical framework used to study the system. Reconstruction methods reveal feasible combinatorial representations of higher-order interactions, stability theory reveals operator-level and coupling-dependent structural effects, and nonlinear reaction-diffusion analysis on directed hypergraphs reveals dynamically relevant higher-order effects through pattern-forming dynamics.

The main results can be summarized across three interconnected levels of analysis.

5.1.1 Reconstruction from Data

We first considered the inverse problem of reconstructing interaction structure from pairwise observations. We formulated the reconstruction problem as a regularized optimization problem, and we introduced deterministic and probabilistic clique-contraction frameworks for computing sparse hypergraph representations consistent with observed graphs. Furthermore, we showed that this reconstruction problem is fundamentally ill-posed, in the sense that multiple distinct higher-order interaction structures may induce the same pairwise representation under clique expansion. As a result, higher-order structure is not uniquely identifiable from pairwise data alone. This establishes a fundamental limitation of static reconstruction, and it highlights the role of modeling assumptions in selecting among admissible higher-order representations.

5.1.2 Stability of Network Dynamical Systems

We then studied dynamical systems on graphs, focusing on how interaction structure influences stability. In static systems, we showed that structure enters through coupling operators whose spectral properties determine how node dynamics are shifted. In switching systems, we derived Lyapunov-based conditions depending only on local degree-level structural quantities. We also identified *intrinsic obstructions to stabilization*. More specifically,

- diffusive coupling introduces a *functional obstruction* through the presence of an unshifted synchronization mode,
- graph structure, such as bipartiteness, can create *structural obstructions* preventing stabilization under signless coupling.

These results demonstrate that structural effects in pairwise systems are mediated through operator-level representations, and they may either enable or limit stabilization.

5.1.3 Nonlinear Reduction on Directed Hypergraphs

Finally, we studied reaction-diffusion systems on directed hypergraphs and analyzed their behavior near bifurcation using weakly nonlinear reduction. We showed that the nonlinear dynamics near onset are governed by reduced amplitude equations whose coefficients depend not on the full hypergraph structure, but only on specific dynamically relevant projections of higher-order interactions. These projections, termed *packing effects*, encode the components of higher-order structure governing nonlinear saturation and pattern selection. This leads to the following two fundamental conclusions

- higher-order structure is not fully observable through nonlinear dynamics
- nonlinear behavior depends only on specific dynamically relevant projections of that structure.

Moreover, this framework led naturally to the notion of *dynamical graph surrogacy*. A hypergraph-coupled system admits a dynamical graph surrogate up to a given order whenever its packing effects vanish, so that its reduced dynamics coincide with those of an appropriate pairwise system. This yields the following important conceptual insight

The absence of observable higher-order effects in the dynamics does not imply the absence of higher-order interactions in the underlying structure.

Higher-order interactions may therefore be present while remaining dynamically invisible within a given analytical regime or approximation.

5.2 A Unified Perspective on Structural Effects

These results yield a unified perspective on structural effects in network dynamical systems. Across all three levels considered, interaction structure is not directly observable. Instead,

it becomes visible only through the analytical framework used to probe the system

$$\text{Structure} \xrightarrow{\text{analysis}} \text{observable effects}$$

Different analyses reveal different structural representations

- reconstruction reveals feasible combinatorial representations, but it fails to uniquely identify higher-order interactions
- stability analysis reveals operator-level structural effects through spectra, coupling operators, and Lyapunov-compatible degree conditions
- nonlinear reduction reveals dynamically relevant higher-order projections through packing effects

This perspective reframes the role of structure in complex systems. Rather than asking

What is the interaction structure?

the present work suggests asking instead

Which aspects of structure are visible through a given analytical or dynamical framework?

In this sense, structural effects are not intrinsic observables of the interaction network itself, but instead they are analysis-dependent manifestations of that structure.

5.3 Implications

The results of this dissertation have broader implications for the modeling, analysis, inference, and control of complex interacting systems.

5.3.1 Limits of Structural Inference

The non-uniqueness of reconstruction and the projection-dependent nature of dynamics together show that structural inference from observations is fundamentally limited. Even with access to dynamical data, only certain aspects of interaction structure can be recovered.

5.3.2 Role of Higher-Order Interactions

Higher-order interactions do not uniformly influence dynamics. Their effects are mediated through specific structural projections and may vanish entirely within certain analytical regimes. Thus, the mere presence of higher-order interactions does not guarantee observable higher-order dynamical effects.

5.3.3 Modeling Considerations

These results also carry important implications for model selection.

- In some regimes, hypergraph models are necessary to capture nonlinear collective behavior and pattern selection.
- In other regimes, graph-based models may suffice due to dynamical graph surrogacy.

Consequently, the appropriate level of structural modeling depends fundamentally on the dynamical regime and on the observable phenomena of interest.

5.4 Future Directions

The framework developed in this dissertation opens several directions for future research.

5.4.1 Beyond Weakly Nonlinear Regimes

The present work develops a nonlinear reduction framework for reaction-diffusion systems on directed hypergraphs near codimension-one steady bifurcations. A natural next step is to extend this framework to broader classes of bifurcation phenomena. Future directions include

- Hopf bifurcations leading to oscillatory instabilities and time-periodic patterns
- higher-codimension bifurcations involving interacting modes
- mode interactions in hypergraph-structured systems, where higher-order interactions may fundamentally alter classical bifurcation scenarios

The present analysis is also restricted to the weakly nonlinear regime near onset. Extending these results to strongly nonlinear and global dynamics remains an important open problem. Additional directions include

- understanding how hyperedge heterogeneity influences instability selection and pattern formation
- studying how higher-order interactions affect transitions between dynamical regimes
- relating discrete hypergraph models to continuum limits

These directions aim toward a comprehensive theory of higher-order dynamics extending classical bifurcation and pattern formation theory to systems with genuinely multi-node interaction structures.

5.4.2 Inference of Dynamically Relevant Higher-Order Structure

The results of this dissertation show that dynamics depends only on specific structural projections termed packing effects. This raises a natural inverse problem

Can dynamically relevant higher-order structure be inferred directly from data?

Rather than reconstructing the full hypergraph, a promising direction is to infer packing effects or other reduced structural quantities directly from time-series observations. Key challenges include

- characterizing identifiability of packing effects
- understanding the role of noise and partial observability
- developing computational methods for inferring minimal higher-order structures consistent with observed dynamics

5.4.3 Control of Higher-Order Dynamical Systems

Another important direction is the development of a theory of control for higher-order dynamical systems. Building on the results of this dissertation, a central question is

How can higher-order structure be manipulated to influence collective behavior?

This includes

- controlling instability and pattern formation
- designing interventions that exploit or suppress higher-order effects
- understanding how higher-order structure affects controllability

Because packing effects determine nonlinear behavior near onset, they provide a natural bridge between higher-order structure and control design.

Toward a Unified Framework: Dynamics, Inference, and Control

These directions suggest a broader closed-loop perspective on higher-order systems

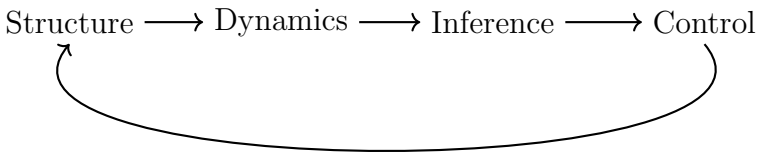

In this view,

- dynamics reveals only certain aspects of structure
- inference seeks to recover those aspects from data
- control seeks to manipulate them to achieve desired outcomes

The aim is therefore to develop a unified mathematical framework in which higher-order structure, dynamics, inference, and intervention are treated in a consistent and interconnected manner.

Appendices

Appendix A Aggregator-Mixer Coupling Examples

A.1 Multilinear Coupling

A particularly simple and analytically tractable subclass of the aggregator–mixer framework is obtained by choosing linear aggregation functions. In this setting, the aggregators ψ_k are taken to be the arithmetic mean of the tail states as follows

$$\psi_k(x_1, \ldots, x_k) = \frac{1}{k} \sum_{\ell=1}^{k} x_\ell \tag{A.1}$$

Choosing the mixer to be the identity map, $\Theta_k(x) = x$, the resulting coupling function becomes

$$\phi_k(x_{j_1}, \ldots, x_{j_k}, x_i) = M_k \left(\frac{\beta_k}{k} \sum_{\ell=1}^{k} x_{j_\ell} + \alpha_k x_i \right) \tag{A.2}$$

This coupling structure generalizes classical linear diffusive interactions on graphs to directed hypergraph settings. In particular, the interaction term depends linearly on the average state of the tail nodes together with a linear contribution from the head node. Such couplings provide a natural higher-order extension of consensus, diffusion, and linear network interaction models.

A.2 Polynomial Coupling

An important subclass of the aggregator–mixer framework is obtained by choosing polynomial aggregation functions. In this setting, the i-th canonical projection of the aggregator ψ_k is taken to be a monomial of degree at least k. More precisely, letting $\{\mathbf{e}_i\}_{1\le i\le d}$ denote the canonical basis of $\mathbb{R}^d$, we assume

$$\mathbf{e}_i^T \psi_k(x_1,\dots,x_k) = \prod_{\ell=1}^{k} x_{\ell,i}^{m_\ell}, \qquad \sum_{\ell=1}^{k} m_\ell \ge k, \qquad m_\ell \ge 1, \tag{A.3}$$

where $x_{\ell,i}$ denotes the i-th component of x_ℓ.

Equivalently, the aggregation function may be expressed using the Hadamard product

$$\psi_k(x_1,\dots,x_k) = \odot_{\ell=1}^{k} \odot_{\nu=1}^{m_\ell} x_\ell \tag{A.4}$$

Choosing the mixer function to be the identity, $\Theta_k = \mathrm{Id}$ the coupling function reduces to the polynomial interaction form

$$\phi_k(x_{j_1},\dots,x_{j_k},x_i) = M_k\left(\beta_k \odot_{\ell=1}^{k} \odot_{\nu=1}^{m_\ell} x_{j_\ell} + \alpha_k \odot_{\ell=1}^{k} \odot_{\nu=1}^{m_\ell} x_i\right) \tag{A.5}$$

A.3 Homogeneous Polynomial Coupling

In the *Polynomial Coupling* above, the aggregators ψ_k, and consequently the coupling functions ϕ_k need not have the same degree for all $k \in \{1,\cdots,\rho-1\}$. This leads in general to *non-homogeneous* polynomial coupling term in (4.12). However, if instead one seeks *homogeneous polynomial* coupling structure, then additional constraints must be imposed on the aggregators ψ_k. More specifically, all aggregators, and therefore all the coupling functions ϕ_k must be chosen to have *the same degree* d. Note that the degree must be *at least* $\rho-1$, namely $d \ge \rho-1$, where $\rho = r(\mathcal{H})$ is the *rank* of the hypergraph. Table A.1 shows an example of the *multiindice* exponents $(m_1,\cdots,m_k)$ to realize a homogeneous polynomial coupling

in the dynamics (4.12). This class of coupling includes multilinear tensor interactions in [14] as a particular case, and it provides a natural higher-order generalization of homogeneous polynomial coupling mechanisms commonly used in tensor-based dynamical systems.

Table A.1: Example of multi-index exponents $(m_1, \dots, m_k) \in \mathbb{N}^k$, where $\mathbb{N} = \{1, 2, \dots\}$ and $1 \le k \le \rho - 1$. These choices yield homogeneous polynomial coupling terms in the dynamics (4.12). The minimum degree of the aggregators ψ_k is $\rho - 1$, where ρ denotes the rank of the hypergraph. Multiplication is interpreted componentwise via the Hadamard product since the variables x_i may be high-dimensional.

ψ_k	$\deg(\psi_k) = \rho - 1$	$\deg(\psi_k) = \rho$	$\dots$
$\psi_1(x_1)$	$x_1^{\rho-1}$	x_1^{ρ}	$\dots$
$\psi_2(x_1, x_2)$	$x_1^{\rho-2}x_2$	$x_1^{\rho-1}x_2$	$\dots$
$\vdots$	$\vdots$	$\vdots$	$\vdots$
$\psi_{\rho-1}(x_1, \dots, x_{\rho-1})$	$x_1 x_2 \cdots x_{\rho-1}$	$x_1^2 x_2 \cdots x_{\rho-1}$	$\dots$

A.4 Trigonometric Coupling

Another important subclass of the aggregator-mixer framework is obtained by combining multilinear aggregation with trigonometric mixing functions. In this setting, the aggregation function ψ_k is chosen to be multilinear, while the canonical projections of the mixer Θ_k are taken to be trigonometric functions such as *sine* or *cosine*. A particularly relevant example arises when choosing the aggregation function to be the summation

$$\psi_k(x_1, \dots, x_k) = \sum_{\ell=1}^{k} x_\ell \tag{A.6}$$

and selecting the mixer so that its canonical projections are given by the sine function,

$$\mathbf{e}_i^T \Theta_k(x) = \sin(x_i), \qquad 1 \le i \le d. \tag{A.7}$$

This yields a higher-order trigonometric coupling structure generalizing classical Kuramoto-type dynamics. To illustrate this connection, suppose for simplicity that $\mathcal{H}$ is a 3-uniform directed B-hypergraph and that the node dynamics are scalar-valued. The corresponding order-2 coupling function on the B-arc $e = (\{j_1, j_2\} \to i)$ takes the form

$$\phi_2(x_{j_1}, x_{j_2}, x_i) = \alpha_2 \sin\big(x_{j_1} + x_{j_2} - 2x_i\big). \tag{A.8}$$

This expression is a direct higher-order extension of the classical Kuramoto interaction term, with pairwise phase differences replaced by collective phase interactions involving multiple tail nodes. The normalization factor is absorbed into the adjacency tensor $\mathsf{A}^{(2)}_{ij_1j_2}$. Consequently, the framework naturally incorporates higher-order Kuramoto-type models on directed hypergraphs within the general aggregator-mixer architecture.

Appendix B Additional Derivations

B.1 Proof of Lemma 4.20

Proof. Fix $i \in \{1, \dots, n_0\},\ j \in \{1, \dots, n\}$. For each $\ell \in \{1, \dots, k\}$, define the constrained index set $\mathcal{J}_\ell(j) := \left\{(j_1, \dots, j_k) \in \{1, \dots, n\}^k \;\middle|\; j_\ell = j\right\}$. Then by definition of the contraction we have, $\mathsf{T}^{\hat{\ell}}_{ij} = \sum_{(j_1,\dots,j_k)\in\mathcal{J}_\ell(j)} \mathsf{T}_{ij_1\cdots j_k}$. Now let $\ell, \ell' \in \{1, \dots, k\}$, and consider the permutation $\pi_{\ell\leftrightarrow\ell'} \in S_k$ that exchanges the positions ℓ and ℓ'. This permutation induces a bijection between the sets $\mathcal{J}_\ell(j)$ and $\mathcal{J}_{\ell'}(j)$ since fixing the value j in the ℓ-th position is equivalent after permutation to fixing j in the ℓ'-th position.

By symmetry of the tensor T in its last k indices, we have $\mathsf{T}_{ij_1\cdots j_k} = \mathsf{T}_{ij_{\pi(1)}\cdots j_{\pi(k)}}$ for every permutation $\pi \in S_k$. In particular, corresponding terms under the above bijection have identical values. Therefore, $\mathsf{T}^{\hat{\ell}}_{ij} = \mathsf{T}^{\hat{\ell}'}_{ij}$. Since the equality holds for all $i \in \{1, \dots, n_0\}, \quad j \in \{1, \dots, n\}$, it follows that $\mathsf{T}^{\hat{\ell}} = \mathsf{T}^{\hat{\ell}'}$. ■

B.2 Proof of Proposition 4.22

Proof. Let $j_1, \cdots, j_p$ be fixed tail indices, and consider a hyperedge $e = (T \to i) \in E_k$ such that $j_1, \cdots, j_p \in T$. Using the definition of the adjacency tensor (4.2), the contribution of e to the contraction $\left\langle \mathsf{A}^{(k)}, \mathsf{1}_{k-p} \right\rangle_{\{p+2,\dots,k+1\}}$ is $(k-p)!\,\frac{w(e)}{k!} = \frac{w(e)}{(k)_p}$. Thus multiplying by $(k)_p/k^p$ and summing over all hyperedges containing $j_1, \cdots, j_p$ yields the result. Note that the restriction to distinct tail indices isolates the genuinely p-way interactions of $\mathsf{T}^{(k,p)}$, since repeated-index entries reduce to lower-order moments. ■

B.3 Proof of Proposition 4.29

Proof. Let $y = \delta\mathbf{x}$ and consider the following cubic order Taylor expansion of the vector field near the bifurcation

$$\dot{y} = J_0 y + \epsilon J_1 y + B(y, y) + C(y, y, y) + O(\|y\|^4 + |\epsilon|\|y\|^2 + \epsilon^2\|y\|), \tag{B.1}$$

where B and C are symmetric bilinear and trilinear maps. Since J_0 has a simple zero eigenvalue with right eigenvector v and left eigenvector w satisfying $w^\top v = 1$, with all remaining eigenvalues have negative real part, the center manifold theorem, guarantees the existence of a one-dimensional locally invariant center manifold locally tangent to $\text{span}\{v\}$ at the origin. Let's parametrize it as follows

$$y = Av + h(A, \epsilon), \tag{B.2}$$

where $A \in \mathbb{R}$ and $h(A, \epsilon)$ takes values in the stable complement of $\text{span}\{v\}$. Let $Q = I - vw^\top$ denote the projection onto this stable complement. We have the following expansion of the correction term owing to the tangency of the center manifold to $\text{span}\{v\}$

$$h(A, \epsilon) = A^2 u + O(|A|^3 + |\epsilon||A|^2) \tag{B.3}$$

for some $u \in \text{Range}(Q)$. The amplitude is defined using the adjoint vector w such that $A = w^\top y$. Since the correction term is transverse to the critical subspace, namely $w^\top h(A, \epsilon)$, differentiating the projection of (B.2) yields $\dot{A} = w^\top \dot{y}$. Substituting the expansion of (B.2)

into (B.1) and keeping only terms up to cubic order, we obtain

$$\dot{A} = w^\top \Big[J_0(Av + A^2u) + \epsilon J_1(Av) + B(Av + A^2u, Av + A^2u) + C(Av, Av, Av) \Big] + \text{h.o.t.} \tag{B.4}$$

Since $J_0 v = 0$ and $w^\top J_0 = 0$, we obtain

$$\dot{A} = \epsilon\, w^\top J_1 v\, A + w^\top B(v, v)\, A^2 + w^\top \Big(2B(v, u) + C(v, v, v) \Big)\, A^3 + \text{h.o.t.} \tag{B.5}$$

Hence

$$\alpha = w^\top J_1 v, \qquad \beta = w^\top B(v, v), \qquad \gamma = w^\top \Big(2B(v, u) + C(v, v, v) \Big) \tag{B.6}$$

It now remains to determine u. In the one hand, substituting the expansion of the ansatz (B.2) into (B.1) then applying the stable projection Q gives $J_0 u + QB(v, v)$ at order A^2. In the other hand, differentiating the expansion of the ansatz (B.2), then applying the stable projection Q yields $Q\dot{y} = 2A\dot{A}u + O(A^2\dot{A}) = O(A^3)$ since $\dot{A} = O(A^2)$ at the bifurcation point. Thus the center manifold invariance condition requires the quadratic component $J_0 u + QB(v, v)$ to vanish. Since $u \in \text{Range}(Q)$, the center-manifold invariance Since $u \in \text{Range}(Q)$, the center-manifold invariance condition requires this component to vanish. Since the zero eigenvalue of J_0 is simple, its restriction to the stable subspace Range(Q) is invertible. Thus the equation has a unique solution. ■

Appendix C Numerical Validation

C.1 Hypergraph Benchmark Sets

$V = \{1, 2, 3, 4, 5, 6\}$

Hyperedge	Directed relation	Weight
e_1	$\{3, 4\} \to 1$	2.00
e_2	$\{5\} \to 1$	0.60
e_3	$\{5\} \to 2$	0.80
e_4	$\{6\} \to 2$	0.80
e_5	$\{3\} \to 2$	0.40
e_6	$\{1\} \to 3$	0.50
e_7	$\{2\} \to 4$	0.50

(a) Hypergraph $\mathcal{H}_A$

$V = \{1, 2, 3, 4, 5, 6\}$

Hyperedge	Directed relation	Weight
e_1	$\{3\} \to 1$	1.00
e_2	$\{4\} \to 1$	1.00
e_3	$\{5\} \to 1$	0.60
e_4	$\{5, 6\} \to 2$	1.60
e_5	$\{3\} \to 2$	0.40
e_6	$\{1\} \to 3$	0.50
e_7	$\{2\} \to 4$	0.50

(b) Hypergraph $\mathcal{H}_B$

Table C.1: Pair of directed weighted hypergraphs $\mathcal{H}_A$ and $\mathcal{H}_B$ used in Figure 4.4

$V = \{1, 2, 3, 4, 5, 6\}$

Hyperedge	Directed relation	Weight
e_1	$\{3, 4\} \to 1$	1.01
e_2	$\{5, 6\} \to 1$	1.00
e_3	$\{3, 6\} \to 2$	0.80
e_4	$\{3\} \to 5$	1.50
e_5	$\{5\} \to 1$	0.60
e_6	$\{1\} \to 3$	0.50
e_7	$\{5\} \to 2$	0.75
e_8	$\{1, 2, 5\} \to 4$	0.50
e_9	$\{4, 5, 6\} \to 1$	0.50

Table C.2: Directed weighted hypergraph $\mathcal{H}$.

C.2 Reduced Dynamics Versus Full System

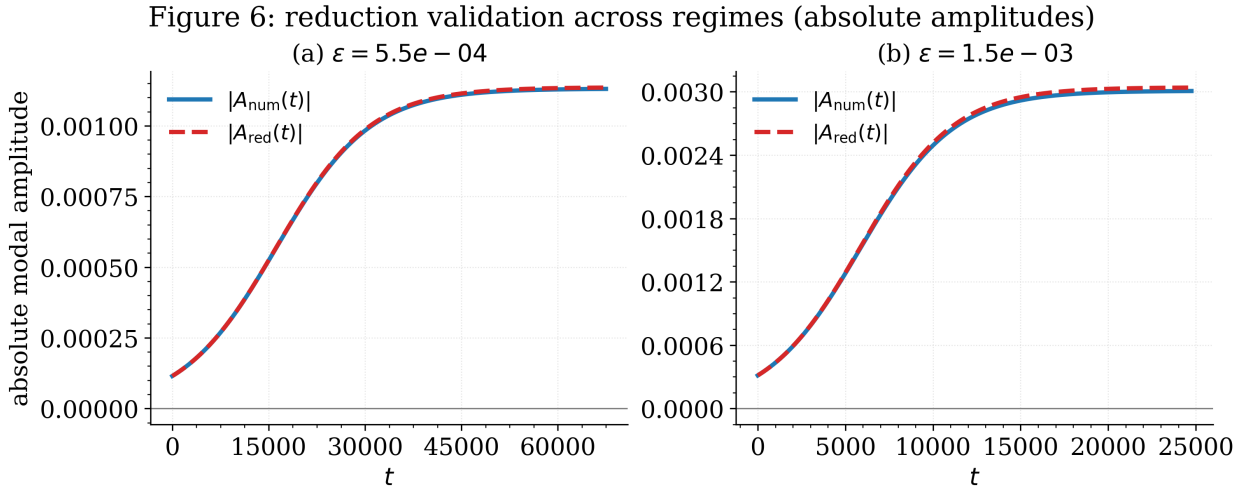

Figure C.1: Reduction validation across regimes. The projected amplitude $A_{\mathrm{num}}(t)$ from the full hypergraph system is compared with the solution $A_{\mathrm{red}}(t)$ of the reduced normal form, initialized with $A_{\mathrm{red}}(0) = A_{\mathrm{num}}(0)$. **Left:** Near-onset regime with $\varepsilon = 5.5 \times 10^{-4}$. The reduced equation accurately reproduces both the transient growth and the saturation amplitude over long timescales, consistent with the validity of the weakly nonlinear reduction close to bifurcation. **Right:** Moderately larger parameter offset with $\varepsilon = 1.5 \times 10^{-3}$. Although the dynamics move farther from the asymptotic weakly nonlinear regime, the reduced model still captures the qualitative evolution and provides a quantitatively accurate approximation of the saturation dynamics. In both cases, the close agreement confirms that the reduced amplitude equation captures the dominant critical-mode dynamics governing pattern formation near onset.

Bibliography

[1] Juan A Acebrón, Luis L Bonilla, Conrad J Pérez Vicente, Félix Ritort, and Renato Spigler. The kuramoto model: A simple paradigm for synchronization phenomena. *Reviews of modern physics*, 77(1):137–185, 2005.

[2] Sameer Agarwal, Kristin Branson, and Serge Belongie. Higher order learning with graphs. In *Proceedings of the 23rd international conference on Machine learning*, pages 17–24, 2006.

[3] Alex Arenas, Albert Díaz-Guilera, Jurgen Kurths, Yamir Moreno, and Changsong Zhou. Synchronization in complex networks. *Physics reports*, 469(3):93–153, 2008.

[4] Giacomo Baggio, Virginia Rutten, Guillaume Hennequin, and Sandro Zampieri. Efficient communication over complex dynamical networks: The role of matrix non-normality. *Science advances*, 6(22):eaba2282, 2020.

[5] Federico Battiston, Giulia Cencetti, Iacopo Iacopini, Vito Latora, Maxime Lucas, Alice Patania, Jean-Gabriel Young, and Giovanni Petri. Networks beyond pairwise interactions: Structure and dynamics. *Physics reports*, 874:1–92, 2020.

[6] Austin R Benson, David F Gleich, and Desmond J Higham. Higher-order network analysis takes off, fueled by old ideas and new data. *SIAM News Blog*, 21(1), 2021.

[7] Austin R Benson, David F Gleich, and Jure Leskovec. Higher-order organization of complex networks. *Science*, 353(6295):163–166, 2016.

[8] Claude Berge. *Hypergraphs: combinatorics of finite sets*, volume 45. Elsevier, 1984.

[9] Anthony M. Bloch. *Nonholonomic Mechanics and Control*. Springer, 2015.

[10] Anthony M Bloch, PS Krishnaprasad, Jerrold E Marsden, and Tudor S Ratiu. Dissipation induced instabilities. In *Annales de l'Institut Henri Poincaré C, Analyse non linéaire*, volume 11, pages 37–90. Elsevier, 1994.

[11] Alain Bretto. Hypergraph theory. *An introduction. Mathematical Engineering. Cham: Springer*, 1:209–216, 2013.

[12] Jack Carr. *Applications of centre manifold theory*. Springer Science & Business Media, 2012.

[13] Damon Centola. *How behavior spreads: The science of complex contagions*, volume 3. Princeton University Press Princeton, NJ, 2018.

[14] Can Chen, Amit Surana, Anthony M Bloch, and Indika Rajapakse. Controllability of hypergraphs. *IEEE Transactions on Network Science and Engineering*, 8(2):1646–1657, 2021.

[15] M. C. Cross and H. S. Greenside. *Pattern Formation and Dynamics in Nonequilibrium Systems*. Cambridge University Press, 2009.

[16] Mark C Cross and Pierre C Hohenberg. Pattern formation outside of equilibrium. *Reviews of modern physics*, 65(3):851, 1993.

[17] Raymond A DeCarlo, Michael S Branicky, Stefan Pettersson, Bengt Lennartson, et al. Perspectives and results on the stability and stabilizability of hybrid systems. *Proceedings of the IEEE*, 88(7):1069–1082, 2000.

[18] Madhav Desai and Vasant Rao. A characterization of the smallest eigenvalue of a graph. *Journal of Graph Theory*, 18(2):181–194, 1994.

[19] Gaogao Dong, Dongli Duan, and Yongxiang Xia. A briefing survey on advances of coupled networks with various patterns. *Frontiers in Physics*, 9:795279, 2021.

[20] Marie Dorchain, Wilfried Segnou, Riccardo Muolo, and Timoteo Carletti. Impact of directionality on the emergence of turing patterns on m-directed higher-order structures. *Chaos, Solitons & Fractals*, 189:115730, 2024.

[21] Michael B Elowitz and Stanislas Leibler. A synthetic oscillatory network of transcriptional regulators. *Nature*, 403(6767):335–338, 2000.

[22] Stefano Galli, Anna Scaglione, and Zhifang Wang. For the grid and through the grid: The role of power line communications in the smart grid. *Proceedings of the IEEE*, 99(6):998–1027, 2011.

[23] Giorgio Gallo, Giustino Longo, Stefano Pallottino, and Sang Nguyen. Directed hypergraphs and applications. *Discrete applied mathematics*, 42(2-3):177–201, 1993.

[24] Gene H Golub and Charles F Van Loan. *Matrix computations*. JHU press, 2013.

[25] John Guckenheimer and Philip Holmes. *Nonlinear oscillations, dynamical systems, and bifurcations of vector fields*. Springer Science & Business Media, 2013.

[26] Roger A Horn and Charles R Johnson. *Matrix analysis*. Cambridge university press, 2012.

[27] Rebecca B Hoyle. *Pattern formation: an introduction to methods*. Cambridge University Press, 2006.

[28] Iacopo Iacopini, Giovanni Petri, Alain Barrat, and Vito Latora. Simplicial models of social contagion. *Nature communications*, 10(1):2485, 2019.

[29] Mahdi Jalili. Enhancing synchronizability of diffusively coupled dynamical networks: a survey. *IEEE transactions on neural networks and learning systems*, 24(7):1009–1022, 2013.

[30] Hassan K. Khalil. *Nonlinear Systems*. Prentice-Hall, 3 edition, 2002.

[31] Steffen Klamt, Utz-Uwe Haus, and Fabian Theis. Hypergraphs and cellular networks. *PLoS computational biology*, 5(5):e1000385, 2009.

[32] Bryan Klimt and Yiming Yang. The enron corpus: A new dataset for email classification research. In *European conference on machine learning*, pages 217–226. Springer, 2004.

[33] Tamara G Kolda and Brett W Bader. Tensor decompositions and applications. *SIAM review*, 51(3):455–500, 2009.

[34] Yoshiki Kuramoto. Self-entrainment of a population of coupled non-linear oscillators. In *International symposium on mathematical problems in theoretical physics: January 23–29, 1975, kyoto university, kyoto/Japan*, pages 420–422. Springer, 2005.

[35] Yuri A Kuznetsov. *Elements of applied bifurcation theory*. Springer, 1998.

[36] Matthew D Kvalheim and Anthony M Bloch. Families of periodic orbits: closed 1-forms and global continuability. *Journal of Differential Equations*, 285:211–257, 2021.

[37] Juho Lee, Yoonho Lee, Jungtaek Kim, Adam Kosiorek, Seungjin Choi, and Yee Whye Teh. Set transformer: A framework for attention-based permutation-invariant neural networks. In *International conference on machine learning*, pages 3744–3753. PMLR, 2019.

[38] Sansan Li, Na Sun, Li Chen, and Xingang Wang. Network synchronization with periodic coupling. *Physical Review E*, 98(1):012304, 2018.

[39] Daniel Liberzon. *Switching in systems and control*, volume 190. Springer, 2003.

[40] Jannik Luboeinski, Luis Claro, Andrés Pomi, and Eduardo Mizraji. Stabilization through self-coupling in networks of small-world and scale-free topology. *Scientific Reports*, 13(1):1089, 2023.

[41] Philip K Maini, Thomas E Woolley, Ruth E Baker, Eamonn A Gaffney, and S Seirin Lee. Turing's model for biological pattern formation and the robustness problem. *Interface focus*, 2(4):487, 2012.

[42] Rossana Mastrandrea, Julie Fournet, and Alain Barrat. Contact patterns in a high school: a comparison between data collected using wearable sensors, contact diaries and friendship surveys. *PloS one*, 10(9):e0136497, 2015.

[43] Ana P Millán, Joaquín J Torres, and Ginestra Bianconi. Explosive higher-order kuramoto dynamics on simplicial complexes. *Physical Review Letters*, 124(21):218301, 2020.

[44] Luc Moreau. Stability of multiagent systems with time-dependent communication links. *IEEE Transactions on automatic control*, 50(2):169–182, 2005.

[45] Moise R Mouyebe and Anthony M Bloch. On the local controllability of a class of quadratic systems. *arXiv preprint arXiv:2410.04770*, 2024.

[46] Moise R Mouyebe and Anthony M Bloch. Coupling induced stabilization of network dynamical systems and switching. In *2025 IEEE 64th Conference on Decision and Control (CDC)*, pages 8091–8097. IEEE, 2025.

[47] Riccardo Muolo, Luca Gallo, Vito Latora, Mattia Frasca, and Timoteo Carletti. Turing patterns in systems with high-order interactions. *Chaos, Solitons & Fractals*, 166:112912, 2023.

[48] Riccardo Muolo, Lorenzo Giambagli, Hiroya Nakao, Duccio Fanelli, and Timoteo Carletti. Turing patterns on discrete topologies: from networks to higher-order structures. In *Proceedings A*, volume 480, page 20240235. The Royal Society, 2024.

[49] James Dickson Murray. *Mathematical biology: II: spatial models and biomedical applications*, volume 18. Springer, 2003.

[50] Hiroya Nakao and Alexander S Mikhailov. Turing patterns in network-organized activator–inhibitor systems. *Nature Physics*, 6(7):544–550, 2010.

[51] Alan C Newell and John A Whitehead. Finite bandwidth, finite amplitude convection. *Journal of Fluid Mechanics*, 38(2):279–303, 1969.

[52] Mark Newman. *Networks*. Oxford university press, 2018.

[53] Jorge L Ocampo-Espindola, István Z Kiss, Christian Bick, and Kyle CA Wedgwood. Strong coupling yields abrupt synchronization transitions in coupled oscillators. *Physical Review Research*, 6(3):033328, 2024.

[54] Reza Olfati-Saber, J Alex Fax, and Richard M Murray. Consensus and cooperation in networked multi-agent systems. *Proceedings of the IEEE*, 95(1):215–233, 2007.

[55] Reza Olfati-Saber and Richard M Murray. Consensus problems in networks of agents with switching topology and time-delays. *IEEE Transactions on automatic control*, 49(9):1520–1533, 2004.

[56] Ashwin Paranjape, Austin R Benson, and Jure Leskovec. Motifs in temporal networks. In *Proceedings of the tenth ACM international conference on web search and data mining*, pages 601–610, 2017.

[57] Louis M Pecora and Thomas L Carroll. Master stability functions for synchronized coupled systems. *Physical review letters*, 80(10):2109, 1998.

[58] Arkady Pikovsky, Michael Rosenblum, Jürgen Kurths, and A Synchronization. *A universal concept in nonlinear sciences*. Cambridge University Press, Princeton, 1985.

[59] Wei Ren and Randal W Beard. Consensus seeking in multiagent systems under dynamically changing interaction topologies. *IEEE Transactions on automatic control*, 50(5):655–661, 2005.

[60] Suman Saha, Arindam Mishra, E Padmanaban, Sourav K Bhowmick, Prodyot K Roy, Bivas Dam, and Syamal K Dana. Coupling conditions for globally stable and robust synchrony of chaotic systems. *Physical Review E*, 95(6):062204, 2017.

[61] Michael T Schaub, Austin R Benson, Paul Horn, Gabor Lippner, and Ali Jadbabaie. Random walks on simplicial complexes and the normalized hodge 1-laplacian. *SIAM Review*, 62(2):353–391, 2020.

[62] Jangir Selimkhanov, Brooks Taylor, Jason Yao, Anna Pilko, John Albeck, Alexander Hoffmann, Lev Tsimring, and Roy Wollman. Accurate information transmission through dynamic biochemical signaling networks. *Science*, 346(6215):1370–1373, 2014.

[63] Eduardo D Sontag et al. On the input-to-state stability property. *Eur. J. Control*, 1(1):24–36, 1995.

[64] Julien C Sprott. *Elegant chaos: algebraically simple chaotic flows*. World Scientific, 2010.

[65] Juliette Stehlé, Nicolas Voirin, Alain Barrat, Ciro Cattuto, Lorenzo Isella, Jean-François Pinton, Marco Quaggiotto, Wouter Van den Broeck, Corinne Régis, Bruno Lina, et al. High-resolution measurements of face-to-face contact patterns in a primary school. *PloS one*, 6(8):e23176, 2011.

[66] Steven H Strogatz. From kuramoto to crawford: exploring the onset of synchronization in populations of coupled oscillators. *Physica D: Nonlinear Phenomena*, 143(1-4):1–20, 2000.

[67] Amit Surana, Can Chen, and Indika Rajapakse. Hypergraph similarity measures. *IEEE Transactions on Network Science and Engineering*, 10(2):658–674, 2022.

[68] Joaquín J Torres and Ginestra Bianconi. Simplicial complexes: higher-order spectral dimension and dynamics. *Journal of Physics: Complexity*, 1(1):015002, 2020.

[69] Lloyd N Trefethen and David Bau. *Numerical linear algebra*. SIAM, 2022.

[70] Alan Mathison Turing. The chemical basis of morphogenesis. *Bulletin of mathematical biology*, 52(1):153–197, 1990.

[71] Stephen Wiggins. *Introduction to applied nonlinear dynamical systems and chaos*. Springer, 2003.

[72] Tao Yang, Ziyang Meng, Guodong Shi, Yiguang Hong, and Karl Henrik Johansson. Network synchronization with nonlinear dynamics and switching interactions. *IEEE Transactions on Automatic Control*, 61(10):3103–3108, 2015.

[73] Manzil Zaheer, Satwik Kottur, Siamak Ravanbakhsh, Barnabas Poczos, Russ R Salakhutdinov, and Alexander J Smola. Deep sets. *Advances in neural information processing systems*, 30, 2017.

[74] Dengyong Zhou, Jiayuan Huang, and Bernhard Schölkopf. Learning with hypergraphs: Clustering, classification, and embedding. *Advances in neural information processing systems*, 19, 2006.